University of Tennessee, Knoxville

TRACE: Tennessee Research and Creative Exchange

Doctoral Dissertations

Graduate School

5-2017

# Biogeochemical Characteristics of Organic Matter in a Karst Groundwater System

Teresa Lynn Brown
*University of Tennessee, Knoxville*, tbrown23@vols.utk.edu

Follow this and additional works at: https://trace.tennessee.edu/utk_graddiss

Part of the Biogeochemistry Commons, Hydrology Commons, and the Speleology Commons

## Recommended Citation

Brown, Teresa Lynn, "Biogeochemical Characteristics of Organic Matter in a Karst Groundwater System. " PhD diss., University of Tennessee, 2017.
https://trace.tennessee.edu/utk_graddiss/4389

This Dissertation is brought to you for free and open access by the Graduate School at TRACE: Tennessee Research and Creative Exchange. It has been accepted for inclusion in Doctoral Dissertations by an authorized administrator of TRACE: Tennessee Research and Creative Exchange. For more information, please contact trace@utk.edu.

To the Graduate Council:

I am submitting herewith a dissertation written by Teresa Lynn Brown entitled "Biogeochemical Characteristics of Organic Matter in a Karst Groundwater System." I have examined the final electronic copy of this dissertation for form and content and recommend that it be accepted in partial fulfillment of the requirements for the degree of Doctor of Philosophy, with a major in Geology.

Annette S. Engel, Major Professor

We have read this dissertation and recommend its acceptance:

Larry D. McKay, Terry C. Hazen, Steve W. Wilhelm, Susan M. Pfiffner

Accepted for the Council:

Dixie L. Thompson

Vice Provost and Dean of the Graduate School

(Original signatures are on file with official student records.)

# Biogeochemical Characteristics of Organic Matter in a Karst Groundwater System

A Dissertation Presented for the
Doctor of Philosophy
Degree
The University of Tennessee, Knoxville

Teresa Lynn Brown
May 2017

Copyright © by Teresa Lynn Brown
All rights reserved.

## Dedication

This work is dedicated to the memory of my late father, Dallas Lloyd Brown, a great teacher who trusted, encouraged, supported, and tried to instill good judgement in me without judging. This level of scholarship would not have been possible without early guidance and counsel provided by my undergraduate mentor, Katherine King-Frazier, a beautiful soul and accomplished scientist who blasted off from this planet far too early. Departed family and friends responsible for my academic aspirations also include great teachers and leaders; Drs. Ruth and R.D. Campbell, Bob and Birdie McCoy, Drs. Bobby and Frank Bowles, Katherine and Martha Sieg, and many others. Lastly, I dedicate this research to the living, specifically our students, because it is their mission focus on the far-reaching consequences of our actions using technology and creativity to minimize impacts on Earth's integrated systems.

**Acknowledgements**

I am most grateful to Dr. Larry McKay (MS advisor) and Dr. Annette Engel (PhD advisor) for taking me on as a "nonconventional" graduate student, giving me the opportunity to pursue my passion and to fulfill my calling when others refused to take my intentions seriously. My dissertation advisory committee composed of Dr. Engel, Dr. McKay, Dr. Susan Pfiffner, Dr. Terry Hazen, and Dr. Steve Wilhelm, was supportive throughout my graduate career, worked to mold me into a better scientist, and was especially helpful when I had to change course due to the constraints of reality. The hydrogeologic analyses in this dissertation could not have been accomplished without the enthusiastic assistance provided by Dr. Sid Jones, Gareth Davies, and my stalwart husband, Bob Hunter, who also constructed several graphs and illustrations in this dissertation. Unwavering support of family and friends is important to every student, and in my case has been epitomized by my dear mother, Nancy C. Hagen, and my good friend, Charles Maus. Vital support for this research was provided by the Cave Conservancy Foundation Fellowship for Karst Studies, and the Jones Endowment and Department of Earth and Planetary Sciences at the University of Tennessee, and the Marathon GeoDE Research Fellowship at Louisiana State University. Finally, I sincerely appreciate all the students, staff, and volunteers who contributed to the success of this research through their hard work on sampling trips, in the laboratory, and in the office.

**Abstract**

Development of regional groundwater carbon budgets hinges on the ability to quantify and monitor biogeochemical processes controlled by microbial recycling of natural dissolved organic matter (DOM) in carbon-limited (oligotrophic) areas. DOM is the major reservoir of organic carbon in aquatic ecosystems. However, isolation and characterization of DOM in oligotrophic freshwater systems has been limited by operational protocols and instrumentation. The goals of this research were to investigate the seasonal dynamics of microbially-driven organic matter degradation in a karst groundwater system influenced by surface water, and to identify analytical tools and biomarkers to measure long-term hydro-ecological trends in the Appalachian region. To this end, a novel, inexpensive solid phase extraction technique was adapted to isolate and concentrate macromolecular functional groups in DOM rapidly from small (< 5 L) volumes of surface and cave stream waters in the field. Isolates of macromolecular functional groups indicated that DOM quality varied both diurnally and seasonally in surface water recharge due to photo-degradation, as well as hydrological and climatological factors. Seasonal DOM quality in the cave stream was constant, despite water residence times (during spring and summer) that ranged from less than 24 hours to more than 7 days. The structure of microbial communities responsible for surface-derived DOM transformations varied significantly between surface recharge and cave stream at low flow conditions. Seasonal DOM transformations also significantly varied with microbial physiological responses to stressors along the flow path, due to transport, temperature fluctuations, and nutrient limitation. This research links environmental and microbial processes in a karst groundwater-surface water system and provides evidence that quantification of carbon cycling in oligotrophic systems based on the macromolecular DOM transformations can be estimated and utilized in regional to global carbon cycle budgets.

**Table of Contents**

Chapter 1. Dissertation Overview: Organic Matter in Freshwater Systems ..... 1

1.0 Abstract ..... 2

1.1 Introduction ..... 2

1.1.1 Conceptual Models for OM Evolution ..... 5

1.1.2 Outstanding Issues in DOM Characterization ..... 8

1.1.3 Indicators of Microbial Community Composition and OM Processing ..... 10

1.2 Overview of Dissertation Research ..... 11

1.3 Description of the Study Area ..... 12

1.3.1 James Branch Catchment ..... 12

1.3.2 Cascade Cave System and Previous Research ..... 14

1.4 Dissertation Organization ..... 15

Chapter 2. An Adaptation of Weak Anion-exchange Chromatography for the Isolation of Natural Organic Matter from Oligotrophic Aquatic Environments ..... 21

2.0 Abstract ..... 22

2.1 Introduction ..... 22

2.2 Methods ..... 27

2.2.1 DEAE Preparation ..... 27

2.2.2 NOM Isolation and Fractionation ..... 28

2.2.3 Natural OM Characterization ..... 29

2.2.4 Calibration and Statistical Analyses ..... 31

2.3 Results ..... 32

2.3.1 DEAE Retention and Elution Efficiencies ..... 32

2.3.2 Spectral Comparison of Original OM, Filtrates, and Isolates ..... 33

2.4 Discussion ..... 35

Chapter 2 Appendix ..... 38

Chapter 3. A Hydrologic Analysis of the Cascade Cave Drainage System Under Low- and High-Flow Conditions ..... 46

3.0 Abstract ..... 47

3.1 Introduction ..... 47

3.2 Materials and Methods ..... 49

3.2.1 Flow Measurements ..... 49

3.2.2 Analysis of Background Fluorescence ..... 50

3.2.3 Dye Selection and Dosage ..... 51

3.2.4 Dye Injections ..... 53

3.2.5 Dye Analyses ..... 54

3.3 Results and Discussion ..... 55

3.3.1 Discharge ..... 55

3.3.2 Background Fluorescence ..... 55

3.3.3 Dye Detection and Recovery ..... 57

3.3.3.1 Tracer Test I ..... 57

3.3.3.2 Tracer Test II ..... 58

3.3.3.3 Tracer Test III ..... 58

3.4 Summary and Conclusions ..... 59

Chapter 3 Appendix ..... 62

Chapter 4. Structural Transformation of Organic Matter Along the Recharge to Discharge Flow Path of an Oligotrophic Cave Stream ..... 74

4.0 Abstract ..... 75

4.1 Introduction ..... 75

4.2 Methods ..... 78

4.2.1 Water Sampling and Physicochemistry ..... 78

4.2.2 DOM Isolation ..... 81

4.2.3 Spectroscopic Characterization ..... 81

4.2.4 Statistical and Data Analyses ..... 83

4.3 Results ..... 84

4.3.1 Hydrochemistry ..... 84

4.3.2 Interpretation of FTIR Spectra ..... 85

4.4 Discussion ..... 89

4.4.1 Hypothesis 1: Seasonal hydrologic variations and temperature perturbations affect DOM quality and the efficiency with which DOM is processed in the subsurface ..... 91

4.4.2 Hypothesis 2: Specific macromolecular indicators of DOM degradation exhibit decreasing IR absorbance with extended residence time and transport in the subsurface ..... 93

4.4.3 Hypothesis 3: Dissolved organic carbon-to-total-nitrogen ratios (OC:TN) decrease downstream coincident with microbial processing and by-product formation ..... 95

4.5 Summary ..... 96

Chapter 4 Appendix ..... 99

Chapter 5. Lipid Biomarkers Revealed Rapid Microbial Community Response to Changing Environmental and Hydrological Conditions ..... 115

5.0 Abstract ..... 116

5.1 Introduction ..... 117

5.1.1 Definitions and Fatty Acid Biosynthesis ..... 118

5.1.2 Fatty Acid Nomenclature ..... 119

5.1.3 Fatty Acid Classes and Biomarkers ..... 121

5.1.4 PLFA Analysis Links Environment to DOM Quality ..... 123

5.2 Objectives and Hypotheses ..... 124

5.3 Methods ..... 126

5.3.1 Water and Sediment Sampling ..... 126

5.3.2 PLFA Extraction and Analysis ..... 127

5.3.3 Quantification and Statistical Analysis ..... 128

5.4 Results ..... 131

5.4.1 Water Chemistry ..... 131

5.4.2 Total Bacterial and Microeukaryotic Biomass ..... 132

5.4.3 PLFA Classes by Sample Type ..... 132

5.4.4 PLFA Profiles for Attached and Suspended Fractions ..... 133

5.4.5 Biomarker Ratios through Time ..... 134

5.4.6 Multivariate Analysis ..... 135

5.5 Discussion ..... 136

5.6 Conclusion ..... 140

Chapter 5 Appendix ..... 142

Chapter 6. Dissertation Conclusions ..... 156

References ..... 161

Appendix ..... 200

Vita ..... 204

**List of Tables**

Table 2.1 Characteristic FTIR functional group frequencies in NOM isolates. ..... 38

Table 2.2 Physicochemical parameters of original reference NOM solutions. ..... 39

Table 2.3 Final physicochemical parameters of DEAE isolates from Suwannee River reference NOM and Nordic Reservoir reference NOM..... 40

Table 2.4 Summary of DEAE cellulose isolation efficiency for Suwannee River NOM and Nordic Reservoir NOM..... 40

Table 3.1 Dye receptors and water samples in Tygarts Creek and the Cascade Cave system for Tracer Test II..... 62

Table 3.2 Summary of dye traces recovered in the Cascade Cave system at various recharge and flow conditions..... 63

Table 4.1 Geochemical and physicochemical data from all samples. ..... 99

Table 4.2 Inorganic and organic nutrient concentrations in the Cascade Cave system. ..... 101

Table 5.1. Phospholipid fatty acid markers characteristic of certain groups of organisms ..... 142

Table 5.2. PLFA classes in the suspended fraction from Fort Falls (top row) and Lake Room (bottom row). All data in mol %, unless otherwise indicated..... 143

Table 5.3. PLFA classes extracted from the attached fraction at Fort Falls (top row) and Lake Room (bottom row). All data presented in mol %, unless otherwise indicated..... 144

Table 5.4. Summary of specific marker PLFA for groups of organisms and physiological status. ..... 145

**List of Figures**

Figure 1.1. General site location map for the Cascade Cave system study area (approximate catchment outlined in white) in Carter County, KY. Source: Olive Hill, KY. 38º21'07.93", 83º06'41.85". Google Earth. October 8, 2013. ..... 17

Figure 1.2. Stratigraphic section of the Carter Caves State Resort Park vicinity (top). Rose diagram of fracture orientations in the area (bottom). Modified from Engel and Engel (2009). 18

Figure 1.3. Conceptual cross-section profile of the Cascade Cave flow path. ..... 19

Figure 1.4. Simplified topography and hydrology of the Cascade Cave System, Kentucky. The lower section of James Branch sinks at Fort Falls to recharge a subsurface tributary to Tygarts Creek. Box Canyon is the linear feature (outlined in bold) in the center of the map. ..... 20

Figure 2.1 Experimental configuration for loading reference NOM solutions onto DEAE cellulose columns. ..... 41

Figure 3.1 Installation of ISCO automatic recorders and flow probes (top right) at Fort Falls (top) and the Lake Room resurgence. The latter was also programmed to collect water samples. ..... 64

Figure 3.2 Locations of passive dye receptors along Tygarts Creek and the Cascade Cave system. ..... 65

Figure 3.3 Uranine passes over Fort Falls during (above) a high flow tracer test on May 28, 2014, and (below) a low flow tracer test on June 9, 2015. ..... 66

Figure 3.4 Water samples were analyzed for fluorescence in the field using Turner Designs Model 10 filter fluorometers turned to detect red dyes for Rhodamine WT (left) and green dyes for Uranine (right). ..... 67

Figure 3.5 Discharge hydrographs for James Branch at Fort Falls (green) and the Cascade Cave stream in the Lake Room (blue) during Tracer Test I. Precipitation data are daily totals. ..... 68

Figure 3.6 Discharge hydrographs for James Branch at Fort Falls (green) and the Cascade Cave stream in the Lake Room (blue) during Tracer Test III. Precipitation data are daily totals. ..... 69

Figure 3.7. Rhodamine WT is visible in the Lake Room resurgence (May 14, 2014) during Tracer Test I from Box Canyon swallet. ..... 70

Figure 3.8 Dye breakthrough curves for Rhodamine WT recovered in the Lake Room during Tracer Test I. Curve A represents a dye injected at Box Canyon Swallet, and Curve B represents dye injected in Jones Cave. ..... 71

Figure 3.9 Dye breakthrough curve for Uranine recovered in the Lake Room, superimposed on the low flow hydrograph, during Tracer Test III. ..... 72

Figure 3.10 Estimated groundwater flow paths delineated during the dye tracer tests. Triangles are dye injection sites, arrows denote positive dye detection sites, red lines represent positively-recovered Rhodamine WT traces, and the green line represents positively-recovered Uranine traces. ..... 73

Figure 4.1. Photographs of field DOM isolation set-up on the surface at Fort Falls (left), and in Cascade Cave (center), with close-up of filter and stacked tubes (right). ..... 102

Figure 4.2. Time series plots, from top to bottom, of pH (semi-log), dissolved oxygen and specific conductivity (µS $cm^{-1}$) along the Cascade Cave system flow path. Green lines, water at the recharge point Fort Falls; dashed lines, water in Jones Cave; solid lines, water in the Lake Room of Cascade Cave. ..... 103

Figure 4.3. Seasonal relationships between DOC (units mg $^{-1}$) and temperature at the surface recharge point of Fort Falls (FF) (green diamonds) and at the Lake Room (LR) in Cascade Cave (blue triangles). Data from Oct. 2012 – June 2014. ..... 104

Figure 4.4. Seasonal relationships between DOC and DN (units mg $^{-1}$) at the surface recharge point of Fort Falls (FF) (green diamonds) and at the Lake Room (LR) in Cascade Cave (blue triangles) in 2013-2014. ..... 105

Figure 4.5. FTIR spectra of DOM isolates from Fort Falls (green) and Lake Room (blue) in early (left) and late (right) winter, and under high flow conditions (~ 0.006 $m^3$ $s^{-1}$ ..... 106

Figure 4.6. FTIR spectra of DOM isolates from Fort Falls (green) and the Lake Room (blue) in late (left) and early (right) summer to compare low flow conditions (~ 0.0006 $m^3$ $s^{-1}$). ..... 107

Figure 4.7. Comparison of FTIR spectra for DOM isolates from adjacent sinking stream inputs to the Cascade Cave system. Water samples from James Branch at Fort Falls (green) and Echo Canyon Branch (orange) were collected in daylight in June 2014. ..... 108

Figure 4.8. Change in DOM isolate spectra along the flow path from Echo Canyon Branch (orange) through Jones Cave (red) to the resurgence at the Lake Room (blue) in Cascade Cave. Water samples were collected during daylight in June 2014. ..... 109

Figure 4.9. FTIR spectra of September 2013 DOM isolates: Left panel, Fort Falls at night (dashed) vs. day (solid); Right panel, Lake Room at night (dashed) vs. day (solid). ..... 110

Figure 4.10. FTIR spectra of September 2013 DOM isolate from the Lake Room at night, expanded from Fig. 4.0.9 (above). ..... 111

Figure 4.11. Second derivatives of DOM isolate FTIR spectra from James Branch at Fort Falls (green) and the Lake Room in Cascade Cave (blue). ..... 112

Figure 4.12. Functional group ratios for DOM isolates from surface recharge at Fort Falls (green) and the Lake Room (blue) in Cascade Cave for the four sample events. ..... 113

Figure 4.13. Relationship of DOM isolate carboxyl, phenolic, and alkane functional groups at Fort Falls (green) and the Lake Room (blue) in Cascade Cave. The Sept. 2013 DOM isolates are circled in red. ..... 114

Figure 5.1 Structure of the cytoplasmic membrane of a cell. (http://www.biologyjunction.com/cell%20%20notes%20bi.htm) ..... 146

Figure 5.2 Generalized structure of saturated (top) and unsaturated (bottom) fatty acids. ..... 147

Figure 5.3. Separatory funnels (a), rotary evaporation (b), and silicic acid column (c) chromatography steps in the modified Bligh Dyer PLFA extraction process ..... 148

Figure 5.4 Seasonal total microbial biomass in the suspended community (open symbols) as pmol PLFA $mL^{-1}$, and in the attached community (closed symbols) as pmol PLFA $g^{-1}$ for the surface stream at Fort Falls (pink triangles) and the Lake Room (blue circles). ..... 149

Figure 5.5 Concentration of PLFA characteristic of prokaryote (bac-) and eukaryote (euk-) contributions to total biomass in suspended and attached fractions from FF (pink) and LR (blue). ..... 150

Figure 5.6 Comparison of average PLFA class distributions by sample type for each site. ..... 151

Figure 5.7 Comparison of PLFA profiles averaged over all sample events for suspended (A) and attached (B) fractions at Fort Falls, and for suspended (C) and attached (D) fractions at Lake Room. Error bars represent one standard deviation. ..... 152

Figure 5.8 Time series analysis of biomarker PLFA ratios from suspended (open) and attached (solid) fractions at FF (pink) and LR (blue): A. *trans/cis* unsaturated PLFA, B. cyclopropyls/precursor PLFA, C. *iso/anteiso* terminally-branched saturates, D. Actinomycetes/sulfate-reducing bacteria. ..... 153

Figure 5.9 Principle components analysis (PCA) of the complete PLFA data set (42 individual PLFA) for the 12 filter samples (suspended) and 12 sediment samples (attached), using PLFA as species. For clarity, only the PLFA with the longest vector lengths (greatest weighs) are shown. Specific sample events are depicted as open and closed circles related to sample type. ..... 154

Figure 5.10 Principle components analysis (PCA) of the complete PLFA data set (42 individual PLFA) for the 12 filter samples (suspended) and 12 sediment samples (attached), using PLFA as species with 8 environmental variables. ..... 155

# Chapter 1. Dissertation Overview: Organic Matter in Freshwater Systems

## 1.0 Abstract

Organic matter (OM) is the most important pool of reduced carbon in aquatic ecosystems. OM links primary production with microbial decomposition and biogeochemical cycling to sustain higher trophic levels. Ecosystem-level assessments require biomonitoring strategies that incorporate metrics for assessing trends in OM quality and quantity in relation to conventional hydrogeochemical parameters, especially for interconnected surface water – groundwater systems vulnerable to land use and climate change impacts. Development of a unified approach to characterize OM has been hindered by divergent conceptual models across disciplines and by disparate operational definitions of natural OM and a variety of isolation techniques. This research focused on the transport and transformation of dissolved and particulate OM in an oligotrophic karst system in order to: 1) adapt a cost-effective isolation technique for OM in naturally low (oligotrophic) concentrations; 2) evaluate seasonal hydrological dynamics of a cave stream influenced by surface water to assess OM residence times; 3) characterize macromolecular functional group changes in OM quality along the flow path over time; and to 4) examine and correlate the abundance, structure, and physiological status of microbial communities in recharge and discharge with OM quality and stream water geochemistry.

## 1.1 Introduction

Continental aquifers constitute a majority of the world's potable water supplies (Van der Leeden et al., 1990), with the largest reservoir of organic carbon in these freshwater environments being derived from particulate, dissolved, and colloidal OM formed through microbial degradation and transformation processes (Thurman, 1985; Wetzel, 1992). Diverse microbial communities control nutrient cycles, and link the carbon cycle to other biogeochemical cycles (Battin et al., 2008a; Finzi et al., 2011). However, the metabolic activities of distinct

metabolic guilds that mineralize OM in groundwater are poorly understood and difficult to measure (McGuire et al., 2010). Quantification and modelling of OM fluxes are also complicated by myriad environmental and hydrological factors that affect OM composition and bioavailability, including watershed characteristics, land use, and climate (Delpla et al., 2009; Marin-Spiotta et al., 2014; Terajima et al., 2013). Moreover, rates at which groundwater microbiomes shift and adapt to environmental change vary according to regional climatic conditions and the extent of surface water – groundwater interactions (Docherty et al., 2012; Wallenstein et al., 2012).

Consequently, the organic carbon budget and fluxes into and from groundwater are not included in continental-scale global change models used by International Panel on Climate Change (IPCC) to develop predictions and scenarios for the future (Friedlingstein et al., 2006; Zhu et al., 2010). Because conventional physicochemical monitoring parameters are relatively insensitive to changing environmental conditions (Jaffe et al., 2008; Kaur et al., 2005), a framework for monitoring OM transformations across and between ecosystems could improve our knowledge of carbon cycling in groundwater, facilitate long-term water supply planning and aquatic habitat protection, and yield new insight into the mechanics of biogeochemical cycling and pollutant fate and transport between interconnected surface – groundwater systems.

The aim of this dissertation research was to refine and test a set of OM characterization methods for use in linking environmental and microbiological variables to carbon cycle processes in groundwater systems that are influenced by surface water. The specific hypotheses for this research address aspects of microbial (i.e., biotic) and abiotic transformations that alter and degrade terrestrial OM in a karst watershed with surface streams feeding a cave stream:

(1) Predictable changes in OM quality and bioavailability can be traced along a discrete hydrologic flow path where water and OM enter a relatively pristine karst groundwater system at the surface-subsurface interface (i.e., swallets, sinking streams) and flow into and through the subsurface.

(2) OM transformations are identifiable by examining aqueous geochemistry, hydrology, and microbial community characterization.

To test these hypotheses, a multi-level approach was employed to examine intrinsic macromolecular changes occurring during progressive OM decomposition and to characterize the resulting macromolecular composition of OM and the associated nutrient pool.

This investigation exploited the accessibility of a typical cave stream to allow the detailed examination of OM transported from the surface into the subsurface as groundwater recharge. Many caves occupy that portion of the critical zone, at the interface between the terrestrial surface and subsurface, where microbial processing of OM occurs along flow paths from headwater stream recharge to discharge at spring resurgences (e.g., Brooks et al., 1999; Jardine et al., 2006). Karst landscapes harbor some of Earth's most important continental aquifers in carbonate rocks with high dissolutional porosity. Karst comprises 20-25% of the ice-free land surface, and nearly 20% of society worldwide, and 40% of the United States of America (USA) population, depends on fresh water supplied from karst systems (Ford et al., 2007; Loaiciga, 2009). Karst aquifers have profound effects on regional hydrologic budgets, such as in the Appalachian Mountains of USA, for example where approximately 25% of annual precipitation is shunted into the subsurface as groundwater recharge, and maintains up to 90% of riverine base flow during an average year (W. E. Sandford et al., 2012).

### 1.1.1 Conceptual Models for OM Evolution

OM is a complex mixture of heterogeneously distributed compounds sourced from the partial oxidative decomposition of plant and animal material, microbial biomass, and metabolic waste and metal complexation byproducts (Fimmen et al., 2007; Leenheer et al., 2003). Soluble, or dissolved, OM (DOM) is typically measured as dissolved organic carbon (DOC) and commonly occurs in natural freshwaters at concentrations 1-5 mg C $L^{-1}$ (0.08-0.42 mMol $L^{-1}$) (e.g., Egli, 2010; Thurman, 1985). Historical studies of OM typically focused on soil or marine aquatic systems, where degradation rates were recognized as being controlled by the chemical composition of the substrate, microbial community structure, nitrogen availability, and environmental conditions (Tenney et al., 1929). There continues to be uncertainty about the ages and mean residence times of OM in soils and freshwater systems, in part due to the lack of standard OM characterization protocols (Filella, 2014; Minor et al., 2014; Nebbioso et al., 2013), although information is emerging from measurements of the isotopic signatures in OM (Marin-Spiotta et al., 2014).

Three general phases of OM decomposition are identified and assigned to increasingly specialized guilds of microbial decomposers: 1) an early stage, where broad groups of fungi and bacteria rapidly consume labile simple sugars over minutes to hours; 2) mid-stage, in which cellulosic compounds are degraded by specific fungal and bacterial groups over days to months; and 3) a late stage, where specialized enzymes possessed by only a few fungi and bacteria are required to break down recalcitrant lignin compounds over timeframes on the order of years to centuries (Jiao et al., 2010; Kalbitz et al., 2003; Moorhead et al., 2006). Various analyses for lignin-derived phenols, which are abundant structural components of vascular plants, have been employed as biomarkers for terrestrial OM inputs to rivers, lakes, and coastal/estuarine systems (Benner et al., 2001; Bianchi et al., 2011; Schmidt et al., 2009). From the analysis of more than

20,000 DOC measurements from the world's oceans (Hansell et al., 2009), the microbial carbon pump (MCP) is now recognized as playing a significant role in the repetitive processing and transformation of OM in oligotrophic sea waters (Jiao et al., 2010). It follows that, in open continental oligotrophic surface-groundwater systems with continuous or episodic inputs of fresh material, the molecular composition of the overall OM pool would represent multiple stages of degradation, as well, and that there would be an accumulation of recalcitrant OM.

Conventional ideas about the nature of OM in freshwater ecosystems were adapted from the Humic Polymer Model for soil OM (Brady et al., 2008), in which a vast pool of stable, recalcitrant organic matter (dubbed "Old C") was thought to persist in soils for decades to millennia (Kleber et al., 2011; Paul et al., 2001). "Old C" was considered hydrophobic, with a propensity to sorb onto inorganic mineral surfaces in the form of large, polymeric humic macromolecules with unique chemical structures (Jobbagy et al., 2000; Kaplan et al., 2003; Kleber et al., 2011). However, lignin and other structurally complex compounds can also be rapidly turned over, and labile substrates such as sugars can be retained in OM (Amelung et al., 2008). Such findings fuel debate about the applicability of the Humic Polymer Model, as well as the assumption that "Old C" decomposition is kinetically controlled by temperature (Schmidt et al., 2011; Von Lutzow et al., 2009). A new paradigm is emerging that views OM as an ecosystem property, with rates of degradation governed by interactions between reactive mineral surfaces and microbial degraders, as influenced by OM quality and environmental conditions (e.g.,Kaiser et al., 2000; Marin-Spiotta et al., 2014; Phillips et al., 2000).

There have been limited investigations on the nature of OM in karst aquifers (e.g., Baker et al., 1999; Einseidl et al., 2007; Farnleitner et al., 2005; Green et al., 2006). Ecosystem studies of springs, epikarstic drips, and cave streams suggest that DOM comprises the largest component

of total organic carbon (TOC) flux because particulate OM is filtered or settled out (Gibert, 1986; Graening et al., 2003; Simon et al., 2001), and because most caves stream communities are carbon-limited (Simon et al., 2003). The prevailing model of OM dynamics in caves depicts a system dependent upon surficial inputs of photosynthetically-produced material from the surface (Simon et al., 2007), with reductions in aromaticity and molecular weight as recharge moves from soil through the epikarst (Baker et al., 1999; Simon et al., 2010; Van Beynen et al., 2000). OM degradation in oligotrophic systems have been associated with concomitant decreases in DOC concentration and increases in the concentrations of dissolved nitrogenous compounds (Allison et al., 2014; Bronk, 2002; Fontaine et al., 2003; Guenet et al., 2010; Neff et al., 2003; Perdrial et al., 2014; Yamashita et al., 2015)._Such molecular-level alterations to OM have been attributed to both biotic (e.g., respiration) and abiotic (e.g., photochemical degradation) processes.

Spectroscopic characterization of bulk DOM solutions, based on molecular absorbance of UV radiation (Rosario-Ortiz et al., 2007; Traina et al., 1990; Weishaar et al., 2003) and fluorescence properties (Baker et al., 2001; Coble, 1996; McKnight et al., 2001), is a common screening technique for DOM quality. However, macromolecular-level characterization needed to inform microbial OM decomposition models requires that groundwater DOM be isolated and concentrated. Previous spectroscopic measurements of DOM fluorescence properties and composition have indicated microbial uptake and mineralization on decadal scales in “fast-flow” portions of granular, fractured, and karstified continental aquifers (Birdwell et al., 2009, 2010; Einseidl et al., 2007). Seasonal observations of bulk DOM characteristics and microbial diversity in caves, springs, and karst aquifers not only indicate the presence of microbially-transformed DOM in groundwater, but suggest that the dynamics of those transformations are also strongly

influenced by external environmental conditions (Brannen et al., 2009; Brown et al., 2011). Updated perspectives on OM dynamics have stimulated research on DOM transfer and transformation at the land-water interface, where progressive microbial decomposition of organic material in the soil zone produces carbon compounds of varying lability and solubility. OM that is not turned over within hours to days, or sorbed onto mineral surfaces, is inevitably leached to groundwater and streams (McGuire et al., 2010) to form an essential pool of labile dissolved and colloidal nutrients in freshwater ecosystems (Battin et al., 2008a).

### 1.1.2 Outstanding Issues in DOM Characterization

Mounting evidence suggests that DOM is a hydrologic parameter of concern because, depending on DOM quality, DOM can serve as a major nutrient source for groundwater-dependent organisms (e.g., Sinsabaugh et al., 2003; Wetzel, 1992), act as a proton and electron donor/acceptor in pH buffering and biogeochemical reactions (e.g., (Cory et al., 2005; Macalady et al., 2011), and play an integral part in the hydrodynamics of contaminant transport (McCarthy et al., 1993). Research has shown that the surface-reactive organic acids in DOM bind and interact with bio- and geochemical compounds, including polysaccharides and amides (Volk et al., 1997), metals (Mason, 2013), exchangeable ions (Cronan, 2009), and organisms (Steinberg et al., 2009). As such, public drinking water supply sources in the USA are routinely screened for elevated levels of DOM as precursors for trihalomethane formation, which are potentially carcinogenic by-products of chlorine disinfection (Nguyen et al., 2013; Reckhow, 1990). DOM has also been implicated in the behavior of more toxic pollutants such as xenobiotics (Steinberg et al., 2006), and engineered and manufactured nanomaterials released into the environment (Klaine et al., 2008). Moreover, as an important ecosystem property, DOM quality links environmental conditions to the function and structure of biological communities through

biogeochemical cycling, and should be a lynchpin for the development of biomonitoring strategies (Goldscheider et al., 2006; Griebler et al., 2010; Judd et al., 2006; Pronk, Goldscheider, & Zopfi, 2009)

A dynamic mixture of OM is difficult to characterize analytically, especially at groundwater DOC concentrations near instrument detection limits (Hansell et al., 2009). Some have argued that nearly every tool available to analytical chemistry has been applied to the characterization of natural OM, but no standardized or uniformly accepted method for identifying DOM structure exists (McDonald et al., 2004). There is consensus that multiple approaches should be employed in tandem to investigate DOM dynamics, albeit the preferred combinations vary according to discipline (McDonald et al., 2004; Minor et al., 2014; Schmidt et al., 2011). In addition to fluorescence spectroscopy methods, a number of techniques are reported in the literature that have been used to characterize OM, and some are used in tandem, including reverse osmosis (RO) (Sun et al., 1998), ultrafiltration (UF) (Simjouw et al., 2005), solid-phase extraction (SPE) (Aiken et al., 1992; Leenheer, 1981; Peuravuori et al., 2002), and freeze-drying (McDonald et al., 2004) prior to further analysis. Each respective isolation technique introduces recognized biases because physical or chemical separation methods (e.g., RO versus SPE) are selective for certain size fractions or functional groups of macromolecules that may not be directly comparable to fractions produced by other methods (Peuravuori et al., 2002; Peuravuori et al., 2005). Additionally, only samples isolated via the combination of RO, freeze-drying, and non-ionic porous resins (e.g., XAD-4, XAD-8) can be compared to reference standards commercially available from the International Humic Substances Society (IHSS) (Aiken et al., 1992; Croue, 2004; Shuman, 1990). For most groundwater and other oligotrophic

waters, defined as DOC < 5 mg C $L^{-1}$, the release of organic carbon artifacts from non-ionic porous resins limits application of the IHSS method for OM isolation.

Regardless, the isolation, extraction, and concentration of DOM macromolecular functional groups is necessary for analysis by advanced spectroscopic techniques, including Nuclear Magnetic Resonance (NMR), X-ray microscopy, Fourier transform infrared (FTIR), and Fourier transform ion cyclotron resonance mass spectrometry (FT-ICR-MS). Lignin compounds, carboxylic acid groups, amines and amides, carbohydrates, and lipids have been detected from lacustrine and estuarine DOM isolates with NMR and FT-ICR-MS (e.g., Lam et al., 2007; Sleighter et al., 2008). FTIR spectroscopy, a more widely-available and relatively inexpensive technology, has long been used to characterize microbial and terrestrial DOM (Abdulla et al., 2010; Garip et al., 2009; Hay et al., 2007; Leenheer, 2009), often in combination with other methods. Recent advances in nondestructive attenuated total reflectance (ATR)-FTIR produce high resolution spectra for very small aliquots of liquid samples (McDonald et al., 2004).

### 1.1.3 Indicators of Microbial Community Composition and OM Processing

Molecular methods are essential tools in the assessment of microbially metabolized DOM in groundwater and sediments because < 1% of environmental microorganisms have been grown in culture (D. C. White et al., 1998). Phospholipid fatty acids (PLFA), which are important components of cell membrane lipids, can be quantitatively extracted and identified by gas chromatography to provide estimates of viable microbial biomass and community diversity at the phenotypic level (White et al., 1979). PLFA profiles are used to distinguish sources of DOM based on fatty acids unique to plants, algae, and other eukaryotes versus PLFA profiles associated with prokaryotes (Volkman, 2006; D. C. White et al., 1998). Taxonomic details of microbial communities cannot be derived from PLFA profiles, but coexisting microbial

functional groups within communities can be identified, including Gram-positive, Gram-negative, Actinomycetes, sulfate reducers, methanogens, fungi, algae, etc. Their metabolic status and responses to disturbance or stressful environmental conditions can also be evaluated through the use of individual PLFA biomarker ratios (White, 1995).

## 1.2 Overview of Dissertation Research

The aim of the empirical research described herein was to refine and test a set of DOM characterization methods for use in linking environmental and microbiological variables to carbon cycle processes in groundwater systems influenced by surface water. Based on the intrinsic macromolecular changes that occur during progressive OM decomposition, the transformation of terrestrial DOM that recharges groundwater at the surface-subsurface interface should be traceable along a discrete subsurface flow path, and should correspond to predictable changes in DOM quality. The research involved developing a novel method for DOM isolation via weak anion exchange to enable the rapid concentration and preservation of hydrophilic DOM in the field. The hydrogeology and hydrochemistry of a relatively pristine, surface-influenced karst system and its contributing catchment basin, were also characterized over multiple seasons and flow conditions. Samples of surface and groundwater DOM were isolated during the timeframe examined for the hydrogeology and hydrochemistry and analyzed for spectroscopic fingerprints of macromolecular functional groups, as well as by-products of photo-degradation, hydrolysis, decarboxylation, and other biodegradation and nutrient cycle processes. The FTIR spectroscopic procedures employed in this research are advantageous in terms of simple sample preparation and rapid results. Finally, microbial community structures and the metabolic status of attached and planktonic microorganisms in the surface water-groundwater system were profiled over space and time using PLFA analyses, which also provided an estimation of viable microbial

biomass in water and sediments. Information about active microbial communities provided support for the reach-scale to catchment-scale macromolecular characterization of DOM, and helped link environmental conditions to DOM structure and quality along the cave stream flow path (Marin-Spiotta et al., 2014). The results of these multiple lines of evidence revealed that OM in groundwater recharge from a sinking stream, was already partially decomposed by abiotic and biotic processes at the surface, and was swiftly transformed by microbially mediated processes in the aerobic, aphotic subsurface. In this oligotrophic cave environment, the loss of DOC was accompanied by an accumulation of dissolved nitrogenous compounds.

The remainder of Chapter 1 focuses on the geologic and hydrologic description of the study area used for the dissertation research, specifically the Cascade Cave system in Kentucky.

## 1.3 Description of the Study Area

### 1.3.1 James Branch Catchment

The study area encompasses a1000 hectare (10 $km^2$) sub-watershed of Tygarts Creek, a tributary to the Ohio River flowing north of Olive Hill, Kentucky, through Carter Caves State Resort Park (CCSRP) (Figure 1.1). Elevations range from 215 m to 335 m above mean sea level in the catchment where natural sandstone arches, cliffs, and deeply-incised karst valleys, set the topography of the northern Cumberland Plateau apart from the adjacent Bluegrass Region. Annual precipitation averages 1090 mm (356 mm as snow) and the mean annual temperature is 11.7 $^{o}$C (MRCC, 2014). Approximately 60% of the catchment is covered in mixed mesophytic forest, with the dominant land use in light agriculture and low density residential occupation. Soils on the plateau primarily consist of the Latham silt loam (45%) on hillslopes and ridges, and the Shelocta silt loam (18%) in alluvial valleys. The well-drained silt loams grade into silty clays up to ~ 90 cm deep. Sinkholes are floored by the Bledsoe-Caneyville-Rock outcrop soil

association, a rich, organic silt loam under-drained by relatively deep (~165 cm), gravelly, silty clay (NRCS, 2014).

Most of upper James Branch catchment is underlain by the Carter Caves Sandstone (Paragon Formation), a tan, cross-bedded and well-sorted quartz sandstone representing a regional unconformity at the Mississippian – Pennsylvanian boundary, approximately 330 Ma (Engel et al., 2009; NRCS, 2014). The sandstone forms a ~20-m thick caprock over carbonates and shales of the Mississippian Slade Formation (Figure 1.2). The Slade Formation is made up of cherty, arenaceous, and oolitic carbonate units with local thicknesses around 25 m (Engel et al., 2009; Englund, 1976; Ettensohn et al., 1984). The entire section, along with underlying siliciclastic units of the Borden Formation, is roughly equivalent to the Pennington Formation, Bangor Limestone, Hartselle Formation, Monteagle/St. Louis Limestones, and Warsaw Formation of south-central Kentucky and the western Cumberland Plateau of Tennessee (Engel et al., 2009). Structurally, the area is located on the eastern limb of the Waverly Arch, a north-south trending feature associated with late Paleozoic tectonic uplift that produced regional stratigraphic dips of 0.3$^{o}$ to 3$^{o}$ ESE. Orthogonal fracture sets in the Slade Formation (Figure 1.2), oriented NE-SW/NW-SE, in addition to a minor N-S set, exert strong structural control over local stream and cave morphology (Engel et al., 2009).

The main surface tributary in the catchment is James Branch, a spring-fed stream that flows NNW across the caprock for 2 km (at ~ 1.9 % gradient) before plunging over a ledge of the Carter Cave Sandstone at a waterfall known as Fort Falls (referred to throughout the dissertation as FF (Figure 1.3). In low (~ 50 L min$^{-1}$) to moderate (>250 L min$^{-1}$) flow conditions, James Branch completely sinks into a swallet at the base of the waterfall and recharges the cave system in the Slade Formation. At high-flow (>1000 L min$^{-1}$) conditions,

James Branch overflows into a series of swallets in the normally dry channel at the base of Box Canyon, a rectangular, steep-walled collapse feature that formed along 90$^{o}$ joint-sets in the bedrock (Lierman et al., 2011).

Drinking water in the area is supplied from an upstream reservoir on Tygart Creek located near Olive Hill and managed by the Carter County Utility District. Most domestic water wells in the Cascade Cave study area were abandoned in the 1980s when public water lines were extended to the community (Plummer, 2014). Remaining active wells are typically used for watering gardens and livestock. No potentiometric maps have been developed for the area.

### 1.3.2 Cascade Cave System and Previous Research

Box Canyon is a blind valley that contains at least five named caves, all but one within the boundaries of CCSRP. Jones Cave (referred to throughout the dissertation as JC) is uppermost in the projected flow path and privately owned. Sandy Cave, near the center of the system, and Cascade Cave, which occupies the lower reaches of the system, are located within the Cascade Caverns Nature Preserve, which is part of the CCSRP (Figure 1.4).

Based on the morphology of the karst system, including overlying surface terrain, the Cascade Cave system can be described as a classical valley-drain plateau margin cave (Crawford, 1996) and is typical of an epigenic karst system that receives inputs from sinking streams, dendritic conduit development, and spring resurgences at or near base level (Quinlan et al., 1989). At base flow, the gaining cave stream appears to flow along a relatively direct route from FF to a single spring resurgence in Cascade Cave known as the Lake Room (referred to throughout the dissertation as LR). Several other small tributaries are thought to contribute to the system, including Box Canyon swallet (referred to throughout the dissertation as BCS), Echo Canyon Branch (referred to throughout the dissertation as ECB), and at least three unnamed in-

feeders to the cave stream that contribute enough flow to effectively double the volume of discharge at the resurgence.

In a previous study, bulk DOM in the Cascade Cave system was characterized by using fluorescence spectroscopy over several seasons (Brannen-Donnelly et al., 2015). The spectra were analyzed from excitation-emission matrices (EEMs), whereby four distinct peak regions associated with humic substances and natural proteinaceous compounds were identified that corresponded to fluorescence spectra from cave drip waters and karst aquifers (Baker et al., 1999; Birdwell et al., 2010), sediment pore waters (Coble, 1996), and other freshwater environments (e.g., McKnight et al., 1994; McKnight et al., 1997). In these hydrogeologic settings, low intensity DOM fluorescence attributed to fulvic acids is commonly observed in the long UV and blue regions of the electromagnetic spectrum (Brown et al., 2009; Newson et al., 2001). Protein-like fluorophores comprise the most intensely fluorescent components of DOM, with peaks in the UV-visible region, near the lower limits of the instrument scan range.

## 1.4 Dissertation Organization

Chapter 2 describes the systematic validation of OM isolation using diethylaminoethyl (DEAE) cellulose weak anion-exchanger to recover soluble functional groups from IHSS reference aquatic NOM. The purpose of adapting the DEAE method of SPE was to optimally extract and concentrate DOM present at the low DOC concentrations typical of natural groundwater and headwaters streams. Upon elution from the DEAE, carbon recovery efficiencies were evaluated with DOC analyses and UV and infrared (IR) spectroscopy.

Chapter 3 examines the hydrogeology of the Cascade Cave groundwater system, where the DEAE SPE procedure was used to isolate and concentrate DOM in the field (described in

Chapter 4). Tracer testing with fluorescent dyes and continuous flow monitoring delineated stream inputs to the cave, identified overflow routes, and facilitated the estimation of mean water residence times in the system.

Chapter 4 explores the Cascade Cave system hydrochemistry and DOM chemistry by using FTIR spectroscopy from DOM isolates. Temporal and spatial patterns were evaluated according to prevailing hydrologic, geochemical, and climatic conditions.

Chapter 5 analyzes PLFA profiles from colloidal and particulate OM to correlate specific PLFAs with environmental and geochemical variables using principle components analysis. This approach provided a means for comparing the structure and status of surface stream and cave stream microbial communities, and their respective responses to changing DOM quality and environmental variables.

Chapter 6 summarizes the results of this research and discusses its implications. The collective results are framed within current ecological concepts about carbon cycle processes in aquifers, and implications are described that have potential impact on the development of long-term biomonitoring networks for integrated freshwater systems.

## Chapter 1 Appendix

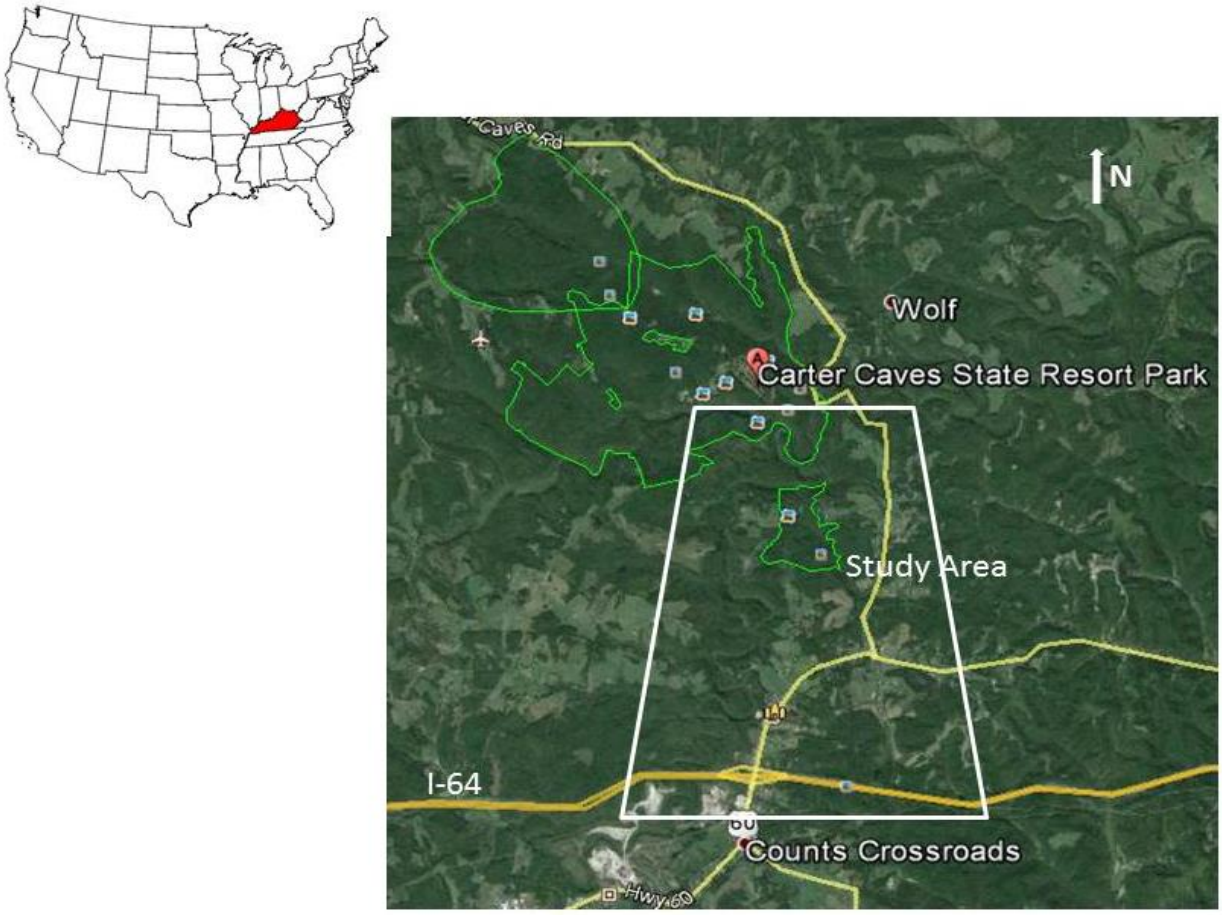


Figure 1.1. General site location map for the Cascade Cave system study area (approximate catchment outlined in white) in Carter County, KY. Source: Olive Hill, KY. 38º21'07.93", 83º06'41.85". Google Earth. October 8, 2013.

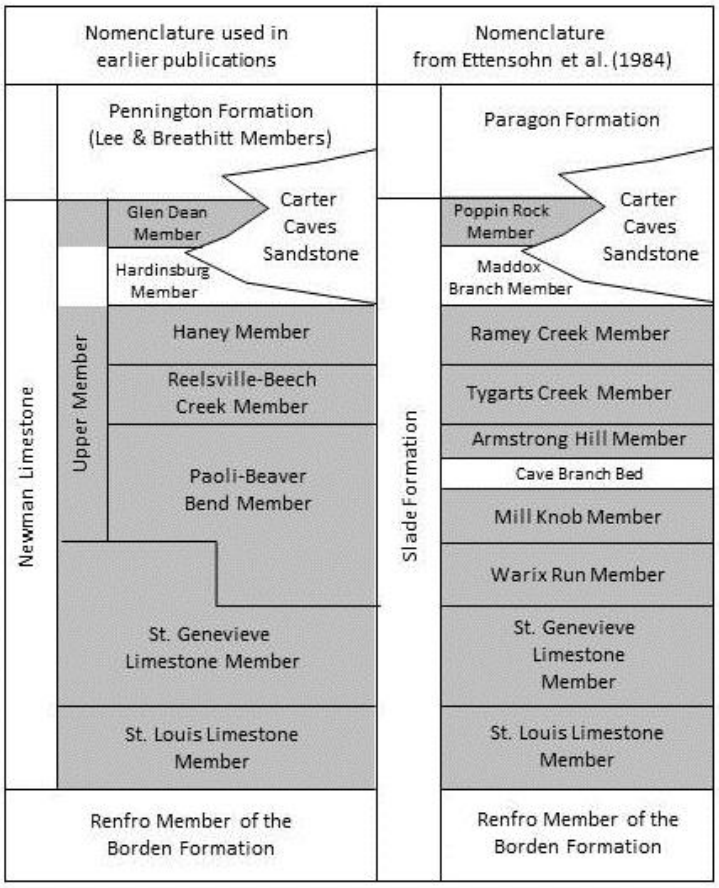


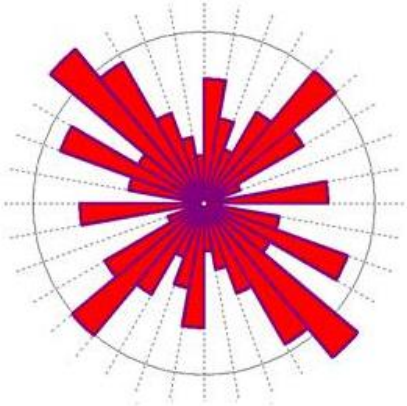

Figure 1.2. Stratigraphic section of the Carter Caves State Resort Park vicinity (top). Rose diagram of fracture orientations in the area (bottom). Modified from Engel and Engel (2009).

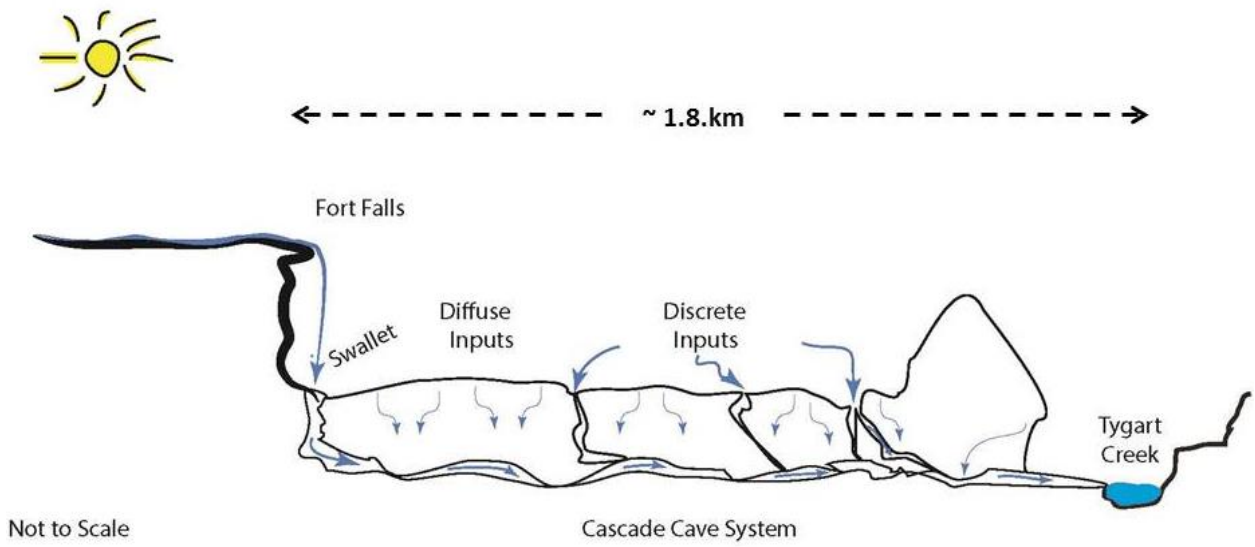


Figure 1.3. Conceptual cross-section profile of the Cascade Cave flow path.

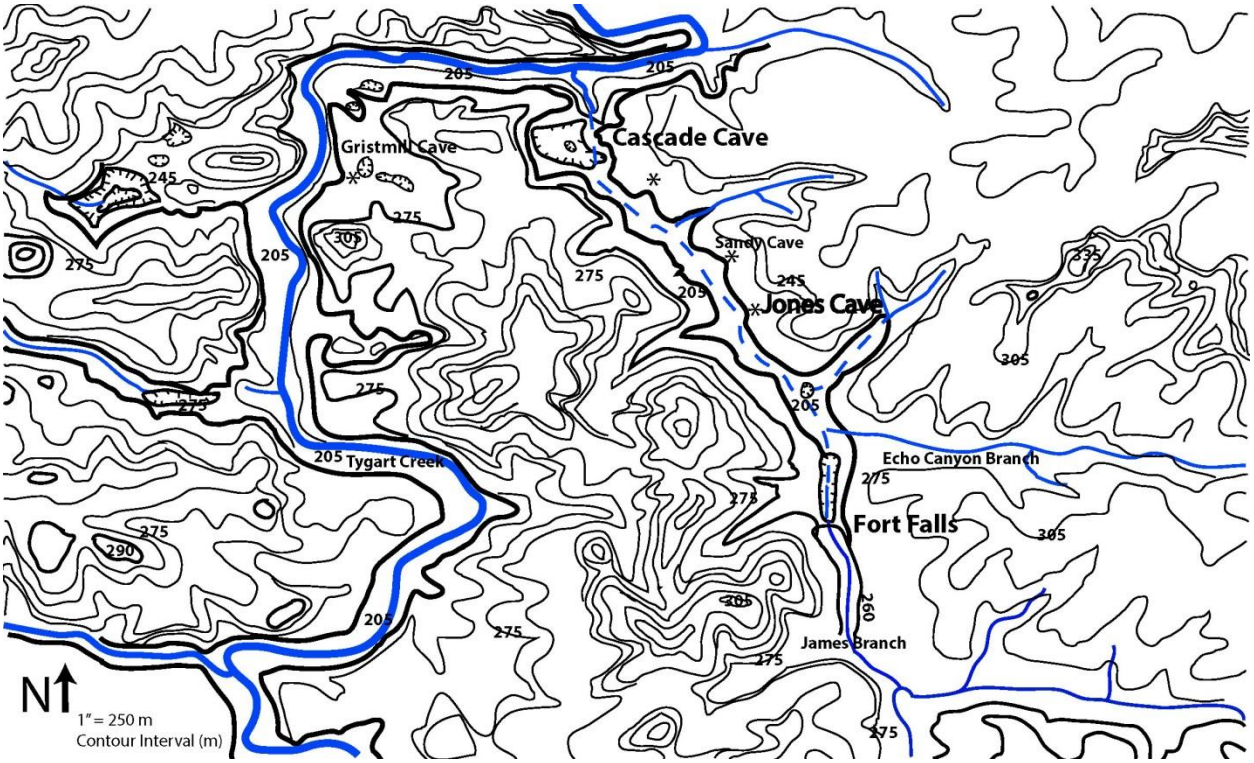


Figure 1.4. Simplified topography and hydrology of the Cascade Cave System, Kentucky. The lower section of James Branch sinks at Fort Falls to recharge a subsurface tributary to Tygarts Creek. Box Canyon is the linear feature (outlined in bold) in the center of the map.

# Chapter 2. An Adaptation of Weak Anion-exchange Chromatography for the Isolation of Natural Organic Matter from Oligotrophic Aquatic Environments

## 2.0 Abstract

The isolation of natural OM fractions from IHSS reference standards was conducted using diethylaminoethyl (DEAE) cellulose weak anion-exchanger to efficiently recover hydrophilic functional groups at the low (< 0.80 mMol $L^{-1}$) organic carbon concentrations typical of natural groundwater and headwaters streams. The aromaticity and organic carbon content of the isolates was estimated using UV absorbance and DOC analyses. Macro-molecular groups in the isolates were characterized via ATR-FTIR and compared with previously-published spectra to discern similarities between the DEAE isolates of the respective OM reference standards, and previously-published acid, base, and neutral fractions isolated with XAD-8 DOC fractionation analysis. Reactive functional groups in the DEAE isolates were identifiable by infrared spectra, and were similar, if not directly comparable, to the fractions isolated with other methods. The DEAE method enables relatively rapid NOM fractionation in the field, requires small volumes (< 5 L) of water, and segregates macromolecules at carbon concentrations well below the limits of other techniques. These attributes warrant the expanded use of DEAE to isolate hydrophilic OM in oligotrophic aquatic systems and can help bridge gaps between laboratory- and field-based investigations.

## 2.1 Introduction

Natural organic matter (OM) is a complex mixture of dissolved, colloidal, and particulate macromolecules composed of the byproducts of microbially-mediated decomposition that is heterogeneously distributed in aquatic ecosystems (Fimmen et al., 2007; Leenheer et al., 2003; Thurman, 1985). Research to characterize OM from different aquatic environments has generated more than 5000 publications in the past three decades (Filella, 2014; Perdue, 2009),

and propelled the scientific community to establish a reference collection of humic substances (MacCarthy, 1976) which is managed and distributed by the IHSS (www.humicsubstances.org). Seven representative natural OM samples have been chemically characterized for use as reference standards and experimental controls, including OM isolated from swamps, soils, peats, an Antarctic lake, and a high-latitude water supply reservoir.

To characterize the nature and type of OM, fractions of humic (i.e., complex mixtures of hydrophobic and hydrophilic organic acids) and nonhumic (i.e., amides, lipids, low-molecular weight acids, polysaccharides) substances must be concentrated, then separated and purified based on physical, including molecular size and weight, and chemical properties (e.g., polarity, hydrophobicity, etc.) (Filella, 2009; Leenheer, 2009; McDonald et al., 2004; Perdue, 2009. For each IHSS reference standard, 120-130 L of source water was filtered (using 0.4-0.45 µm pore size), concentrated by reverse osmosis (RO), or in some cases underwent rotary evaporation and lyophilization, prior to pulverization, homogenization, and storage {Serkiz, 1990 #393; Society, 2016).

OM isolation is effectively done using solid phase extraction (SPE) or column adsorption chromatography because of the ionic and acidic nature of organic matter (Leenheer, 1981; Sirotkina et al., 1974; Sun et al., 1998; Thurman, 1985, although RO is an attractive isolation method because it does not significantly alter the OM during fractionation {Serkiz, 1990 #393). The IHSS adopted a multiple-step procedure in which the pre-filtered OM is acidified then sequentially sorbed to, and desorbed from, nonionic, macroporous acrylic resins (Amberlite® XAD-8 and XAD-4) (Aiken et al., 1992; Leenheer, 1981; Thurman et al., 1981). This method fractionates OM into humic acid (HA) and fulvic acid (FA) fractions that primarily differ in solubility (i.e., HA are insoluble in acidic solutions). The fraction that passes through the resin

generally includes carboxylic groups, carbohydrates, and amino groups, whereas mostly FA and some HA adsorb to the resin (Leenheer, 2009; Perdue, 2009; Peuravuori et al., 2002; Society, 2016, and with average OM recovery (~ 64%) quantifiable as DOC concentration ([DOC]) {Shuman, 1990 #298; Thurman, 1985. For most aquatic OM, the XAD isolation method has been shown to be analytically reproducible, with fast sorption kinetics due to high resin capacity and stability {Town, 1993 #397). OM analysis characterization post-isolation is accomplished by UV absorbance, fluorescence, or vibrational spectroscopy, and/or $^{13}$C-NMR, and gas chromatography-mass spectrometry (GC-MS) (Leenheer, 2009; Stevenson, 1994; Thurman, 1985). Interpretations of the results of these analyses are strongly dependent upon the isolation process and its selectiveness for certain functional groups and/or macromolecules (Peuravuori et al., 2005. As such, NOM operational definitions and classifications are almost exclusively based on separation of hydrophobic or hydrophilic acids, bases, and neutral fractions on XAD resins and in-series cation and anion exchangers {Filella, 2009 #390).

Despite the apparent advantages, the numerous limitations of the XAD method have been documented in the literature. XAD-isolated fractions may not be representative of the original OM because of intrinsic OM hydrophobicity (Perdue, 2009), preferential retention of higher molecular weight and more aromatic fractions (Croue, 2004; Shuman, 1990), 2004), and inefficient adsorption of hydrophilic fractions due to acid-base and desalting manipulations (Croue, 2004; Frimmel, 1998; Janoš, 2003; Pettersson et al., 1994). Large volumes of water (typically 10s to 100s of liters) must be filtered, preserved, and acidified to accumulate sufficient OM for isolation (Aiken et al., 1992), which restricts the types of aquatic samples that can be analyzed using this method. Laborious solvent (i.e., Soxhlet) extraction cleaning steps are necessary to reduce leaching of organic by-products from the resin into the sample isolates

(Company, 2000; Eaton, 2005), although carbon artifacts can still be common (Daignault et al., 1988; Thacker et al., 2005; Town et al., 1993). In addition, and probably most significant among the limitations, Amberlite® XAD-8 resin is no longer produced and the recommended replacement, Superlite ™ DAX-8 (Farnworth, 1995) separates a more specific fraction of aliphatic OM than its predecessor (Peuravuori et al., 2002).

OM isolation by other SPE approaches, such as using the weak anion exchange resin, diethylaminoethyl (DEAE) cellulose [$-OC_2H_4N(C_2H_5)_2$], have also been developed. DEAE consists of a tertiary amine moiety (pKa 10.9) bonded to an inert cellulose backbone that has the potential to retain organic compounds effectively between pH 4 and 8 (Smith et al., 1991). OM containing negatively-charged, high and low molecular weight functional groups rapidly sorb by electrostatic interactions. The sorbent is then eluted by alkaline hydrolysis, which reduces the generation of solvent waste associated with DAX/XAD methods (Miles et al., 1983; Smith et al., 1991). The DEAE isolation method does not segregate identical OM fractions as the DAX/XAD process, but, with comparable DOC recoveries, the DEAE isolation method separates a combination of the non-humic hydrophilic OM that is structurally similar to IHSS fulvic acid fractions (Janoš, 2003; Miles et al., 1983; Peuravuori et al., 1997). Peuravuori et al. (1997) found that DEAE isolated approximately 20% more carboxyl groups than the DAX/XAD procedure, with optimum recovery (80-90%) of organic acids.

DEAE use has received less attention (Ibrahim et al., 2008; Miles et al., 1983; Peuravuori et al., 2005; Peuravuori et al., 1997), and has not been thoroughly evaluated as a fractionation procedure for a range of natural waters or for low carbon-containing natural waters (Boult et al., 2001; Pettersson et al., 1994; Peuravuori et al., 2002). Known disadvantages of a DEAE approach include non-retention of neutral species and irreversible sorption of some inorganic and

humic material (Hejzlar et al., 1994; Miles et al., 1983; Smith et al., 1991). But, known advantages of using DEAE instead of other sorbents include that it eliminates the need for flammable and potentially toxic organic solvents, while still having acceptable recoveries (~75-98%) of OM macromolecules without the need for pH adjustment or excessive pre-cleaning (Hejzlar et al., 1994; Ibrahim et al., 2008; Peuravuori et al., 2005). Additionally, DEAE isolation of OM has been reported as cost-effective and convenient, with the potential for being field portable due to the minimal volumes of water (< 5 L) needed to obtain measureable OM concentrations.

The main goal for any OM isolation, purification, and fractionation method is to gain a better understanding of OM transformation and transport dynamics {Tranvik, 2010 #322}. It has been challenging to characterize OM sources and fractions in oligotrophic groundwater and headwater stream ecosystems because reactive macromolecules occur at concentrations near minimum detection limits (MDL) as [DOC] (Thurman, 1985). Consequently, the objectives of this research were to modify and adapt the DEAE fractionation procedure for use with oligotrophic natural waters ([DOC] <10 mg $L^{-1}$) to (i) recover a high percentage of non-humic OM consistently and without adding carbon during fractionation, (ii) concentrate the dilute OM from conservative volumes (<5 L) of water, and (iii) characterize isolated macromolecular functional groups with spectroscopic analysis to yield comparable information to the published literature. Two well-characterized IHSS reference standards, Suwannee River (SR) natural OM and Nordic Reservoir (NR) natural OM (Clifford et al., 2010; Glover et al., 2005; Hay et al., 2007; Ritchie et al., 2003)(Table 2.1), were selected as the aqueous test media to represent organic matter that originates from very different aquatic environments. Because the goal was to obtain non-humic, hydrophilic fractions, the potential sorption of humic compounds by DEAE

was not critical to the interpretation of the resulting OM fractions. The adaptation and validation of this modified SPE method using DEAE will advance the isolation and concentration of signature OM macromolecules from inside remote cave streams and pools, where water volumes could be potentially limited. Currently, to our knowledge, there are no universally accepted methods to segregate and concentrate OM rapidly in the field based on a method that performs equally well in the laboratory. The method could also be adapted for other types of field research where volumes of water are low, or where field locations make it nearly impossible to transport and deploy the equipment needed (i.e., pumps, columns, tubing) to isolate OM by using the conventional methods based on RO and DAX/XAD.

## 2.2 Methods

### 2.2.1 DEAE Preparation

Empty, fritted (20-µm), 60 mL polytetrafluoroethylene SPE tubes (Supelco Analytical, Sigma-Aldrich Corporation, USA) were conditioned in reagent-grade methanol and air-dried to reduce the potential for phthalate leaching. For each column, 1.2 g pre-swollen microgranular DEAE (Whatman™ DE-53; 2 meq $g^{-1}$ exchange capacity) was placed in a muffled (to 545 $^{o}$C) 30 mL borosilicate glass beaker and suspended in 6 mL 0.1 M NaOH. The slurry was stirred at 350 rpm for 5 min, adjusted to neutral pH during stirring with HCl, and allowed to settle. The supernatant was then decanted and the process repeated to produce a final wet volume of 5 mL of cleaned and pre-conditioned DEAE slurry, at circumneutral pH, prior to transferring into a fritted polyethylene tube with a top frit inserted with a columnar tool. The desired final DEAE bed volume not less than 3 mL because media compaction can occur during column preparation, which can reduce flow rates and increase isolation time.

Prepared columns were capped, labeled, and refrigerated in the dark at 4ºC until use. Prior to column loading, columns were flushed with 15 mL 18 MΩ distilled, deionized (DD) water (average [DOC] was below detect limit). Rubber stoppers fitted with stainless steel, 14 gauge needles were placed on top of muffled borosilicate glass, side-arm flasks to assist with connecting the columns to the flasks during isolation (Figure 2.1). Aliquots of flush water were checked for DOC leaching via absorbance spectroscopy, explained below. During the course of this study, the [DOC] of blank DEAE columns was consistently < 1 mg $L^{-1}$, even for DEAE used that was beyond the manufacturer's recommended expiration date. Only after about two years did we note that excess carbon and amides began to appear in filtrates and blank isolates due to DEAE degradation. All OM isolation results described herein used newly purchased materials.

### 2.2.2 NOM Isolation and Fractionation

Fifteen different experimental solutions of SR or NR natural OM (purchased directly from IHSS) were made in 2 L of 18 MΩ DD water by dissolving the freeze-dried, powdered OM standards in concentration of 2.5, 5.0, 7.5, 10, and 15 mg $L^{-1}$. Each of the experimental solutions was made in triplicate, stirred, and allowed to equilibrate overnight in the dark at room temperature (~21 ºC) prior to use (Alberts et al., 2004; Maurice et al., 2002). Separately, 2 L of the OM solutions (Table 2.2) were loaded directly, without pH adjustment, onto a prepared and pre-wetted (with 18 MΩ DD water) DEAE column by using weighted Tygon® tubing (0.125 cm ID) connected to a muffled glass flask (Figure 2.1). Sample flasks and columns were protected from the light during loading and handling to prevent photo-degradation. Following brief application of a syringe vacuum to the luer tip of the column, a gravity drip flow rate of 10 - 20 mL $min^{-1}$ was initiated (Hejzlar et al., 1994). Tubing blanks and column blanks with no added OM were also run in triplicate. The fluid collected in the flask (the filtrate) was collected and

transferred to muffled 40 ml amber VOA vials (Thermo Scientific) and stored at 4$^{o}$ C in the dark prior to analysis.

For isolate elution, each of the loaded columns were wetted with three bed volumes (9 mL) of 18 MΩ DD water (discarded) and eluted with eight bed volumes (25 mL) of 0.1 M NaOH for cation exchange, as well as for maximum recovery of adsorbed non-humic matter and to prevent hydrolysis of the DEAE cellulose (Miles et al., 1983; Smith et al., 1991; Tuschall et al., 1985). Isolates were immediately acidified to pH 5-6 with HCl and transferred into muffled 40 ml amber VOA vials for storage at 4$^{o}$ C until analysis.

### 2.2.3 Natural OM Characterization

The pH of original OM solutions, flush water, filtrates, and eluted isolates was measured at ambient temperature (20 ± 2$^{o}$C) with a Denver Instrument Ultrabasic pH/mV meter equipped with an ATC electrode that had been calibrated at pH 4.00, 7.00, and 10.00 prior to measurements. OM retention efficiencies and excess DOC contributions were determined by measuring [DOC] and UV absorbance of the original OM solutions, filtrates, DEAE blanks, and tubing blanks, and by analyzing the solution spectra from FTIR spectroscopy. Total carbon (TC) was determined using a Shimadzu TOC-V carbon analyzer, after which acidified samples were sparged to remove inorganic carbon as $CO_2$. The difference between TOC and total inorganic carbon was reported as [DOC]. The instrument was standardized with $C_8H_5KO_4$, and the minimum detection limit (MDL) was 0.1 mg $L^{-1}$. Precision between duplicate injections was reported as 2% of the relative percent difference (RPD) for [DOC] > 4 mg $L^{-1}$, and 5% RPD for [DOC] < 4 mg $L^{-1}$.

Few quantifiable parameters exist for OM, other than [DOC] commonly used to characterize NOM in aquatic environments (Filella, 2009; Wetzel, 1992). Because the organic

carbon component of OM consists of numerous aromatic and conjugated alkene structures containing acidic, basic, and neutral functional groups that absorb light over a range of wavelengths, [DOC] has been correlated with UV absorbance at 254 nm ($UVA_{254}$) and other wavelengths (Eaton, 2005; Korshin et al., 1997; Traina et al., 1990), chemical compositions (Fram et al., 1999; Pettersson et al., 1994; Weishaar et al., 2003), aromaticity (McKnight et al., 2001), and reactivity (Korshin et al., 1997; Reckhow et al., 1990). UV absorbance was measured on an Evolution 200 series scanning spectrophotometer (Thermo Fisher Scientific, Inc., USA) in the wavelength range 240-600 nm using 1 cm quartz cuvettes. Solutions were scanned at room temperature at pH 5-6, and those with $UVA_{254} > 3$ $cm^{-1}$ were diluted by 50% prior to being measured again. $UVA_{254}$ data were compared to distilled water blanks. If the [DOC] is divided from the specific UV absorbance at 254 nm ($SUVA_{254}$), then values could indicate contributions from aromatic OM (Chin et al., 1997; Potter et al., 2005). $SUVA_{254}$ values are reported in L $cm^{-1}$ $mg^{-1}$ (Weishaar et al., 2003). UV absorbance scans at 280 nm ($UVA_{280}$) were also done to determine the molar absorptivity ($\varepsilon_{280}$) for the organic carbon, in mol C $cm^{-1}$ (Lakowicz, 2013).

The infrared (IR) absorbance spectra of original OM, filtrates, and isolates were measured with an Agilent Cary 660 FTIR single-beam spectrometer with a DTGS detector over a spectral range of 4000-600 $cm^{-1}$. Liquid samples (approximately 40 µL) were applied directly onto the Ge crystal mounted in an Attenuated Total Reflectance (ATR) accessory. The background solution for the DEAE filtrates was 18 MΩ DD water, and 0.1 M NaOH (at pH 5.6) was used as the background for the DEAE isolates. Thirty-two scans at a resolution of 4 $cm^{-1}$ were collected for each spectrum, which were baseline-corrected and -smoothed (11-pt). Isolate spectra from OM solutions at concentrations < 10 mg $L^{-1}$ were also ATR-corrected. All spectra were truncated to expand the area of interest in the 1800-1000 $cm^{-1}$ region (Garip et al., 2009;

Hay et al., 2007; Maurice et al., 2002; Schmitt et al., 1995), and spectral ranges were assigned to macromolecular functional groups based on previously published band positions (Table 2.1). Because many OM infrared absorption bands have strong pH dependence, and highly-oxygenated groups (e.g., carboxyls) exhibit wide spectral shifts in response to redox conditions and metal complexation (Hay et al., 2007; Macalady et al., 2011), experimental DEAE isolates were spectroscopically analyzed at pH 5 to pH 6 to bracket the estimated pKa values of many aquatic carboxyl groups (Ritchie et al., 2003). This intensified the infrared (IR) absorptivity of de-protonated carboxyl groups and amides due to increased H-bonding and aggregation (Wershaw, 2004).

### 2.2.4 Calibration and Statistical Analyses

Calibration curves were calculated using solutions of all the concentrations of both SR and NR reference OM. Each OM concentration was determined in triplicate and the relative standard deviations were calculated for the efficiency of OM recovery based on [DOC], $UVA_{254}$, and $\varepsilon_{280}$. Statistical significance between [DOC] for NR and SR solutions and $UVA_{254}$ of respective isolates was determined using a two-tailed Student's t-test (A. M. Ellison et al., 2004). Significance was set at $p < 0.05$.

DEAE cellulose elution efficiency was estimated by comparing the isolate $UVA_{254}$ to the DOC content of the original experimental solution, such as to calculate $SUVA_{254}$ values (Simjouw et al., 2005). The validity of using $UVA_{254}$ as a quantitative surrogate for estimating [DOC] recovery was supported by linear regression analyses (SAS Version 9.4).

## 2.3 Results

### 2.3.1 DEAE Retention and Elution Efficiencies

The two IHSS OM reference standards, SR and NR, were used to evaluate the effectiveness of DEAE to adsorb and fractionate different OM fractions through anion exchange, and by using NaOH eluent across low [DOC] typically encountered in pristine, natural groundwaters and headwater streams, ranging from approximately 0.8 mg $L^{-1}$ to 6.0 mg $L^{-1}$. The physicochemical characteristics of the original reference standards are summarized in (Table 2.2), and the final isolate characteristics are presented in (Table 2.3). Calculated $SUVA_{254}$ of the original OM were comparable to those reported by Amery et al. (2009) using SR and NR OM to test a modified DAX-8 fractionation method for soil OM. Total estimated retention of OM by DEAE was 75% for SR and 70% for NR, based on the difference in [DOC] between the original OM samples and the corresponding DEAE filtrates (

Table 2.4).

Linear regression analyses found no significant difference between the slopes of NR and SR isolates, which supported the use of $UVA_{254}$ as a quantitative surrogate for estimating [DOC] recovery (Figure 2.2). The calculated y-intercepts for each OM isolate indicated that the isolate $UVA_{254}$ value could be correlated with the original OM solution [DOC] below 1.0 mg $L^{-1}$. Linear correlations between [DOC] and $UVA_{254}$ were weakest for higher concentrations of the original OM material used for solutions (15 mg $L^{-1}$); however, there were still good linear correlations for all isolate [DOC] < 6 mg $L^{-1}$. Irreversibly-sorbed materials were visible on both the SR columns (i.e., dark reddish stain) and the NR columns (i.e., dark brown stain) after alkaline elution, as previously reported (e.g., Miles et al., 1983). Irreversible sorption comprised 24% and 14% of the original OM as DOC for SR and NR columns, respectively, and the values were consistent

with previously reported values of 22.6% (Hejzlar et al., 1994) and 15% (Miles et al., 1983) for irreversible adsorption of humic substances (

Table 2.4). This humic material has also been reported to consist of certain phenol functional groups that react and permanently bond with the DEAE (Sirotkina et al., 1974), but could include inorganics contained in the ash component (>40% for NR) of the original OM (Society, 2016).

### 2.3.2 Spectral Comparison of Original OM, Filtrates, and Isolates

Earlier studies found similar carboxylic features in the ATR-FTIR spectra of various IHSS reference OM (Hay et al., 2007; Peuravuori et al., 2005; Ratpukdi et al., 2009); however, the isolate spectra in this study exhibited some differences, which may possibly be related to the original OM solution pH values (Table 2.2). Original SR OM solutions showed a sharp carbonyl ester band at 1743 $cm^{-1}$ (Murdock et al., 2009), compared to a much less intense peak in the original NR OM solutions. NR OM solutions also exhibited a small, carboxylate asymmetric stretching ($\nu_{as}$) band (Abdulla et al., 2010; Hay et al., 2007) at 1590 $cm^{-1}$ (Figure 2.). Weak bands at 1457-1445 $cm^{-1}$ in both reference OM solutions may represent $CH_2$ scissoring within aliphatic compounds, such as alcohols or phenolic functional groups (Abdulla et al., 2010; Simjouw et al., 2005). Small peaks at 1274-1261 $cm^{-1}$ and 1168-1087 $cm^{-1}$ superimposed on a broad band are interpreted as C-O asymmetric stretching of amino-sugars and polysaccharide compounds (Kacurakova et al., 2000; Max et al., 2004).

DEAE filtrates exhibited less intense IR absorbance than the original OM solutions, and SR and NR filtrates shared few spectral bands in common, as would be expected based on their initial chemistries (Figure 2.4). The SR filtrate (15 mg $L^{-1}$ OM) had a small carbonyl ester peak at 1743 $cm^{-1}$, but also sharp peaks at 1706 $cm^{-1}$ and 1538 $cm^{-1}$ that were identified as the C=O

stretching of a carboxylic acid and carboxylate, respectively. There was also the asymmetric deformation of a methyl group at 1465 $cm^{-1}$ (Maurice et al., 2002; Max and Chapados, 2004; Abdulla et al., 2010). The spectral profile for the NR filtrate (15 mg $L^{-1}$ OM) had a shoulder at 1675 $cm^{-1}$, and bands at 1623 $cm^{-1}$ and 1577 $cm^{-1}$ were considered the carboxylate $\nu_{as}$. The 1475 $cm^{-1}$ band was also a methyl group deformation, based on interpretations by Abdulla et al. (2010).

Overall, spectra obtained from low [DOC] solutions were comparable to those produced by Hay and Myneni (2007) for SR OM and NR OM, at solution concentrations of 500 mg $L^{-1}$, and adjusted to pH 5 and pH 6. Our SR and NR OM isolates exhibited nearly identical spectra, with IR absorbance intensities up to an order of magnitude greater than the original OM and filtrates (Figure 2.). Two carboxylate bands dominated the spectral profiles of both isolates: (i) band I occurred at 1581-1635 $cm^{-1}$ in the SR isolate and at 1595-1633 $cm^{-1}$ in the NR isolate, which was representative of the carboxylate $\nu_{as}$, and (ii) band II ranged from 1328-1380 $cm^{-1}$ in the SR isolate and from 1340-1367 $cm^{-1}$ in the NR isolate, which was representative of the symmetric carboxylate stretching frequency ($\nu_s$). Isolates from the 10 mg/L and 15 mg/L OM solutions exhibited $\nu_{as}$ values greater than 1600 $cm^{-1}$, possibly due to stronger interactions between deprotonated carboxyls and positively-charged amides in the more concentrated solutions (Hay and Myneni, 2007; Perdue, 2009). Additionally, band widths (at full width, half-maximum) for $\nu_{as}$ were 129 $cm^{-1}$ for SR and 108 $cm^{-1}$ for NR, which could indicate heterogeneous carboxyl group absorption in the 1600 $cm^{-1}$ region (Hay and Myneni, 2007).

## 2.4 Discussion

Advances in OM research have been jeopardized because of the lack of standardization among SPE methods, heavy reliance upon particular SPE isolation procedures and SPE-specific operational definitions, and unpredictable periods of limited access to commercial (proprietary) adsorbents. Although some researchers argue that there is not one single technique that can separate and isolate OM into different fractions that mimic what is observed in natural systems (Croue, 2004), others claim that even a combination of methods may not efficiently yield quantitative results based on the relative contributions of different OM sources in a system (e.g., Filella, 2009). Moreover, much of the published research on aquatic OM has been conducted in marine systems, where salinity interferes with the sorption of low molecular weight organic acids onto DEAE cellulose, OM fractionation on non-ionic macroporous resins (e.g., DAX/XAD-8, DAX/XAD-4) and RO concentration have been favored (Peuravuori et al., 2005; Peuravuori et al., 1997). The objective of this effort was to modify and adapt DEAE for use with small volumes of low ionic strength, oligotrophic waters ([DOC] <10 mg $L^{-1}$), and the isolates and concentrates overlapped with the "average" fraction of the multiple hydrophobic and hydrophilic fractions produced by the DAX/XAD method (Peuravuori et al., 2005). The procedure developed is relatively rapid (~ 2 hours) and produces non-humic, anionic OM. The DEAE isolation method also minimized contributions of carbon artifacts, and reduced silicate interference with IR absorbance and other downstream analyses that have been recognized limitations of the DAX/XAD method (Maurice et al., 2002; Hay and Myneni, 2007).

From our DEAE isolations, compared to original OM solution concentrations, recoveries [as DOC] were 51-53% relative to the totals, which were reasonable given the average organic carbon content of SR and NR OM (IHSS, 2016). Our OM recoveries relative to [DOC] retained on the DEAE cellulose were 68% and 75% for SR and NR, respectively. Higher OM recoveries from natural

waters isolated by DEAE have been reported (e.g., Pettersson et al., 1994; Peuravuori et al., 1997), perhaps because RO-isolation preferentially produces higher molecular weight OM (Perdue, 2009). More importantly, DEAE effectively concentrated recovered OM as [DOC] by an order of magnitude (

Table 2.4) and by approximately 50-fold compared to what has been done using other methods. From the concentrated macromolecular functional groups, OM characterization by UV-Vis and IR spectroscopy was done, and $SUVA_{254}$ and $\varepsilon_{280}$ values were also comparable to the original OM solutions.

The molecular structure and composition of functional groups, such as organic acids, can provide important information about OM properties (Einseidl et al., 2007; Hessen et al., 2013; McDonald et al., 2004). OM chemical reactivity depends on the concentration and structural environment of oxygenated functional groups, predominantly carboxylic acids, but also carbonyl, alcoholic, and phenolic groups with ester or ether linkages (Thurman, 1985; Hay and Myneni, 2007; Leenheer, 2009). Carboxylic acid groups (e.g., -COOH, $-COO^-$) are anionic in natural waters, and therefore dissociated as aromatic or aliphatic compounds with pKa values that range from < 3.5 – 5.0 derived from direct titrations of IHSS reference and standard OM (Hay et al., 2007; Leenheer et al., 2003; Ritchie et al., 2003). They readily form intermolecular associations with polysaccharide and protein polar groups (Wershaw, 2004) that control the bioavailability of OM-associated nutrients (Cozzolino et al., 2001; Sun et al., 1997). Therefore, being able to isolate and characterize carboxylic acid groups is important to understanding OM hydrodynamics and nutrient cycling. DAX/XAD isolates of OM typically have average pKa values ranging between 3-5 (Shuman, 1990); however, based on linear correlations between $\nu_{as}$ and pKa for various aliphatic monocarboxylates, this DEAE isolation method may have

concentrated carboxyl groups with much lower average pKa values, specifically pKa = 2.03 for NR and pKa = 2.26 for SR (Cabaniss et al., 1995).

Additional research needs to be done to understand the significance of these results for aquatic OM characterization in carbon-poor waters, and specifically for investigations into OM reactivity. In conclusion, this is the first known report of a DEAE cellulose application to isolate and concentrate reactive functional groups from small volumes (< 5 L) under low [DOC] (< 1 mg $L^{-1}$ (<0.08 mMol $L^{-1}$) to 6 mg $L^{-1}$ (0.5 mMol $L^{-1}$)) concentrations. This method also worked reliably with < 2 L water volumes. OM isolation approaches, regardless of the technique, provide insights into the composition and functionality of humic and non-humic substances. Each OM isolation and concentration method has disadvantages, not the least of those being the close relationship between isolation method and the spectroscopic properties of the resulting fraction (Peuravuori et al., 2002). As was the motivation herein, testing modified and alternative isolation techniques on IHSS reference materials for inter-laboratory comparisons and inter-calibration (Amery et al., 2009) are important. But, in oligotrophic aquatic systems, where the differentiation of operationally-defined OM fractions has not traditionally been a research priority, the isolation of macromolecular functional groups on DEAE cellulose does yield concentrated fractions that can be structurally distinguished based on UV and IR spectral properties. The DEAE isolation approach highlighted structural variations between SR and NR that were not apparent in the DAX/XAD isolate FTIR spectra (Hay and Myneni, 2007; Leenheer, 2009). Therefore, the DEAE isolation approach was employed in the field during this research for the characterization of OM in natural, oligotrophic groundwater systems, such as caves, and it is recommended that researchers test this method in other field research and environmental systems.

## Chapter 2 Appendix

Table 2.1 Characteristic FTIR functional group frequencies in NOM isolates.

| Band position & range ($cm^{-1}$) | Bond mode | Functional group assignment |
|---|---|---|
| 1770 (± 10) | C=O stretch | Ester (γ-Lactones) |
| 1740 (± 10) | C=O stretch | Ester (Aliphatic) |
| 1710 (± 15) | C=O stretch | Carboxylic acid (-COOH) |
| ~1650 | C=O | Amide I (CON-) |
| 1600 (± 40) | Asymmetric stretch | Carboxylate ($-COO^-$) |
| ~ 1550 | C=O | Amide II (-CONH-) |
| 1350 (± 50) | O-H in-plane bend | Polysaccharide "a" |
| 1230 (± 30) | C-O asymmetric stretch | Phenol (Ar-OH) |
| 1100 (± 100) | C-O asymmetric stretch | Polysaccharide "b" |

Sources: Stevenson, 1994; Coates, 2000; Simjouw et al., 2005; Leenheer, 2009; Abdulla et al., 2010

Table 2.2 Physicochemical parameters of original reference NOM solutions.

| NOM (mg/L) | pH | DOC[1] (mg/L) | SD[2](RPD) | $UVA_{254}$ (cm) | SUVA (L $cm^{-1}$ $mg^{-1}$) | $UVA_{280}$ (cm) | $\varepsilon_{280}$ (mol $C^{-1}$ $cm^{-1}$) |
|---|---|---|---|---|---|---|---|
| Suwannee River | | | | | | | |
| 2.5 | 5.37 | 1.44 | 0.12 (8%) | 0.05 | 0.03 | 0.04 | 306 |
| 5.0 | 5.19 | 2.42 | 0.23 (9%) | 0.10 | 0.04 | 0.07 | 368 |
| 7.5 | 5.14 | 3.51 | 0.15 (4%) | 0.14 | 0.04 | 0.10 | 334 |
| 10.0 | 5.17 | 4.55 | 0.12 (3%) | 0.18 | 0.04 | 0.13 | 346 |
| 15.0 | 4.57 | 5.91 | 0.56 (9%) | 0.25 | 0.04 | 0.18 | 372 |
| Nordic Reservoir | | | | | | | |
| 2.5 | 6.30 | 0.79 | 0.07 (8%) | 0.04 | 0.05 | 0.03 | 457 |
| 5.0 | 6.24 | 1.67 | 0.17 (10%) | 0.07 | 0.04 | 0.05 | 373 |
| 7.5 | 6.01 | 2.59 | 0.09 (4%) | 0.10 | 0.04 | 0.08 | 353 |
| 10.0 | 6.19 | 3.39 | 0.21 (6%) | 0.15 | 0.04 | 0.12 | 411 |
| 15.0 | 6.23 | 4.30 | 0.16 (4%) | 0.19 | 0.04 | 0.14 | 387 |

1. DOC, dissolved organic carbon (average)
2. SD, Standard Deviation (n = 3)
3. RPD, Relative Percent Difference

Table 2.3 Final physicochemical parameters of DEAE isolates from Suwannee River reference NOM and Nordic Reservoir reference NOM.

| Isolate (mg/L) | pH | SUVA $_{254}$[1] (L cm$^{-1}$ mg$^{-1}$) | $\varepsilon_{280}$ (mol C$^{-1}$ cm$^{-1}$) | Isolate (mg/L) | pH | SUVA $_{254}$[1] (L cm$^{-1}$ mg$^{-1}$) | $\varepsilon_{280}$ (mol C$^{-1}$ cm$^{-1}$) |
|---|---|---|---|---|---|---|---|
| SR2.5 | 5.69 | 0.43 | 3030 | NR2.5 | 5.90 | 0.60 | 3782 |
| SR5.0 | 5.70 | 0.57 | 4343 | NR5.0 | 5.69 | 0.64 | 5418 |
| SR7.5 | 5.73 | 0.65 | 5480 | NR7.5 | 5.81 | 0.73 | 6149 |
| SR10.0 | 5.88 | 0.63 | 5889 | NR10.0 | 5.85 | 0.78 | 7393 |
| SR15.0 | 5.34 | 0.77 | 7816 | NR15.0 | 5.74 | 1.02 | 8811 |

[1] Isolate $UVA_{254}$/[NOM DOC]

Table 2.4 Summary of DEAE cellulose isolation efficiency for Suwannee River NOM and Nordic Reservoir NOM.

| Original NOM Concentration (mg/L) | Loaded DOC[1] (mg/L) | Retained DOC[2] (mg/L) | Isolated DOC[3] (mg/L) | % Recovery[4] | % Concentrated[5] |
|---|---|---|---|---|---|
| SR 2.5 | 2.88 | 2.16 | 1.58 | 55 | 63 |
| SR 5.0 | 4.84 | 3.63 | 2.46 | 51 | 55 |
| SR 7.5 | 7.02 | 5.27 | 3.48 | 50 | 50 |
| SR 10.0 | 9.10 | 6.82 | 4.18 | 46 | 49 |
| SR 15.0 | 11.82 | 8.87 | 6.13 | 52 | 56 |
| NR 2.5 | 1.58 | 1.11 | 1.11 | 70 | 80 |
| NR 5.0 | 3.34 | 2.34 | 1.64 | 49 | 55 |
| NR 7.5 | 5.18 | 3.62 | 2.36 | 46 | 52 |
| NR 10.0 | 6.78 | 4.75 | 3.05 | 45 | 51 |
| NR 15.0 | 8.60 | 6.02 | 4.58 | 53 | 61 |

1. Average in 2 L NOM solution
2. Based on dissolved organic carbon concentration of filtrate
3. Based on $UVA_{254}$
4. (Isolated DOC/Loaded DOC)100

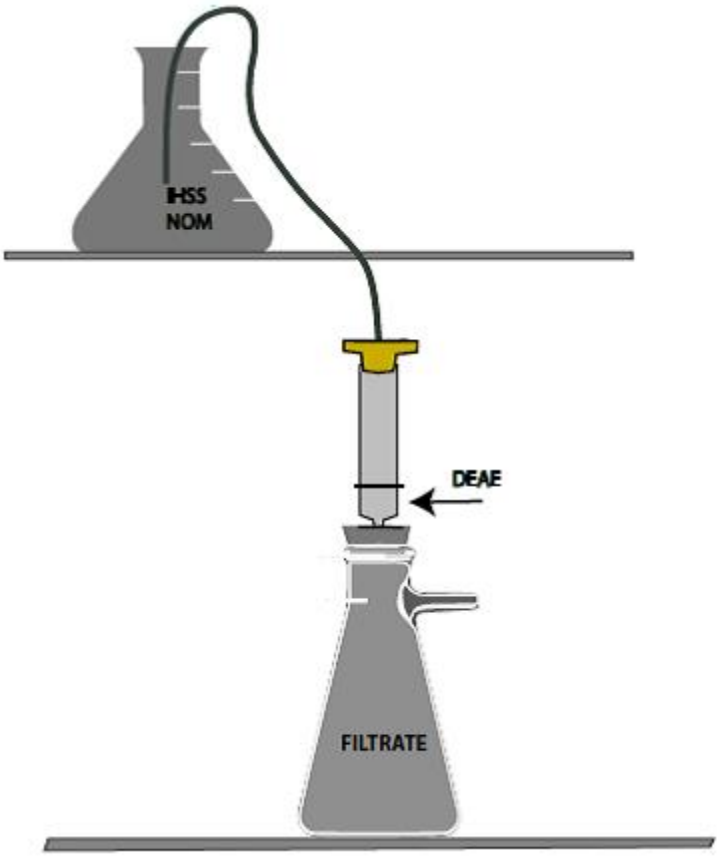


Figure 2.1 Experimental configuration for loading reference NOM solutions onto DEAE cellulose columns.

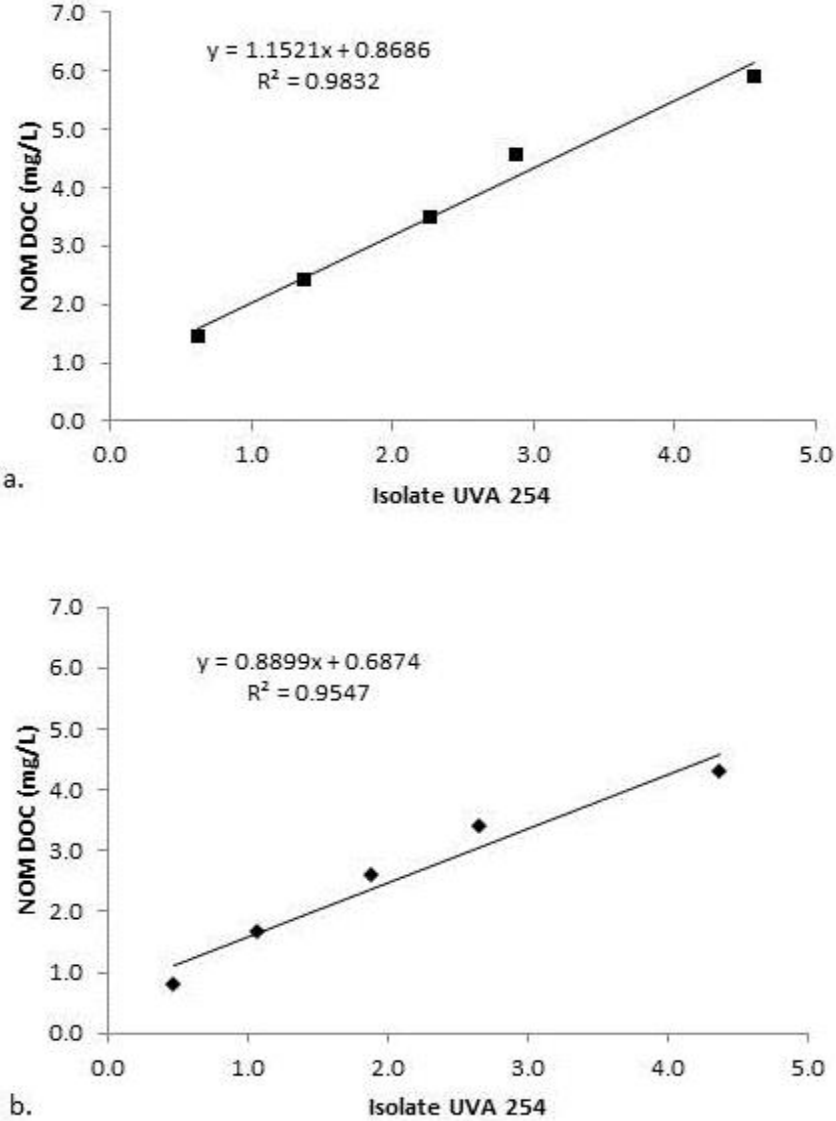


Figure 2.2. Relationship of DEAE isolate absorbance at 254 nm ($UVA_{254}$) to dissolved organic carbon (DOC) concentration in the original NOM. a. Suwannee River NOM; b. Nordic Reservoir NOM.

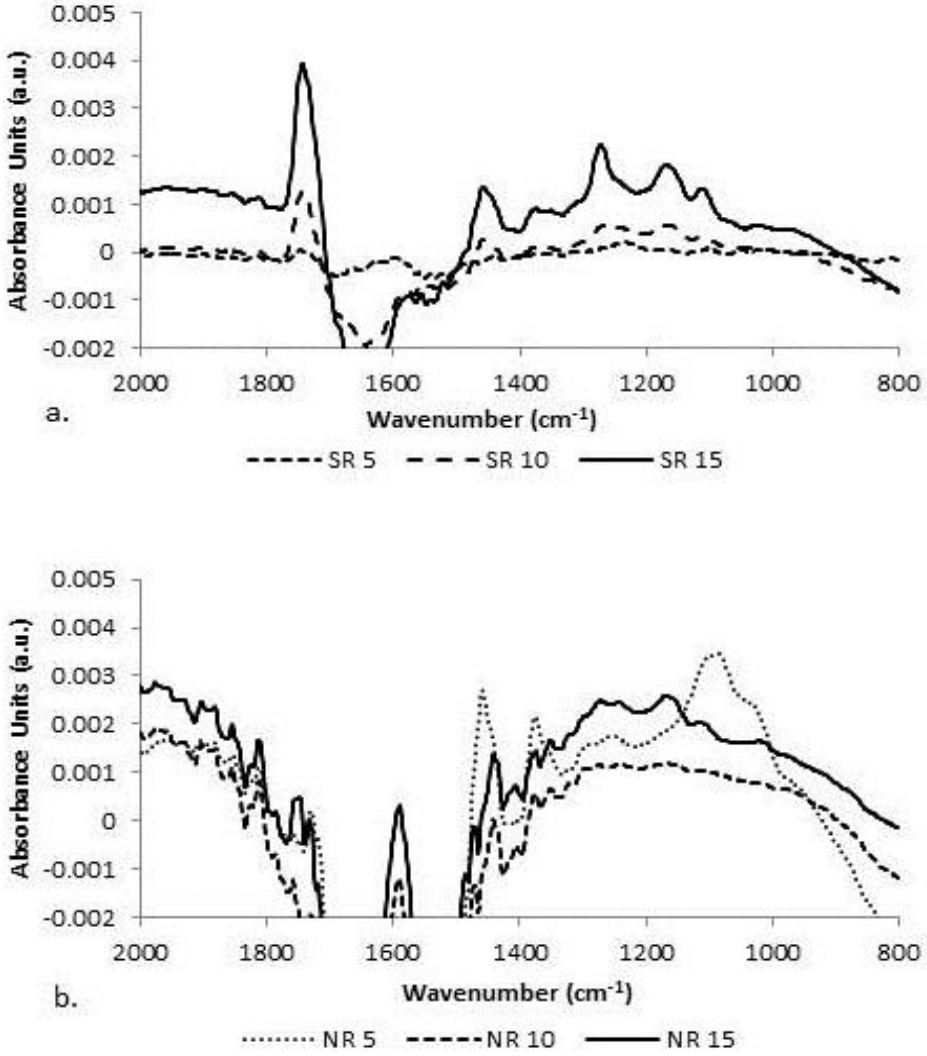


Figure 2.3. Uncorrected ATR-FTIR absorbance spectra of original IHSS NOM solutions. a. Suwannee River NOM, b. Nordic Reservoir NOM.

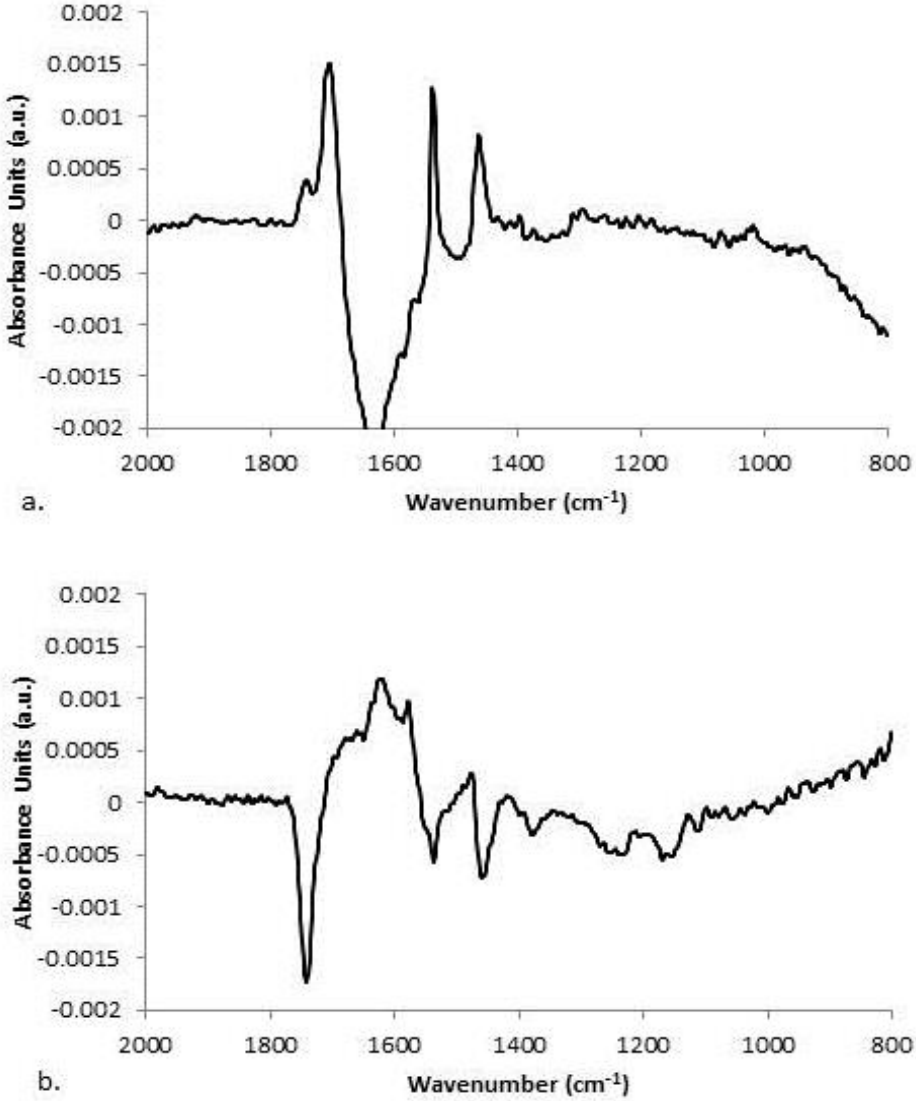


Figure 2.4. Figure Uncorrected ATR-FTIR spectra for NOM DEAE filtrates. a. Suwannee River; b. Nordic Reservoir.

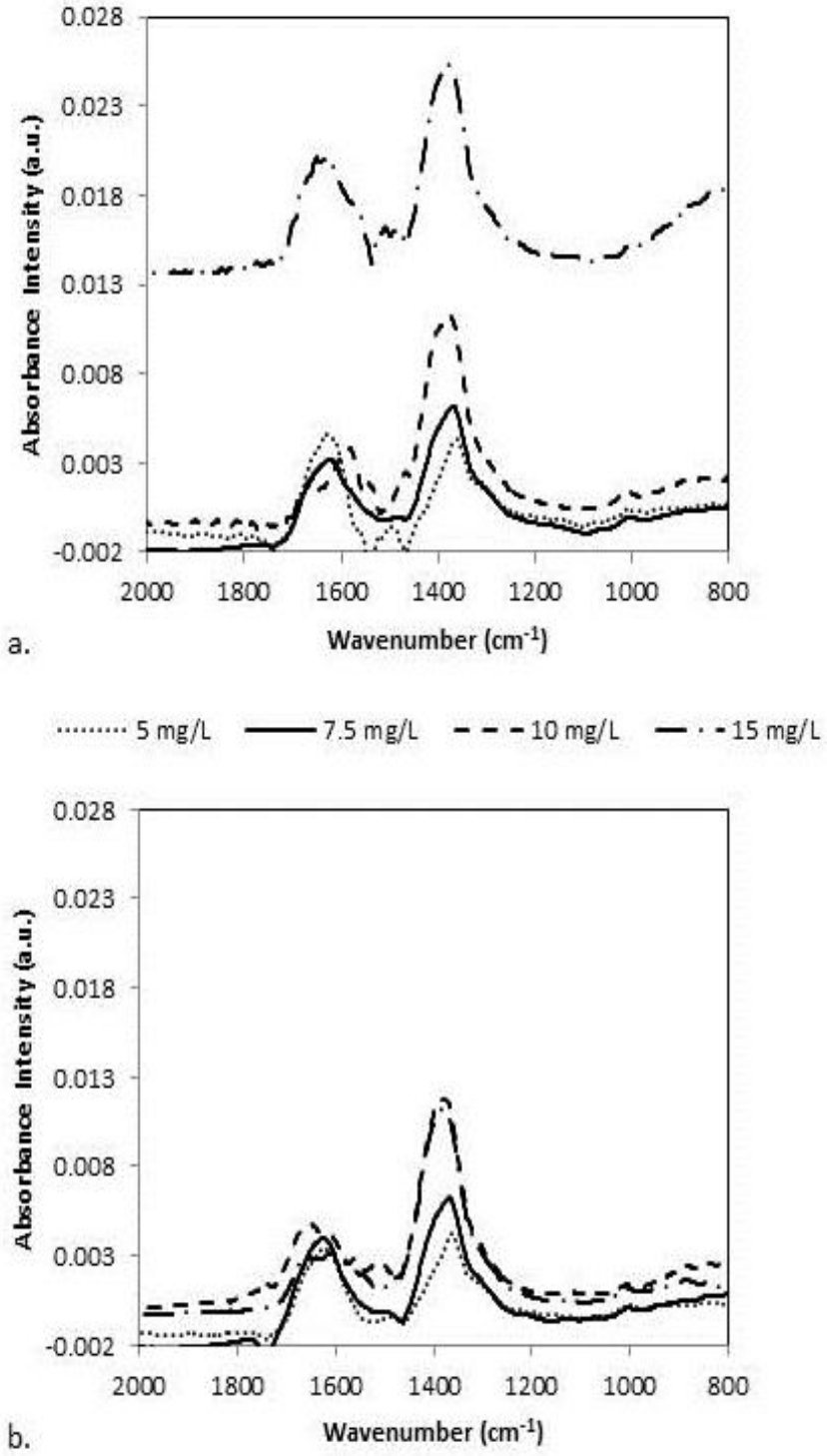


Figure 2.5. ATR-FTIR absorbance spectra for blank-subtracted NOM isolates at pH 5-6. a. Suwannee River NOM, b. Nordic Reservoir NOM.

# Chapter 3. A Hydrologic Analysis of the Cascade Cave Drainage System Under Low- and High-Flow Conditions

## 3.0 Abstract

Subsurface flow paths and velocities for the Cascade Cave system were constrained through continuous flow measurements and dye tracer tests to estimate residence times for dissolved organic matter (DOM) transformation. Flow conditions ranged from a low of 0.0 $m^3 s^{-1}$ (dry channel) to around 1.2 $m^3 s^{-1}$ in James Branch (Fort Falls), and from approximately 0.13 $m^3 s^{-1}$ to 2.7 $m^3 s^{-1}$ in the cave stream (Lake Room) during the tracer test studies. Both sites exhibited strong episodicity to precipitation events, and at least three additional inputs of DOM to the Cascade Cave system were identified that were likely sources of high quality (i.e., less photodegraded) organic matter.

## 3.1 Introduction

An understanding of DOM cycling dynamics in karst requires a systematic evaluation of landscape and hydrologic controls that influence the flux of organic matter and nutrients into cave ecosystems (Berggren et al., 2009; Eimers et al., 2008; Mulholland et al., 1997). Any assessment of organic matter budgets and transformations in a cave system should account for wide variations in recharge and residence time, but this has rarely been done. Consequently, as part of a larger project to understand carbon cycling and transformations in the Cascade Cave system in northeastern Kentucky (Engel et al., 2009), the goals for this study were to generate continuous flow measurements and estimate groundwater travel times from dye tracer tests under various hydrologic conditions, and to identify inputs of fresh DOM along the flowpath.

Like other carbonate-hosted karst systems, such as those occurring along the margins of the Cumberland Plateau, some assumptions already existed about water budget and flux for the Cascade Cave system, a surface-water influenced system that responds rapidly to precipitation

and snowmelt-induced recharge events. Fractures and bedding planes that become dissolutionally-enlarged develop into preferential water flow paths and exhibit strong vadose zone anisotropy at high-flow conditions (Ford et al., 1994). Sinking stream recharge and spring discharge can increase by orders of magnitude during storm events, which results in the introduction and transport of elevated levels of particulate matter and bacteria (Göppert et al., 2008; Pronk, Goldscheider, Zopfi, et al., 2009). Despite their reputation for episodicity, or flashiness, regional carbonate aquifers in the temperate United States of America exist at base flow conditions ~ 90% of the time (Harlow et al., 2005; A. E. Sandford et al., 2012; Worthington, 2009).

Therefore, the main hypothesis was that the major surface tributary in the catchment, James Branch, is the primary source of water flowing into the subsurface karst system, where under base (i.e., low, ~ 50 L $min^{-1}$) to moderate (>250 L $min^{-1}$) flow conditions, surface stream water completely sinks into a swallet and recharges the cave system. At high-flow (> 1000 L $min^{-1}$), James Branch overflows into a series of swallets in the normally dry channel and other temporally-active hydrologic recharge features contribute water and DOM to the cave system.

For a study like this, it is important to have minimal potential for significant background fluorescence caused by anthropogenic activities (e.g., laundry detergents, wastewater from livestock, landfill leachate, wood preservatives, hydraulic fluids, hydrocarbons, and antifreeze (Käss et al., 1998; Thrailkill et al., 1983); (T. Aley, 1999; Baker et al., 2004). Fluorescence spectroscopy is a popular research tool for labeling cells and other biological material, and for rapidly distinguishing components of a mixture based on the photoreactive properties of aromatic organic molecules. When bombarded with high-energy electromagnetic radiation, fluorescent molecules absorb energy and transition to a higher electronic state. Photons are released at

specific excitation wavelengths (λEx), and again, as the molecule returns to ground state (emission wavelength; λEm). Characteristic fluorescence spectra and their intensities can be detected with high sensitivity, and spectral changes over time can signal compositional variations (Lakowicz, 2013). Aromatic natural fluorophores are ubiquitous in aquatic DOM and can cause analytical interference with low concentrations of tracer dyes (e.g., Alexander, 2005). Artificial fluorophores are also common in surface water-influenced groundwater systems impacted by nonpoint sources of pollution (T. Aley, 1999; Käss et al., 1998; Smart et al., 2002).

The Cascade Cave system is protected as part of the Kentucky State Park system and is located in a rural region with low-density households, agriculture, or livestock production. These conditions make the Cascade Cave system an ideal study area to understand natural DOM cycling with the addition of hydrological properties. This chapter describes the thorough evaluation of background fluorescence from natural and anthropogenic sources that was conducted prior to the selection and injection of fluorescent tracer dyes that could be detected at very low concentrations for the hydrological characterization of the Cascade Cave catchment.

## 3.2 Materials and Methods

### 3.2.1 Flow Measurements

Continuous flow measurements at FF and LR were collected at 30-minute intervals over several rainy days in May 2014 using ISCO model 6712 automatic samplers equipped with Module 720 submerged flow probes. The same equipment was employed for two weeks in June 2015 to document low flow conditions, lag times, and recession profiles. James Branch discharge was monitored approximately 35 m upstream from FF, at a section where the channel measured 1.2 m in width. Downstream flow was monitored at the resurgence from the LR where

channel width measured 4.45 m (Figure 3.1). Daily and monthly precipitation data were obtained from an onsite National Oceanic and Atmospheric Administration (NOAA) weather station, USC00156012 (NOAA, 2015), operated by an employee of Carter Cave State Resort Park.

The ISCOs were programmed to compute discharge using Manning's Equation (Hornberger et al., 1998), based on uniform flow in a trapezoidal open channel, in which the channel bottom slope, energy grade line, and water surface slope were similar: $V = [k (R^{2/3}S^{1/2})]/n$, where $V$ = velocity (m $s^{-1}$), k = 1.46 (U.S.C.S) or 1.0 (S.I.), R = hydraulic radius (m), S = channel slope (m/m), n = Manning's Roughness Coefficient. The n-value of 0.025 represented the estimated friction contributed by channel roughness and sinuosity in a natural stream with little vegetation (Hornberger et al., 1998). Discharge (Q in $m^3 s^{-1}$) was computed as $Q = VA$, where A = cross-sectional area of channel ($m^2$).

### 3.2.2 Analysis of Background Fluorescence

Passive dye receptors were constructed of 4.25 g pre-rinsed, laboratory-grade activated charcoal (6 to 12 mesh) in packets of nylon screening material (T. J. Aley, 1999), and were anchored in multiple locations (e.g., springs, pools, and streams) in the watershed (Figure 3.2; Table 3.1). Receptors remained in place for up to three weeks before being collected, after which they were rinsed in-situ to remove excess sediment, placed in Whirlpak bags, labeled, and stored on ice during transport to the laboratory. Prior to elution, the charcoal receptors were rinsed in distilled water to remove sediment, and emptied into 250 mL beakers. Dye receptors were eluted overnight in 20 mL aliquots of 5% aqua ammonia (29% $NH_3$) and 95% isopropyl alcohol solution (70% alcohol, 30% MΩ distilled and deionized water), and then adjusted to >

pH 10 with KOH flakes, following previously described methods (e.g., T. Aley, 1999; Kass, 1998). Eluent was decanted off the supersaturated layer and charcoal prior to analysis.

Charcoal receptors provide a cumulative indication of background fluorescence, so unfiltered water (i.e., grab) samples were also collected in muffled (to 545 $^{o}$C), 40-mL amber glass vials to test for the immediate presence of fluorescent compounds. Water samples were labeled, wrapped in foil, and stored on ice during transport to the laboratory, where they were temporarily refrigerated at 4$^{o}$C. Charcoal eluent and water samples were allowed to reach room temperature (approximately 25$^{o}$C) prior to fluorescence analysis, which was conducted within 72 hours of sample collection.

Fluorescence intensity (FI), in relative units (r.u.), was measured on a Perkin Elmer LS55 luminescence spectrophotometer equipped with a 20-watt Xenon lamp, using rectangular 3.0 mL quartz cuvettes (1 cm path length). The spectrophotometer was calibrated with MΩ distilled deionized water to attain a stable Raman signal-to-noise ratio below 500:1. The instrument setting was a synchronous scan method (220 to 650 nm) with 20-nm offset ($\Delta\lambda$) between $\lambda_{Ex}$ and $\lambda_{Em}$. This method allowed the simultaneous differentiation of natural background fluorescence and multiple artificial background or tracer dye fluorescence (Brown et al., 2009; Käss et al., 1998). Instrumental precision, based on the repetitive measure of signal height, was < 1% relative percent difference (RPD). To test for potential contamination of the charcoal, one MΩ distilled deionized water blank and eluent from one blank dye receptor were analyzed between every three receptors collected from the field.

### 3.2.3 Dye Selection and Dosage

Dyes selected for the tracer tests were composed of low-toxicity, relatively conservative solutes with distinct fluorescent properties that enabled the detection of multiple dyes at very low

(i.e., non-visible) concentrations and that would not overlap with fluorescence from anthropogenic sources (Field et al., 1995; Goldscheider et al., 2008). Uranine/sodium fluorescein (CAS RN 518-47-8)($C_{20}H_{10}Na_2O_5$), and Rhodamine WT (CAS RN 37299-86-8)($C_{29}H_{29}N_2NaO_5$) are the most widely used tracer dyes in the United States, with proven performances in terms of high solubility and chemical stability in typical karst systems (T. Aley, 1999; Goldscheider et al., 2008; Käss et al., 1998). These dyes have been approved for use in public drinking water supply source delineation in several countries (Wolkersdorfer et al., 2012), and are listed in the American National Standards Institute (ANSI)/National Sanitation Foundation (NSF) Standard 60 Drinking Water Treatment Chemicals (www.ansi.org).

Rhodamine WT was used in liquid form, as a 20% solution, and Uranine was used in both powdered form, and in liquid form (50% solution). Minimum estimated dye dosages were calculated using a formula (Worthington et al., 2003) developed for tracing in karst systems based on discharge and flowpath distance: $M = 1.9 \times 10^{-5} (LQC)^{0.95}$, where M = tracer mass [kg], L = flowpath length [km], Q = discharge [L $s^{-1}$], and C = target peak concentration [µg $L^{-1}$]. The formula assumes that dye densities are near that of water. No previous dye trace data were available from the Cascade Cave system, such as through Kentucky's Division of Water, when the initial traces were being planned. Therefore, empirical information about the behavior of dyes was lacking. Minimum target concentrations were established several orders of magnitude higher [500 µg $L^{-1}$] than reported dye detection limits [0.05-0.005 µg $L^{-1}$] to account for tortuosity, turbidity, dead zones, dye loss due to sorption/desorption, and instrument variability (Goldscheider et al., 2008).

Calculated dye dosages were used only as minimum guidelines for planning the qualitative tracer tests, and were adjusted in the field according to site-specific conditions, as

discussed below. Carter Cave State Resort Park officials were consulted prior to each dye trace, and voluntary dye trace notifications were filed with the Kentucky Division of Water through their website, http://water.ky.gov/groundwater/Pages/DyeTraceNotification.aspx.

### 3.2.4 Dye Injections

Three rounds of tracer tests were conducted under various ambient moisture and flow conditions. For all three tracer tests, dyes were directly recovered in the field from both 50 mL grab samples (including from filtered water if the sample was turbid) and 300 mL water samples collected by the ISCO automatic sampler. Grab samples were collected twice daily and the automated samplers were programmed to collect water at 1- and 2-hour intervals during the high and moderate flow events, and at 8-hour intervals during the low flow events.

Tracer test I comprised two dye injections at different locations conducted under low (~56 L $min^{-1}$) and high (~380 L $min^{-1}$) flow conditions on May 13 and 15, 2014, respectively. The first trace involved the injection of 200 mL of liquid Rhodamine WT into a small spring-fed stream flowing into the Box Canyon swallet (BCS). The second trace was an injection of 600 mL of Rhodamine WT into Jones Cave (JC), approximately 75 hours after the injection at BCS and following a 6.4 mm precipitation event. Dyes were recovered through the use of grab samples, passive receptors, and a ISCO sampler in the Lake Room (LR) of Cascade Cave (which is the farthest the water travels in the cave before resurging and flowing into a surface stream before reaching Tygarts Creek).

Tracer test II also consisted of two dye injections at different locations under relatively high flow conditions (~1040 L $min^{-1}$). Powdered Uranine (0.23 kg) was injected at Fort Falls (FF) (Figure 3.3), and 300 mL of Rhodamine WT was injected into Echo Canyon Branch (ECB) on May 28, 2014. Tornado and flood hazard warnings were forecast, so ISCOs were not

deployed and passive receptors and grab samples were used to recover dye in LR and at potential overflow resurgences along Tygart Creek.

Tracer test III involved the injection of 900 mL of liquid Uranine at FF during low flow conditions (~38 L $min^{-1}$) on June 9, 2015 (Figure 3.3). Discharge at FF and LR was monitored throughout test III with a pair of ISCO automatic samplers, as described above. Dye was recovered from grab samples, passive receptors, and ISCO water samplers located in Jones Cave, LR, and Tygarts Creek.

### 3.2.5 Dye Analyses

In all but the last few days of tracer test III, water sample fluorescence was measured in the field within 10 hours of collection using two Turner Designs Model 10 filter fluorometers equipped with far-UV mercury vapor lamps (Figure 3.4). Measurements from the passive dye receptors collected at the end of each tracer test were within 72 hours of being eluted, as described above. Each fluorometer was dedicated to the detection of a specific dye through the use of color filter sets to exclude extraneous light, and pass narrowly targeted bands of light that bracket the excitation and emission maxima for Rhodamine WT ($\lambda_{Ex}$ 560 – $\lambda_{Em}$ 580 nm, red) and Uranine ($\lambda_{Ex}$ 495 – $\lambda_{Em}$ 515 nm, green), respectively (Käss et al., 1998; Wilson et al., 1986). Turner Model 10 fluorometers utilize cylindrical 10 mL glass cuvettes inserted into a temperature-controlled sample holder to minimize the influence of heat from the lamp. Fluorometer sensitivity could controlled manually or selected automatically at scales of x100, x30, x10, x3, x1, x0.3, x0.1. Samples with visible color were diluted by 50% prior to analysis. The fluorometers were blanked with MΩ distilled deionized water between each sample, and instrument drift was recorded as < 1% RPD for the red fluorometer and < 4% for the green fluorometer. Minimum detection limits for these particular field fluorometers were previously

confirmed in the 0.01 µg $L^{-1}$ range through the preparation of standard calibration curves for each dye used in the tracer study.

## 3.3 Results and Discussion

### 3.3.1 Discharge

Discharge in James Branch at FF ranged from 0 $m^3$ $s^{-1}$ because of a completely dry channel to nearly 1.2 $m^3$ $s^{-1}$ (considered to be high flow) during tracer tests I and III, respectively. The highest storm flows that occurred during the tracer test II were not measured. Stream flows in both James Branch (at FF) and ECB were observed to go dry during extended periods of time between precipitation events. Discharge from the Cascade Cave system at LR ranged from 0.13 $m^3$ $s^{-1}$ (low flow) to nearly 2.7 $m^3$ $s^{-1}$ (high flow) during tracer tests I and III.

Both FF and LR exhibited flashy behavior and responded rapidly to rain events, but the intensity of episodicity varied with antecedent moisture conditions. Figure 3.5 and Figure 3.6 present the discharge hydrographs for FF and LR, respectively, during tracer tests I and III, when discharge was measured at 30-minute intervals, but precipitation data are only daily totals. During tracer test I, rain storms continued through the test period. During tracer test III, no rain occurred for the first 7 days after dye injection.

### 3.3.2 Background Fluorescence

Background samples (e.g., grab and passive receptors) collected two weeks prior to a tracer test, and within 24 hours prior to the individual tests, showed no evidence of abnormal fluorescence. Data from the seasonal monitoring effort also showed no indications of artificial or introduced fluorescent compounds that could have interfered with the detection of the selected

tracer dyes. Likewise, dye receptors placed upstream from dye injection points, and dye recovery sites on Tygarts Creek were negative for fluorescent interference during the tracer tests. Natural DOM fluorescence associated with humic substances ($\lambda_{Em}$ 400-480 nm) exhibited broad low-intensity peaks during winter and early spring, and generally increased during storm events. The most intense natural fluorescence was associated with protein-like compounds ($\lambda_{Em}$ 300-350 nm) that increased in late summer and early fall. These findings were consistent with previously published data on natural fluorophores in surface-water influenced karst groundwater systems (e.g., Baker et al., 2001; Brannen et al., 2009; Brown et al., 2009; Mostofa et al., 2007), including the Cascade Cave system (Brannen-Donnelly and Engel, 2015).

The narrow filter band range on the Turner Model 10 fluorometers not only eliminated secondary Rayleigh, Raman, and Tyndall scatter peaks caused by colloidal matter in the water, but also removed all but the tails of natural background fluorescence spectra. During the 2014 traces, average background fluorescence measured on the red fluorometer was 0.2 r.u., ~0.02% of the instrument range, and 0.4 r.u. on the green fluorometer, ~0.04% of the instrument range. During the 2015 trace, average background fluorescence measured on the green fluorometer was 0.02 r.u., ~ 0.002% of the instrument range. The order of magnitude difference in background fluorescence during the low flow tracer test was likely due to a lack of precipitation-driven recharge to flush humic substances into the system. Some quenching of dye fluorescence by humic substances may have occurred during the high flow tracer test; however, this was circumvented through an increase in the minimum calculated dye dosage.

### 3.3.3 Dye Detection and Recovery

Dye injection locations, hydrologic conditions, and estimated travel times of each trace are summarized in Table 3.1 and Table 3.2. Details for individual dye recoveries are described below.

#### 3.3.3.1 Tracer Test I

Recharge contribution from BCS was confirmed at the LR ISCO approximately 18 hours after dye injection, which was a flowpath length of 440 m. Rhodamine WT dye was visually confirmed in LR at 10:30 a.m. on May 14, 2014 (Figure 3.7), and was tracked back to an in-feeder (Station B-1) in Cascade Cave approximately 20 m upstream from LR. Sample station B1 was found to be geochemically distinct from the cave stream during previous research (A.S. Engel, personal communication), and was thought to be the same insurgence traced from Waterfall Cave, located 100 m NW of Cascade Cave in 2008 (O'Dell, 2015). As illustrated by the sharp peak and classic shape of the breakthrough curve (Figure 3.8A), dye concentrations peaked in 22 hours and decreased to background levels within 55 hours post-injection. The average time of travel (to peak dye concentration) was calculated at ~20 m $hr^{-1}$. The dye breakthrough curve suggests a direct route between the injection and recovery sites, with little dispersion at low flow conditions (Goldscheider et al., 2008).

The first trace from JC was initially detected in the LR ISCO samples about 7 hours after injection, with peak dye concentration measured 11 hours after injection (Figure 3.8B). At least four shoulders on the rising and falling limbs can be discerned on the broad shape of the breakthrough curve. Rainfall throughout the whole tracer test contributed ~16 mm of precipitation to the system. Estimated transit times along the 956 m flowpath ranged from a minimum of ~137 m $hr^{-1}$ at the leading edge of the plume to ~87 m $hr^{-1}$ at the peak dye

concentration. Fluorescence dropped to background levels within 14 hours. These results indicate considerable dispersion occurred along the flowpath at high flow. The broadened curve could be attributed to the presence of bifurcations and overflow routes that bypassed a large pool at the upstream end of Cascade Cave (determined from dye receptors). Shoulders may reflect storm pulses from lateral in-feeder streams along the flowpath that retarded the arrival times of the tracer dye (Ford et al., 1994).

#### 3.3.3.2 Tracer Test II

Contribution to recharge from FF was detected as Uranine on dye receptors and in grab samples at JC and LR. The high flow velocity from FF to LR was estimated at < 17 hours. Travel times could not be determined more precisely due to the wide spacing of water samples collected during the storms. Contribution to recharge from ECB was confirmed by positive Rhodamine WT dye recovery from receptors and grab samples in JC, LR, the Gristmill Cave resurgence, and Tygarts Creek at Dr. Lewis bridge (travel time < 13 hours). However, a hydraulic connection between FF, Gristmill Cave, and Tygarts Creek at Dr. Lewis bridge was not confirmed. Nevertheless, under these flow conditions, JC functioned as a distributary overflow route to Gristmill Cave and Tygarts Creek. The flowpath and travel time results mean that DOM contributions from ECB would be fresher than DOM sourced from FF, as well as end up in the cave stream much faster than from FF.

#### 3.3.3.3 Tracer Test III

Discharge in James Branch had dwindled by the time of dye injection at FF, and completely ceased to flow at the ISCO probe the following day. Water continued to trickle over Fort Falls, fed by underflow from the sandstone caprock. Five days (115 hours) after dye

injection, the leading edge of the Uranine plume was detected in a grab sample from JC, approximately 812 m downstream from the injection site (a minimum transit time of 7.1 m $hr^{-1}$).

Subsequent grab samples indicated that the peak of the plume passed through JC on day 6 (144 hr), an average estimated low flow velocity of ~ 5.6 m $hr^{-1}$. Eight days (185 hr) after injection, dye was detected in ISCO samples collected at LR (velocity ~9.6 m $hr^{-1}$) after a 38.6 mm rain event. Dye concentrations were diluted relative to the fluorescence measured at JC, and continued to decrease to background levels after three more days (Figure 3.9), with a shoulder appearing on the recession limb of the dye breakthrough curve by day nine. The dye breakthrough curve had similar features to those from tracer test I between JC and LR at high flow conditions. The response could be associated with stormwater pulses that temporarily delayed dye movement through some part of the system. Storm pulses also exacerbate anisotropy when rapidly recharged surface waters exceed the carrying capacity of trunk conduits (Worthington et al., 2009). Moreover, these results confirm that FF and ECB are not major sources of recharge to the cave stream at low flow conditions. Consequently, streamflow at LR under low flow conditions is likely sustained by subsurface in-feeders and epikarstic seepage.

## 3.4 Summary and Conclusions

The range of hydrologic variability in a karst groundwater system is important to the analysis of DOM transformations and cycling. It has been reported that bacterial uptake of DOM in surface streams increases during stormflow conditions (e.g., Buffam et al., 2001); however, dissolved and particulate OM may be flushed into and transported through a cave system too rapidly for measurable microbial transformations to take place. Conversely, long transit times under low flow conditions may facilitate a high degree of sorption and structural alteration of

OM along the flow path. Low flow conditions would appear to present the optimal opportunities for monitoring DOM transformations in many karst systems, especially if inputs of epikarstic and rhizopheric DOM are of interest. The dye breakthrough curves provide clues to the nature and interconnectivity of swallets, sinking streams, and caves along the flowpath.

For the first time at the Cascade Cave system, as well as for karst in northeastern Kentucky and the Carter Caves State Resort Park, the resulting flow velocities and travel times provide new ways of constraining variations in hydrologic conditions for the cave systems and of characterizing DOM transport through inaccessible sections of the complex underground flow network. Figure 3.10 graphically presents estimated groundwater flow paths identified by the dye tracer tests, from recharge points at FF and ECB through the Cascade Cave system and into Tygarts Creek. The tracer tests also confirm that recharge from James Branch can be partially shunted to Tygarts Creek and Gristmill Cave during high flow conditions. Both James Branch and the Cascade Cave stream exhibited strong discharge episodicity during low flow storm events, as illustrated by the rapid recession curves on their respective hydrographs (Nimmo et al., 2015). The degree of episodicity at low flow conditions (tracer test III) may be more pronounced than at moderate to high flows (tracer tests I and II) due to reduced epikarstic inputs and diffuse recharge during the dry season. Nevertheless, the resulting maximum and minimum travel times from FF to LR, ranging from ~17 hours at high flow conditions (0.03 m $s^{-1}$) to > 185 hours at low flow conditions (0.003 m $s^{-1}$), is typical for cave systems in the Cumberland Plateau region. Based on results compiled from >2000 natural gradient tracer tests from unconfined carbonate aquifers, velocities range from 0.02 to 0.05 m $s^{-1}$ (Quinlan et al., 1996), although it is suspected that these values are biased towards high flow tracer tests due to the time commitment required for low flow tests.

Previous work considered that most of the water and DOM were sourced from primarily James Branch at FF (Brannen-Donnelly and Engel, 2015). However, the results from the dye traces confirm that there are at least three additional sources of DOM input to the Cascade Cave system. These infeeders appear to play a prominent role in sustaining flow in the lower half of the system and may contribute continuous inputs of fresh DOM to the cave stream, even if the contributions were episodic in nature. Residence times along the flowpath from FF to LR were estimated at < 24 hours during high flow conditions (~0.03 m $s^{-1}$) to a week at low flow conditions (~0.003 m $s^{-1}$). Recharge from the epikarst in the form of cave drip waters and diffuse seepage was unquantifiable, but may significantly sustain the discharge differential between FF and LR. The lability, or freshness, of DOM recharged to the system at various hydrologic conditions is evaluated in Chapter 4 of this dissertation. However, given these uncertainties, a DOC mass balance on the system may be more complex than previously considered, and it may be difficult to duplicate carbon budgets for the Cascade Cave system that would be similar to those completed for other systems (Simon et al., 2003). Additional quantitative dye tracing could help to constrain high and low flow conditions in other parts of the system, which should provide more information on carbon budgets, residence times, and turnover rates.

## Chapter 3 Appendix

Table 3.1 Dye receptors and water samples in Tygarts Creek and the Cascade Cave system for Tracer Test II.

| Site ID | Description | Latitude | Longitude | Date Placed | Date Collected | Dye Recovery |
|---|---|---|---|---|---|---|
| Minnix #1 | Resurgence<br>W. bank | 38º20’18.67” | 83º07’24.77” | 052814 | 053114 | Neg. |
| Giant Tire | E. bank | 38º20’19.84” | 83o07’16.00” | 052814 | Missing | N.A. |
| Stamper Spring | Resurgence<br>E. bank | 38º30’28.58” | 83º07’04.02” | 052814 | Missing<br>053114 * | N.A.<br>Neg. |
| Horsetail Spring | Underflow<br>E. bank | 38º20’37.90” | 83º06’54.77” | 052814 | 053114 | Neg. |
| Barber Spring | Resurgence<br>E. bank | 38º20’44.06” | 83º07’01.00” | 052814 | 053014<br>053114 * | Neg.<br>Neg. |
| Giant #1 | Resurgence<br>W. bank | 38º20’45.82” | 83º07’17.30” | 052814 | 053114 | Neg. |
| On-the-Shale Spr. | Resurgence<br>E. bank | 38º21’10.07” | 83º07’20.48” | 052814 | 053114 | Neg. |
| Gristmill Spring | E. bank | 38º21’17.54” | 83º07’13.77” | 053114 | 053114 * | Pos.<br>Pos. |
| Dr. Lewis Bridge* | Center of stream | 38º21’31.34” | 83º07’10.70” | 052814 | 053114 * | Pos.<br>Pos. |
| Cascade Stream | Resurgence<br>E. bank | 38º21’28.11” | 83º06’43.54” | 052814 | 053114 * | Pos.<br>Pos. |
| Deadman Gulch | Spring stream | 38º21’30.95” | 83º06’27.95” | 052814 | 053114 * | Neg.<br>Neg. |
| Rt. 60 Bridge | W. bank | 38º22’02.33” | 83º06’33.22” | 052814<br>053014 | 053014<br>053114 | Pos.<br>Pos. |
| FF | Upstream Channel | 38º20’32.50” | 83º06’23.11” | 051514<br>052814 | 052814 *<br>053114 | Neg.<br>Neg. |
| ECB | Upstream Channel | 38º20’43.79” | 83º06’06.05” | 051514<br>052814 | 052814 *<br>053114 | Neg.<br>Neg. |
| JC | In cave stream | 38º20’59.62” | 83º06’23.96” | 051514<br>052814<br>053014 | 052814 *<br>053014 *<br>053114 * | Neg.<br>Pos.<br>Pos. |
| LR | In cave stream | 38º20’32.50” | 83º06’23.11” | 051514<br>052814<br>053014 | 052814 *<br>053014 *<br>053114 * | Neg.<br>Pos.<br>Pos. |

* GS indicates grab samples collected concurrently with packet collection. N.A. = Not Analyzed. Neg. = No dye recovery. Pos. = Positive dye recovery.

Table 3.2 Summary of dye traces recovered in the Cascade Cave system at various recharge and flow conditions.

| Injection Site | Date | Detection Site | Length (m) | Flow | Est. Discharge* (L $min^{-1}$) | Est. Avg. Velocity (m $hr^{-1}$) | Mean velocity (m $s^{-1}$) |
|---|---|---|---|---|---|---|---|
| Box Canyon Swallet | 051314 | LR | 440 | Low | 56 | 20 | 0.006 |
| Jones Cave | 051514 | LR | 956 | High | 388 | 87 | 0.024 |
| Echo Canyon Branch | 052814 | JC | ~500 | HIgh | 187 | ~112 | ~0.03 |
| Fort Falls | 052814 | LR | 1768 | High | 1040 | ~104 | ~0.029 |
| Fort Falls | 060915 | JC | 812 | Low | 38 | 5.6 | 0.002 |
| Fort Falls | 060915 | LR | 1768 | Low | 38 | 9.6 | 0.003 |

* At time of dye injection

Figure 3.1 Installation of ISCO automatic recorders and flow probes (top right) at Fort Falls (top) and the Lake Room resurgence. The latter was also programmed to collect water samples.

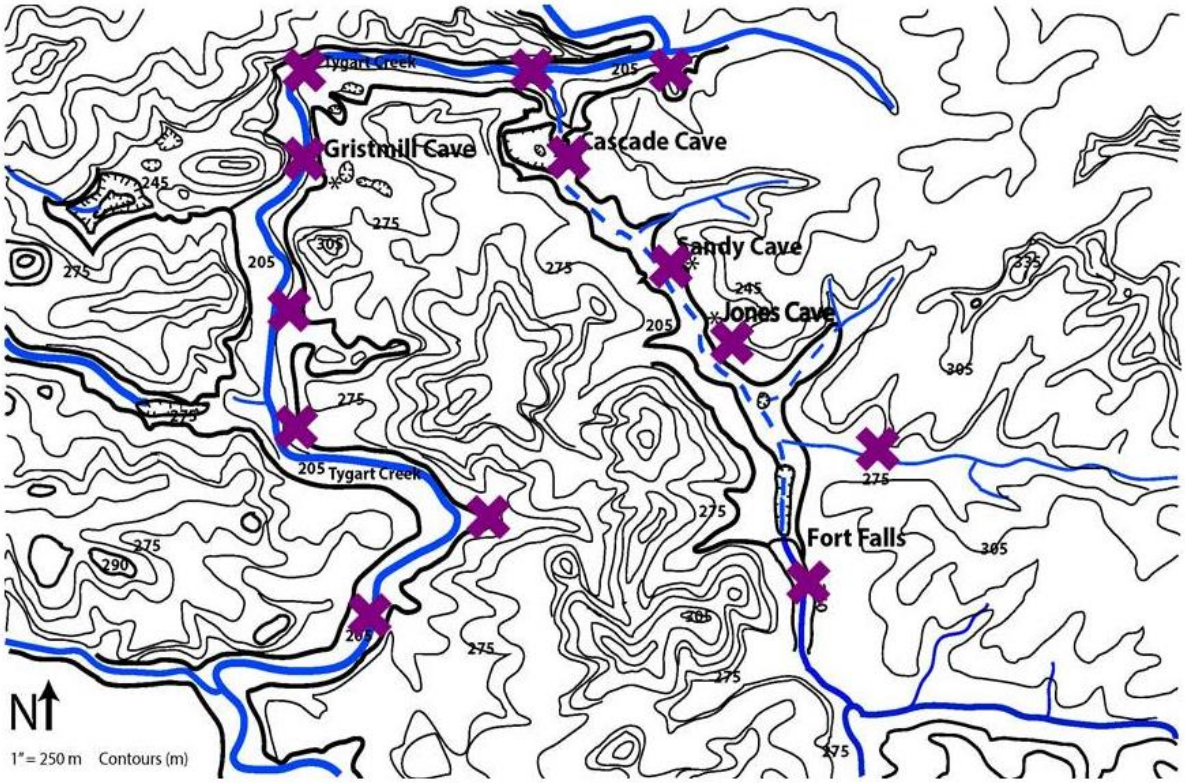


Figure 3.2 Locations of passive dye receptors along Tygarts Creek and the Cascade Cave system.

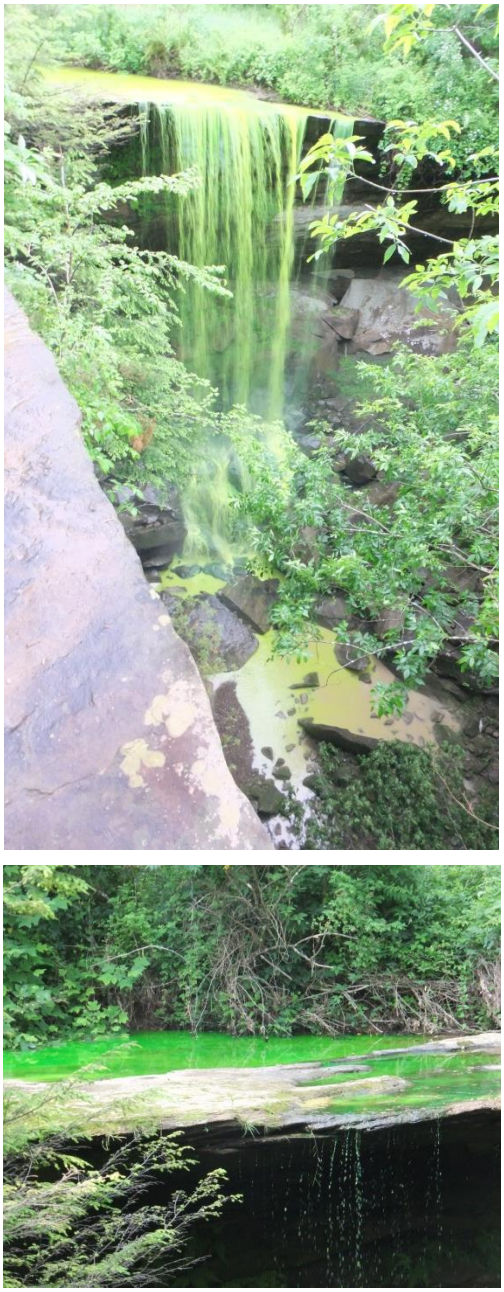

Figure 3.3 Uranine passes over Fort Falls during (above) a high flow tracer test on May 28, 2014, and (below) a low flow tracer test on June 9, 2015.

Figure 3.4 Water samples were analyzed for fluorescence in the field using Turner Designs Model 10 filter fluorometers turned to detect red dyes for Rhodamine WT (left) and green dyes for Uranine (right).

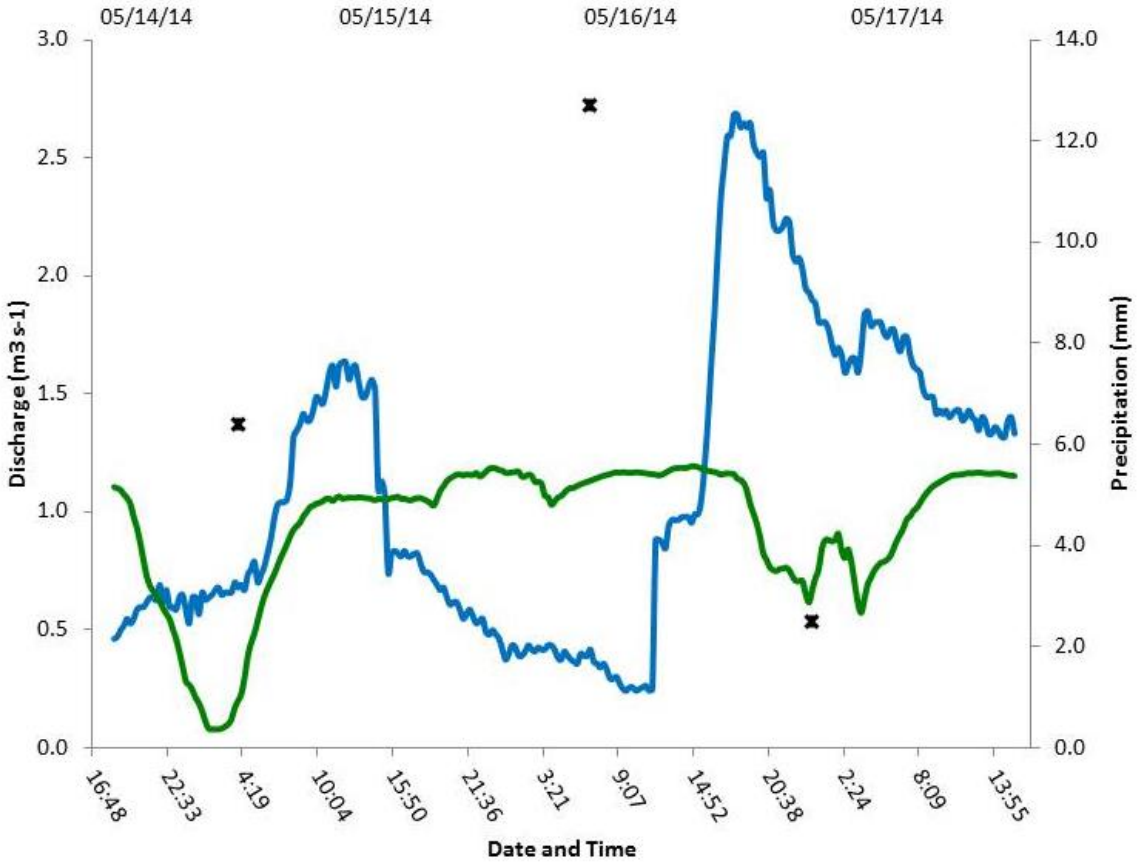


Figure 3.5 Discharge hydrographs for James Branch at Fort Falls (green) and the Cascade Cave stream in the Lake Room (blue) during Tracer Test I. Precipitation data are daily totals.

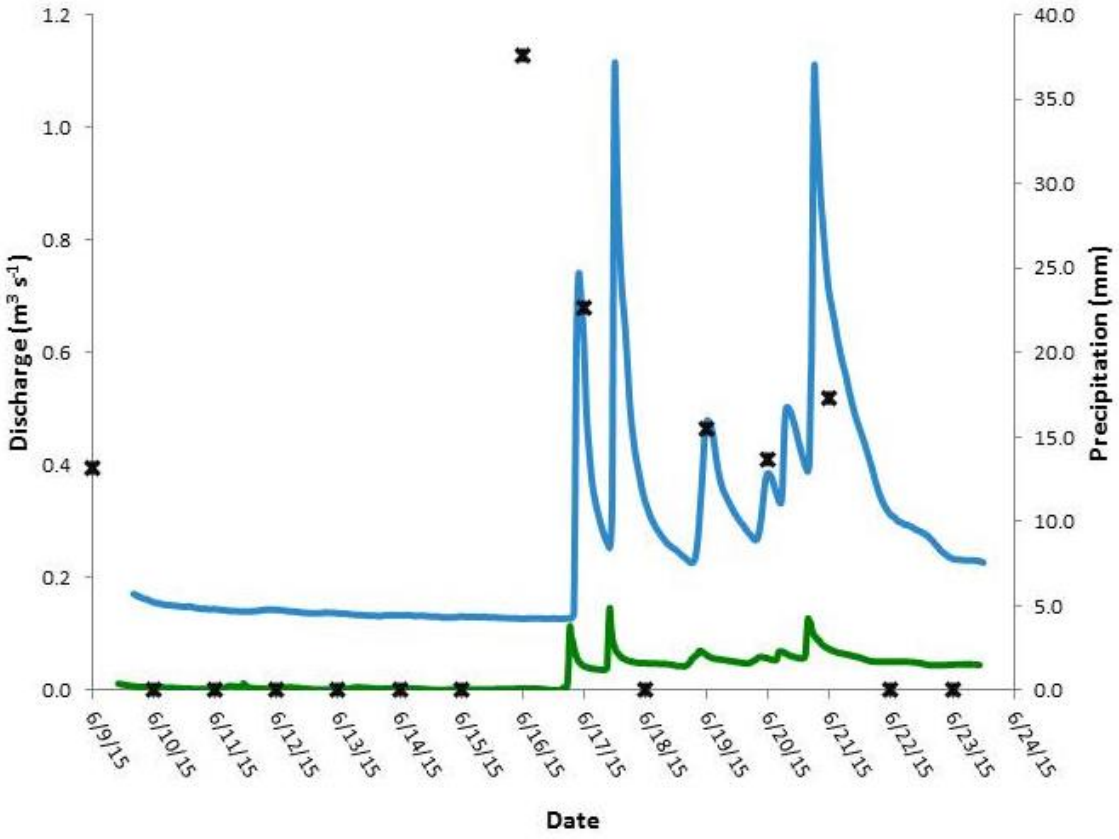


Figure 3.6 Discharge hydrographs for James Branch at Fort Falls (green) and the Cascade Cave stream in the Lake Room (blue) during Tracer Test III. Precipitation data are daily totals.

Figure 3.7. Rhodamine WT is visible in the Lake Room resurgence (May 14, 2014) during Tracer Test I from Box Canyon swallet.

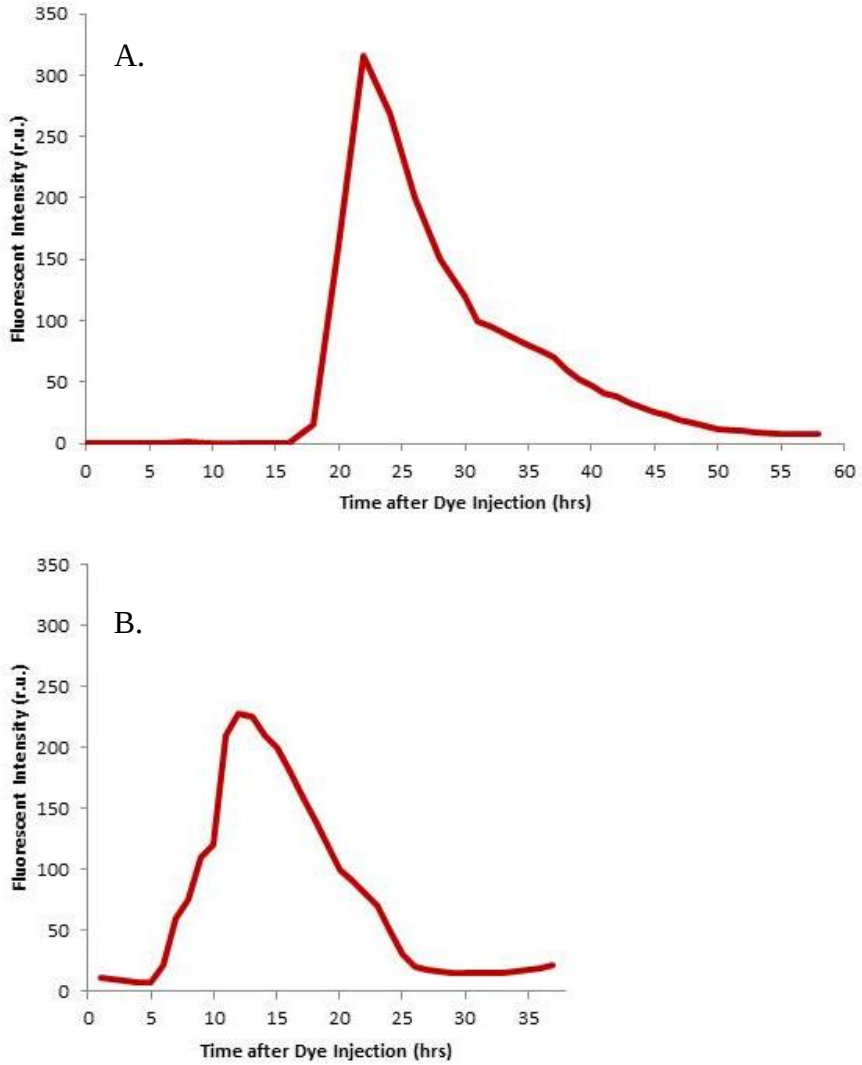


Figure 3.8 Dye breakthrough curves for Rhodamine WT recovered in the Lake Room during Tracer Test I. Curve A represents a dye injected at Box Canyon Swallet, and Curve B represents dye injected in Jones Cave.

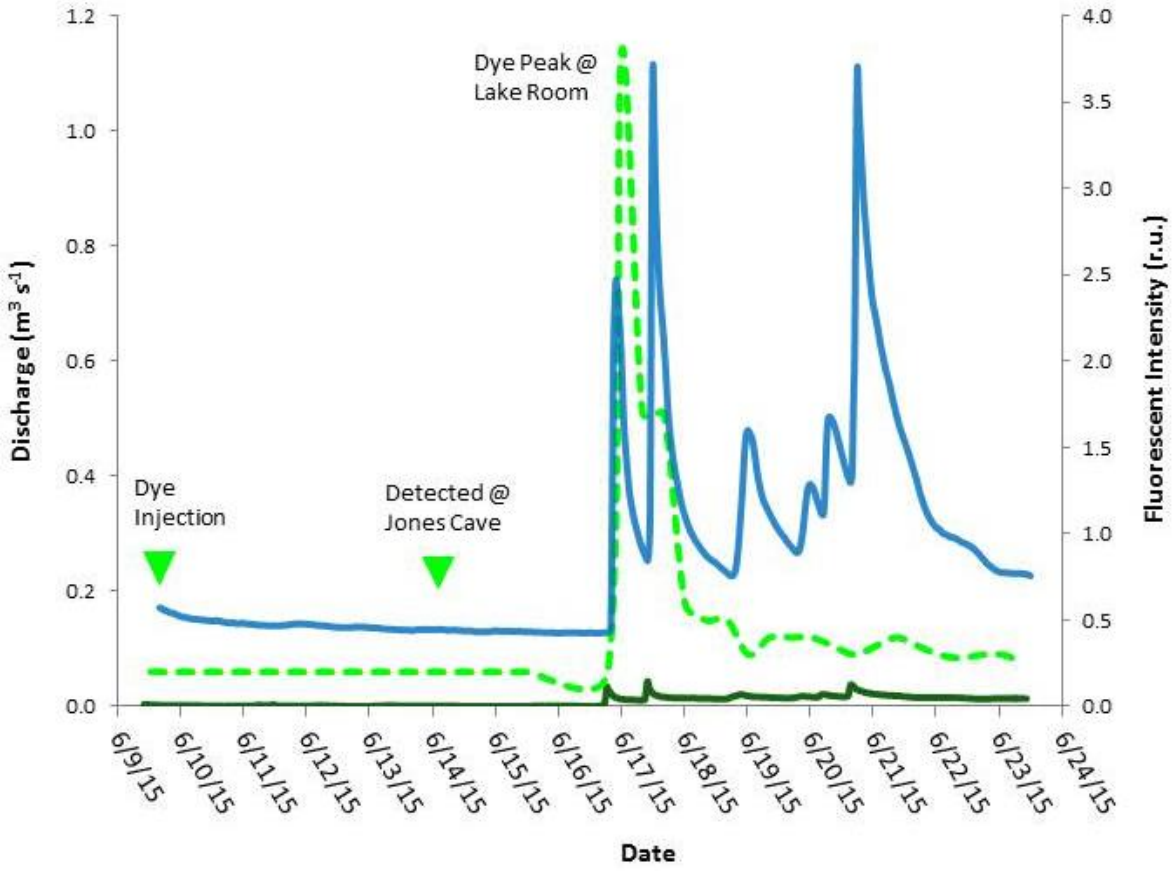


Figure 3.9 Dye breakthrough curve for Uranine recovered in the Lake Room, superimposed on the low flow hydrograph, during Tracer Test III.

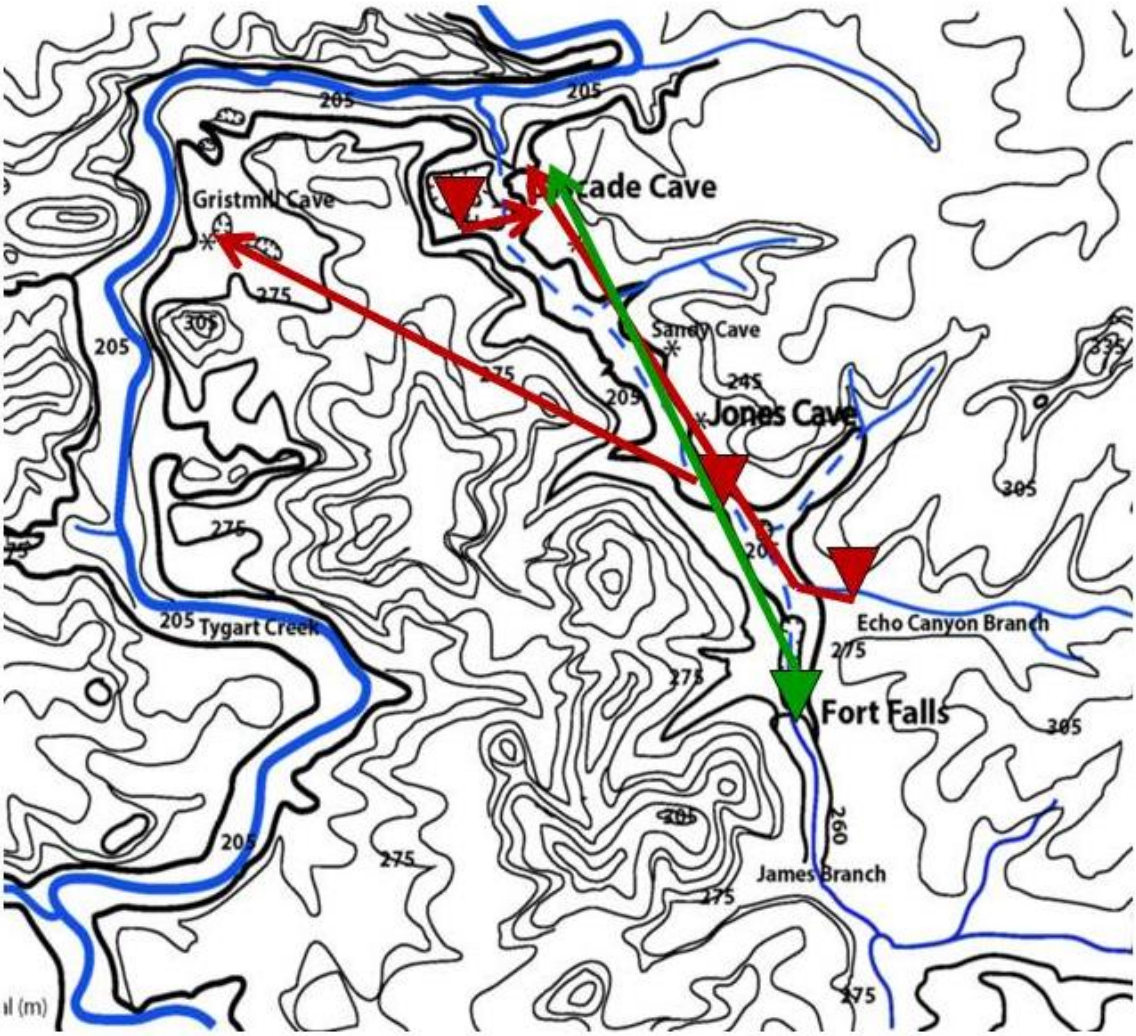


Figure 3.10 Estimated groundwater flow paths delineated during the dye tracer tests. Triangles are dye injection sites, arrows denote positive dye detection sites, red lines represent positively-recovered Rhodamine WT traces, and the green line represents positively-recovered Uranine traces.

# Chapter 4. Structural Transformation of Organic Matter Along the Recharge to Discharge Flow Path of an Oligotrophic Cave Stream

## 4.0 Abstract

The transformations of DOM in surface water and groundwater from the inter-connected karst system including Cascade Cave in Kentucky was examined after concentrating, isolating, and characterizing macromolecular functional groups along the hydrologic flow path. Solid phase extraction chromatography, based on DEAE weak anion exchange for carbon-limited environments, was used to isolate low molecular weight, hydrophilic DOM for chemical characterization by FTIR spectroscopy. The flow path hydrochemistry was monitored seasonally over a period of 4 years (2010-2014). Due to dilution effects during winter, which had high flow conditions, the summer, low flow events were the most informative for discerning microbial transformation effects from the DOM isolates. The quality of DOM (as [DOC]) decreased significantly between the surface and subsurface streams at low flow conditions, and [DOC] was much less variable in groundwater over all seasons and flow conditions. Photo-degraded recharge was poor in esters, phenols, and certain polysaccharides, whereas DOM in fresher recharge was highly aromatic, and was rapidly transformed and degraded, which was observed as changes in amide I and II bands. The predominance of carboxyl functional groups and increasing total dissolved nitrogen concentrations in groundwater DOM isolates were also interpreted as indicative of OM transformation and degradation.

## 4.1 Introduction

Although continental aquifers have the potential to influence the global carbon cycle by "sequestering" organic carbon in excess of ocean floor burial (e.g., Tranvik et al., 2009), recent revisions of global greenhouse gas and carbon fluxes do not address continental aquifer systems (Zhu et al., 2010). The International Panel on Climate Change (IPCC) recently acknowledged

limits on modeling decadal to millennial carbon flux from global terrestrial reservoirs (e.g., soils, lakes, vegetation), and suggested that regional investigations on natural organic matter (OM) turnover and sequestration would be the most appropriate scale for studies because of variations between catchments and groundwater basins (Ciais et al., 2014) .

In regional-scale karst catchments, natural OM (e.g., largely photosynthetically produced detritus) at the surface can broadly diffuse into epikarst or be funneled into recharge sites, i.e., swallets and sinking streams (e.g., Fisher et al., 1973; Simon et al., 2001). Karst systems contain diverse microbial habitats, where aerobic, heterotrophic bacteria metabolize OM and transfer nutrients to downstream aquatic food webs (e.g., Baker et al., 2000; Einseidl et al., 2007; Farnleitner et al., 2005; Simon et al., 2003). Microbial mineralization of OM supports more than 95% of total heterotrophic respiration (Lavelle et al., 2001), and as such, photosynthetically-produced OM in karst groundwater recharge enters a pipeline-like bioreactor, whereby OM can be microbially transformed to different OM compounds, and ultimately to carbon dioxide ($CO_2$) while in transit to spring resurgences, rivers, and lakes on the surface (e.g., Brannen-Donnelly et al., 2015; Brooks et al., 1999; Jardine et al., 2006).

Terrestrial OM that is transported into karst by storms and snowmelt may also become buried and sorbed onto clay and sediment deposits (Kaiser et al., 2005), where it would be inaccessible for degradation and potentially sequestered for years if left undisturbed. Moreover, mixtures of OM from conduit and diffuse recharge can result in OM at any one point along the recharge-to-discharge flow path that represents different stages of transformation. One advantage to studying the fate and transport of natural OM in karst systems compared to other types of terrestrial hydrogeologic systems is that the recharge-to-discharge flow path can be accessible from cave passages large enough for humans to enter. Another advantage is that photo-

degradation of terrestrial OM does not occur and fresh autochthonous OM production by photosynthesis is not possible in the dark (Birdwell et al., 2010; Brannen et al., 2009).

However, despite these advantages, limited research has been done to characterize OM from different points along a karst flow path (Baker et al., 1999; Baker et al., 2001; Birdwell et al., 2009), but also to quantify the rates of OM transformation along a karst flow path (Birdwell et al., 2009, 2010; e.g., Brannen et al., 2009; Brown et al., 2011; Brown et al., 2009; Jardine et al., 2006; Simon et al., 2007). Therefore, the aim of this research was to investigate microbial transformations of OM, as dissolved organic matter (DOM), by examining changes in the macromolecular structure of DOM as water moved along a recharge-to-discharge flow path from a sinking surface stream to a cave stream. Acidic and ionic macromolecular functional groups in DOM were isolated using diethylaminoethyl (DEAE) cellulose weak anion exchange column chromatography, and chemically characterized by using Fourier Transform Infrared (FTIR) spectroscopy. To my knowledge, these approaches have not been previously applied to the characterization of DOM from oligotrophic karst systems, and complement UV-Vis and fluorescence spectroscopy methods used in our laboratory and elsewhere to describe the nature and behavior of DOM from oligotrophic karst waters (Baker et al., 1999; Birdwell et al., 2010; Brannen et al., 2009; Brown et al., 2009; Göppert et al., 2008)

The first of three hypotheses tested by this research was based on observations made during previous research referenced above, and states that: (1) seasonal hydrologic variations and temperature perturbations affect DOM quality and the efficiency with which DOM is processed in the subsurface (as measured from dissolved organic carbon concentrations [DOC]). The second hypothesis was based upon the assumption that DEAE isolates would concentrate macromolecular groups typically associated with aquatic OM, and states that (2) specific

macromolecular indicators of DOM degradation exhibit decreasing IR absorbance with extended residence time and transport in the subsurface. The third hypothesis was based on the reported accumulation of nitrogenous compounds associated with microbial degradation, and states that (3) dissolved organic carbon-to-total-nitrogen ratios (OC:TN) decrease downstream coincident with microbial processing and by-product formation. The findings underscore the fundamental need for basic information about the nature and behavior of OM in karst, and about transformations caused by microbial metabolic processes. In particular, the need for well-tested and comparable alternatives for isolating and characterizing macromolecular functional groups from bulk OM found in a range of ecological settings has been acknowledged (McDonald et al., 2004; Perdue, 2009). Collectively, these results can be applied to other shallow groundwater systems, where the implications are that regional-scale aquifer contributions to greenhouse gas and carbon fluxes can be estimated.

## 4.2 Methods

### 4.2.1 Water Sampling and Physicochemistry

The study was conducted from October 2012 until June 2015 in the Cascade Cave System, Carter Caves State Resort Park, Kentucky. The field site and hydrology are described in detail in Chapters 1 and 3 of this dissertation. Surface water was collected immediately above the ledge at Fort Falls (FF) and in Echo Canyon Branch (ECB), a small sinking stream in a shaded channel with a direct hydrologic connection to Jones Cave (JC) (Figure 1.4). Cave stream water was collected from the dark zone in JC, Sandy Cave, and at the Lake Room (LR) in Cascade Cave, which is also ~10 m upstream from the resurgence. Winter samples were collected under high flow conditions (~1000 L $min^{-1}$ or more) fed by rainfall or snow melt, and summer sample

events were collected at moderate to low flow (~200-40 L $min^{-1}$). All samples were collected during daylight hours, except for those collected during the September 2013 low-flow sampling event, when water samples were collected at two-hour intervals for 24 hours with ISCO automatic samplers located at both FF and LR. Two sets of water samples were collected 12-hours apart (2:30/3:30 p.m. and 2:30/3:30 a.m.) at FF and LR for the isolation of DOM components.

At each sampling location and time, aqueous geochemistry parameters were measured in the field using standard electrode methods, including pH and temperature with an Accumet AP115 portable meter and dissolved oxygen (DO), specific conductance, and temperature with a YSI 85 multimeter. Alkalinity was determined in the field via manual titration to the end-point (pH 4.3) using 0.1 N sulfuric acid (Eaton, 2005). Water samples were collected by filtering to 0.2 µm through Millipore polyvinylidene fluoride (PVDF) filters (EMD Millipore, Merck KGaA, Germany) either by manual filtration using a polypropylene filter holder and sterile syringes or using a Geotech peristaltic pump with polyethylene tubing and a polycarbonate in-line filter holder (142mm) (Geotech Environmental Equipment, Denver, Colorado, USA). Filtered water samples were collected in separate HDPE bottles for major ion analyses and alkalinity, and in separate muffled (to 545$^{o}$C) 40 mL glass vials for dissolved inorganic carbon (DIC), dissolved organic carbon (DOC), dissolved nitrogen (DN), fluorescence, and UV absorbance spectroscopy.

Unfiltered water samples were collected in separate glass vials for total inorganic and organic carbon analyses (TIC, TOC) and total nitrogen (TN) content. Cation samples were preserved with trace metal grade nitric acid, after HDPE bottles were pre-washed with dilute HCl. Water samples and filters were packed on ice for delivery to the laboratory, where samples were stored at 4$^{o}$C until analyses. Major ions were measured on a Dionex ICS-2000 ion

chromatograph, on which accuracy was checked using ion standards to within two standard deviations.

Total carbon (TC) and dissolved carbon (DC) were determined using a Shimadzu TOC-V carbon analyzer by the combustion-infrared detection method (Standard Method 5310B; Standard Methods Online, Standard Methods for the Examination of Water and Wastewater, http://standardmethods.org/), in which acidified samples were sparged to remove inorganic carbon (measured as $CO_2$) (Eaton, 2005). The difference between TC and TIC was reported as the concentration of TOC ([TOC]), and the difference between DC and DIC reported as the total concentration of DOC, [DOC]. The instrument was standardized with $C_8H_5KO_4$, and the minimum detection limit (MDL) was 0.1 mg/L. Precision between duplicate injections was 2% of the relative percent difference (RPD) for [DOC] > 4 mg $L^{-1}$, and 5% RPD for [DOC] < 4 mg $L^{-1}$. It was not assumed that all DIC was necessarily part of DOM.

Seasonal variations in carbon flux through the system were quantified as percent organic carbon (% OC) of the TC load at each site:

$$\%OC = ([DOC]/([DIC]+[DOC])) * 100$$

TN and DN content were measured via high temperature catalytic oxidation with chemiluminescence detection (ASTM D5176-08), at MDL 0.01 mg $L^{-1}$ (ASTM, 2015). This method was selected as being more representative of nitrogen compounds in DOM (e.g., Perakis et al., 2002; Petrone et al., 2009; Simpson et al., 2012), after some previous analyses of dissolved nitrogen species as nitrite and ammonia ($NO_2$, $NH_3$) were measured at or below MDLs.

### 4.2.2 DOM Isolation

DEAE cellulose weak anion exchange column chromatography was utilized to concentrate and isolate acidic and ionic macromolecular functional groups (Thurman, 1985). Column preparation, sample loading, and elution procedures are discussed in detail in Chapter 2 of this dissertation using standard solutions obtained from the International Humic Substances Society (IHSS). For the field isolation of DOM, four liters of water were filtered to 0.2 µm, as described above. Water was loaded onto the DEAE columns in darkness (Figure 4.1), and the columns were stoppered, transported on dry ice, and stored at 4ºC until elution in the laboratory (within 48 hours). If field conditions precluded column loading onsite, then filtered waters were transported back to the laboratory on ice, and allowed to reach room temperature before being loaded onto individual DEAE columns.

### 4.2.3 Spectroscopic Characterization

Few quantifiable parameters exist for OM, other than [DOC] commonly used to characterize OM in aquatic environments (Wetzel, 1992; Filella, 2009). Because the organic carbon component of OM consists of aromatic and conjugated alkene structures that absorb light over a range of wavelengths, [DOC] has been correlated with UV absorbance at 254 nm ($UVA_{254}$) and other wavelengths (Eaton, 2005; Korshin et al., 1997; Traina et al., 1990), chemical compositions (Fram et al., 1999; Pettersson et al., 1994; Weishaar et al., 2003), aromaticity (e.g.,McKnight et al., 2001), and reactivity (e.g.,Reckhow et al., 1990). UV absorbance of bulk and isolate DOM samples was measured on an Evolution 200 series scanning spectrophotometer (Thermo Fisher Scientific, Inc., USA) in the wavelength range 240 to 600 nm. OM build-up on the 1 cm quartz cuvettes was routinely checked using 18 MΩ distilled/deionized (DD) water blanks. Solutions were scanned at room temperature at pH 5 to 6,

and samples with $UVA_{254} > 3$ $cm^{-1}$ were diluted by 50% and re-measured to improve the signal-to-noise ratio. Specific Absorbance ($SUVA_{254}$) values were calculated for each sample as $UVA_{254}$/[DOC] and reported in L $cm^{-1}$ $mg^{-1}$ (Weishaar et al., 2003).

Infrared (IR) absorbance spectroscopy enables the identification of chemical functional groups in molecules by measuring atomic vibrational and rotational reactions to light (Skoog et al., 2007). Major chemical groups in DOM isolates and DEAE filtrates were characterized by using FTIR spectroscopy to identify changes in macromolecular structure from recharge to resurgence. Six functional groups were identified as potential biomarkers of microbial and decompositional processes: carboxylic acids, esters (as fatty acids), amides, saturated hydrocarbons (alkanes), polyphenols (lignin), and carbohydrates (polysaccharides) (Abdulla et al., 2010; Garip et al., 2009; Schumacher et al., 2006)

The IR absorbance of original OM, filtrates, OM isolates, and blank isolates was measured with an Agilent Cary 660 FTIR single-beam spectrometer with a DTGS detector over a spectral range of 4000-600 $cm^{-1}$. Liquid samples (approximately 40 µL) were applied directly onto the Ge crystal mounted in an Attenuated Total Reflectance (ATR) accessory. The background solution for the DEAE filtrates was 18 MΩ DD water for original OM and filtrates, and 0.1 M NaOH (at pH 5.6) for the DEAE isolates. Thirty-two scans at a resolution of 4 $cm^{-1}$ were collected for each spectrum, which were ATR- and baseline-corrected and smoothed (11-pt). Blank isolate spectra were subtracted from OM isolate spectra to delete artifacts from the weak anion exchange resin.

To eliminate large hydroxyl bands, spectra were truncated by subtracting all bands but those of interest, the 1800-1000 $cm^{-1}$ region. Bands for protonated carboxyl groups (–COOH) were assigned to wavenumbers 1720 $cm^{-1}$, indicative of C=O stretching, and ~1418 $cm^{-1}$,

associated with O-H in-plane bending. De-protonated carboxylic groups were identified from two peaks at ~ 1600 $cm^{-1}$ and ~1400 $cm^{-1}$, associated with the asymmetric and symmetric stretching of –COO, respectively (Abdulla et al., 2010; Hay et al., 2007; Schumacher et al., 2006). Other functional groups, such as polyphenols at ~1500 $cm^{-1}$ (vibration of the aromatic ring), and aliphatic and aromatic esters (C=O stretching) at 1740 $cm^{-1}$ and 1780 $cm^{-1}$, respectively, were identified according to previously published band assignments for aquatic natural OM (see Table 2.1 in Chapter 2) (e.g., Leenheer, 2009; Ratpukdi et al., 2009; Tremblay et al., 2011). To overcome interpretation difficulties caused by overlapping bands from the 1700-1600 $cm^{-1}$ and 1200-1000 $cm^{-1}$ regions, absorbance bands characteristic of specific macromolecules were grouped, and their relative intensities summed for later quantitative comparison. Weak, small bands masked by stronger bands were differentiated through the second derivative of the original FTIR spectra, according to the Fourier method (Abdulla et al., 2010).

IR absorption band intensity ratios have been used as indicators of decomposition and microbial processing (e.g., Grube et al., 2006; Ritchie et al., 2008; Tinti et al., 2015). Functional group bands present in the least absorptive DOM isolate spectra (e.g., Sept. 2013, LR-night) were selected as indicative of the most highly processed, refractory OM remaining downstream. Functional group ratios were calculated using absorbance intensities for bands representative of amides divided by bands representative of carboxylic acids and absorption intensities of phenol bands divided by bands representative of carboxyl and alkane groups.

### 4.2.4 Statistical and Data Analyses

Correlations between sample sites, flow conditions, and the hydrochemical constituents in unfractionated water samples were explored using a Completely Randomized Design (CRD)

Split Plot (2-Way) ANOVA with a compound symmetry heterogeneous variance/co-variance matrix (Littell et al., 2006). Total DN data was statistically analyzed using Wilcoxon Two-Sample Test to determine significant differences between sample sites (A. Ellison et al., 2004). To account for different sources of variability, the macromolecular functional group data for the DOM isolates was analyzed for dependency using a CRD Split-Split Plot (3-way) ANOVA with an unstructured variance/co-variance matrix (Littell et al., 2006). A 95% confidence interval was used, with significance determined by P-value <0.05. All statistical assumptions were met and all analyses were performed using SAS software, Version 9.4 (SAS Institute, Inc., Cary, NC).

## 4.3 Results

### 4.3.1 Hydrochemistry

Physicochemical and ion data for sampling sites at FF and ECB, the upper cave stream in JC, and the lower cave stream in LR of Cascade Cave are compiled in Chapter 4 Appendix Table 4.1). Water temperatures on the surface ranged from a high of nearly 30$^{o}$C in the summer to a low around 5$^{o}$C in winter, whereas cave stream temperatures varied around 15$^{o}$C in summer and 5$^{o}$C in winter. Time series plots of temperature, pH, and specific conductivity (Figure 4.2) illustrate seasonal and spatial variations along the flowpath. Specific conductivity and DO concentrations varied inversely, such that the lowest conductivity corresponded with higher DO concentrations in winter at high flow conditions. Similarly, the highest conductivity values and the lowest DO concentrations occurred in summer at low flow conditions. Geometric means of alkalinity at FF, JC, and LR (n = 3) were 143 mg $L^{-1}$, 118 mg $L^{-1}$, and 147 mg $L^{-1}$ (as $CaCO_3$), respectively.

Inorganic and organic carbon and nitrogen data are presented in Table 4.2 for both unfiltered (TIC, TOC, TN) and filtered (DIC, DOC, DN) water samples. ([DOC]) at LR varied

within a much narrower range across all seasons and flow conditions than at FF (Figure 4.3). Variations in [DOC] at FF were statistically significant (P-value = 0.009) between high and low flow conditions, and [DOC] varied significantly between FF and LR at low flow conditions (P-value = 0.0045), but not at high flow. $SUVA_{254}$ values ranged from 0.02 L mg $C^{-1}$ $m^{-1}$ for cave waters to 0.03 L mg $C^{-1}$ $m^{-1}$ for surface waters in the study area. Similar values have been previously reported to indicate aromatic carbon content in DOM (e.g., McKnight et al., 2001; Weishaar et al., 2003). [DOC] showed positive, statistically significant correlations with chloride (P-value = 0.0176), potassium (P-value = 0.0257), and magnesium (P-value = 0.0041) concentrations. [TOC] and [DOC] decreased along the flowpath and remained < 5 mg $L^{-1}$, classifying the waters of the basin as oligotrophic, or nutrient-limited, from an ecological perspective (Egli, 2010). DN concentration increased along the flow path during all seasons except for the high flow event in March 2014 (Figure 4.4). Lack of data precluded more robust analyses, but a simple t-test indicated that DN concentrations were significantly different between FF and LR (P-value = 0.04).

### 4.3.2 Interpretation of FTIR Spectra

The infrared absorbance spectra of DOM isolates from surface water recharge (James Branch at FF) and cave stream discharge (from LR) were compared for winter, high flow conditions and summer, low flow conditions. Figure 4.5 presents DOM isolate spectra for FF and LR during a snowmelt-driven, high-flow event in mid-January 2014, and a rain-fed, high-flow event in mid-March 2014. In January, isolates from both FF and LR exhibited nearly equally intense bands of aliphatic and acetyl esters and amide II (split peaks at 1570-1530 $cm^{-1}$) functional groups, in addition to polysaccharides and organo-silicate compounds (~1100 $cm^{-1}$). The LR DOM isolate exhibited a strong amide I (1650 $cm^{-1}$) band not present in FF, and slightly

greater phenol (1510 $cm^{-1}$) and alkane (1430 $cm^{-1}$) absorbance. Carboxyl group spectra differed between FF and LR, in that the former contained a band associated with protonated carboxylic acids (–COOH) at 1670 $cm^{-1}$, plus shoulders at 1700 $cm^{-1}$ and 1685 $cm^{-1}$. LR contained the same protonated carboxylic acid groups, along with shoulders at 1620 $cm^{-1}$ and 1400 $cm^{-1}$ associated with de-protonated carboxylates (–COO). Both March DOM isolates exhibited the absorbance band pairs associated with –COO at 1640 $cm^{-1}$ and prominent split amide II peaks that were 4.6% and 5.5% more intense in the FF DOM isolate. The FF DOM isolate was also 5.1% richer in aromatic esters, and had 5.8% greater phenol and 3.8% greater alkane content relative to the LR DOM isolate. The LR DOM isolate exceeded the FF DOM isolate in organo-silicate compound absorbance and acetyl esters (1250 $cm^{-1}$).

Figure 4.6 presents FTIR spectra from early September 2013, when the LR isolate was enriched in all macromolecular functional groups with respect to recharge at FF. Ratios of functional group band intensities correlated with 41% greater phenolic absorbance in LR, and 15% and 30% greater polysaccharide and amide II absorbance, respectively. Aliphatic esters were greater by 37%, de-protonated carboxyl groups greater by 11%, and a sharp alkane peak (1460 $cm^{-1}$) in the spectra of both DOM isolates was 28% more intense at LR. By comparison, the June 2014 spectra were overall more aromatic (Figure 4.6), with the LR DOM isolate only slightly richer in aromatic esters, protonated carboxyl groups, and amide II, and polysaccharide macro-molecules than the FF DOM isolate.

Two additional sites were sampled during this event, including JC and ECB. As demonstrated from the dye trace results presented in Chapter 3 of this dissertation, FF and ECB waters converged in JC, and the groundwater flow path continues from JC through to LR. The FTIR DOM isolate spectra (Figure 4.7) indicated that the quality of DOM recharged from ECB

was about 17% more aromatic (i.e., esters and phenols) than DOM recharged from FF, and contained up to 10% more polysaccharide (1360-1340 $cm^{-1}$) and amide II macromolecules, 21% more carboxyl groups, and ~ 7% more organo-silicate compounds. The higher values indicated fresher DOM contributions. The DOM isolate spectra from JC and ECB exhibited strong bands of amide I and phenols, whereas the amide I band was replaced by carboxylic acid in the isolates from FF and LR, and phenol was represented by a low shoulder that was slightly more intense in LR. Ratios of carboxyl groups to phenols and esters indicate that these macromolecular groups co-varied (2.0 for all) at each point along the flow path. No distinct alkane bands were detected in the June DOM isolates.

Because ECB contributed fresher recharge to the cave system along a presumed shorter path length (~ 500 m), its DOM isolate spectra was used to examine changes in DOM composition along the flow path to LR in June 2014 (Figure 4.8). Groundwater DOM isolated from JC exhibited ~ 6% increase in amides I and II over recharge from ECB, which showed a band shift (structural change) from the carboxyl group peak at 1680 $cm^{-1}$. No change in aromatic esters was observed between ECB and JC; however, phenols and polysaccharides increased slightly (~ 2.5%). At LR, ~ 956 m downstream from JC, the amide I band was absent and replaced by a low carboxyl group band. Ratios of functional group band intensities correlated to a 13.5% decrease in aromatic esters, a 15.1% decrease in phenol, a decrease and structural shift in the amide II band, and a 7% decrease in polysaccharide content.

The effects of photochemical degradation on recharge DOM were also assessed during the summer low flow sampling events. In September, DOM was isolated from samples collected at FF and LR approximately 12 hours apart (2:30 p.m./2:30 a.m. and 3:30 p.m./3:30 a.m., respectively). As illustrated in Figure 4.9, the DOM quality of surface water recharged at night

was richer in organic macromolecules than surface water DOM recharged during daylight, specifically, as aliphatic esters (40% greater), phenols and alkanes ( ~ 30% greater), and substantially greater polysaccharides (1172 $cm^{-1}$ and 1106 $cm^{-1}$). Certain bands were only present at night, including acetyl esters (1245 $cm^{-1}$) and polysaccharides at 1305 $cm^{-1}$ and 1052 $cm^{-1}$. A similar comparison of DOM isolates from LR shows that at night, the cave stream contained the lowest IR absorptivity observed during this study. Plotted on a finer scale, the night time LR DOM isolate spectra reveal distinct bands of aliphatic ester, alkanes (1460 $cm^{-1}$ and 1375 $cm^{-1}$), and organo-silicate macromolecules, with very low shoulders associated with amide II and polysaccharide functional groups (Figure 4.10).

Least squares of the means analyses in the statistical mixed model (Littell et al., 2006) indicated that carboxyl groups were not significantly different from ester groups and phenols, but that esters and phenols were significantly different from each other. Amides (combined) were dissimilar from all other macromolecular groups in the DOM isolates. Amide I was typically only present in freshly recharged DOM (e.g., winter high flow and June ECB and JC). Amide II bands were present as split peaks in all DOM isolates except those from September 2013, when amide II was present as a single low peak at 1550 $cm^{-1}$.

The FTIR spectra of these DOM isolates exhibited some broad bands with many shoulders, especially in the 1400 $cm^{-1}$ to 1180 $cm^{-1}$ range. Broad bands with shoulders indicate the presence of overlapping peaks that potentially obscure structural information about the complex mixture. Shoulders were resolved through the application of the second-order Savitzky-Golay method to generate second derivative spectra that point downward for all major bands in the original spectra (Abdulla et al., 2010). One disadvantage of this technique is a decrease in the signal-to-noise ratio in second derivative spectra (Skoog et al., 2007). In most

cases, examination of the second derivative spectra revealed no further insights, for example in June 2014 (Figure 4.11); however, an order-of-magnitude decrease in absorbance intensity between the DOM isolates from Sept. 2013 FF and LR implied that the downstream DOM existed in the leanest, least complex state in late summer.

The filtrate fractions from the DEAE isolation process consisted of organic compounds not irreversibly retained on the anion exchange resin, and exhibited spectra that were dissimilar from their corresponding isolates, with an order of magnitude lower absorption intensities. Carboxylic groups were preferentially concentrated in filtrate fractions, based on strong bands at 1600 $cm^{-1}$, 1440 $cm^{-1}$, and 1400 $cm^{-1}$. Weak, shifted phenol bands (~1500 $cm^{-1}$) and possible amide III bands (small peaks at ~1265 $cm^{-1}$) were also present. The filtrate spectra were almost identical for both FF and LR, and due to the limited information provided, filtrates were not considered further in this study.

## 4.4 Discussion

Transformations of DOM molecular structures in an oligotrophic karst groundwater system were investigated from recharge to resurgence to elucidate aquatic carbon cycling processes in the critical zone. It was hypothesized that the progressive decomposition of surface organic matter by microorganisms could be traced along the groundwater flow path based on changes in DOM macromolecular structure. In practice, tracking the degradation of a parcel of organic matter throughout the Cascade Cave system was complicated by the influence of numerous discrete, diffuse, and direct inputs entering the cave via tree roots, epikarstic drip waters, and other small sinking streams. The resulting DOM composition in the Lake Room at

any given time was the product of pulsed and continuous inputs, in addition to surface environmental conditions, water residence time, and microbial turn-over of labile constituents.

Nonetheless, the statistical analyses revealed trends in the DOM quality of recharge and cave waters discussed below with regard to the previously stated hypotheses. FTIR spectroscopy expresses even very small changes in the composition and structure of a molecule as substantial differences in the size and shape of absorption bands (Skoog et al., 2007). As such, IR absorption band intensity ratios have been used as indicators of decomposition and microbial processing (e.g., Grube et al., 2006; Tinti et al., 2015). Key spectral signatures of fresh DOM specifically include aromatic amides and polyphenols, which have been associated with recycled microbial biomass (McKnight et al., 1994), N- containing polysaccharides (Maie et al., 2006), high molecular weight DOM (Amon et al., 1996; Benner, 2003), riverine or terrigenous inputs of DOM in marine systems (Yamashita et al., 2015), and root exudates (D'Orazio et al., 2009; Hattenschwiler et al., 2000).

Functional group bands present in the least absorptive DOM isolate spectra (September 2013, early morning, Lake Room) were selected as indicative of the most highly processed, refractory OM in the karst groundwater system, and were dominated by aliphatic esters and alkane groups. Esters are relatively stable to hydrolysis reactions and have previously been reported to persist in streams at circumneutral pH (Neilson, 2008). Here, the highest concentrations of esters occurred in non-photo-degraded recharge waters, and may represent the esterification of phytol, a plant-based, branched-chain alcohol produced during chlorophyll metabolism (Santos et al., 2013). Alkanes are stable, simple hydrocarbons produced by bacteria, algae, aquatic macrophytes, and terrigenous plants (Bianchi and Canuel, 2011). Alkanes serve as internal energy and carbon storage compounds in certain strains of bacteria of the genus

*Micrococcus*, *Neisseria*, *Pseudomonas*, *Acinetobacter*, and several actinomycetes, and are utilized during periods of C-starvation (Rontani, 2010).

The carboxyl group is the most highly reactive, oxygen functional group in natural OM, due to its charge, acidity, and surface binding capacities (Abdulla et al., 2010; Cabaniss, 1991; Leenheer et al., 1995). Carboxylic acids and carboxylates formed strong bands in all the Cascade Cave system DOM isolates, with the exception of the late summer, low flow samples. Using $^{13}C$ and $^{15}N$ CPMAS NMR, Lankes et al. (2008) found strong molecular associations between polysaccharide, amide, and carboxyl group signals, leading them to suggest that carboxyls are part of all the structural components of natural OM, and their characteristic spectral signals are the result of biogenesis or oxidative by-products. Indeed, carboxyl to phenol and ester ratios in the Cascade Cave system DOM isolates co-varied at all points sampled along the flow path, and the lack of carboxyls in late summer reflects the lowest quality, most extensively-degraded DOM. The relationships between functional groups in the Cascade Cave system DOM isolates are explored further below with respect to the working hypotheses.

### 4.4.1 Hypothesis 1: Seasonal hydrologic variations and temperature perturbations affect DOM quality and the efficiency with which DOM is processed in the subsurface

DOM quality and quantity in recharge waters varied seasonally, spatially, and diurnally, but generally became more aromatic with warming soil and water temperatures, and increased photosynthetic activity. Early winter vs late winter DOM isolate spectra from FF were poorly differentiated from the cave stream isolate spectra due to dilution effects. Surface recharge contained aromatic esters and phenols in March that were strongly preserved in the June ECB DOM isolate. The similarity between surface and cave stream DOM spectra during the cold season recharge indicated that surface recharge was less influenced by photo-degradation, due to

weaker UV radiation in winter, and by reduced microbial activity due to low temperatures and shorter water residence times (<24 hr). Surface recharge at FF was more enriched in macromolecular groups (including polysaccharides) in March for the only time during the study, and the DOM isolate spectra exhibited the transformation of aromatic esters at FF to acetyl esters at LR indicative of microbial processing.

Comparison of the DOM quality of recharge waters in summer months indicated that aromaticity peaked in early summer and reverted to more aliphatic character during the hot, dry, low flow conditions of late summer. The macromolecular composition of recharge DOM during early summer low flow conditions was dominated by aromatic esters, amides and polysaccharides. In late summer, the DOM composition of recharge waters was more aliphatic than earlier in the season, consistent with photo-degraded excretions from algae and heterotrophic grazers, the main sources of autochthonous organic matter in small lakes and streams (Thurman, 1985). DOC concentrations were greatest in the surface stream and lowest in the cave stream in summer, consistent with trends identified in comparable headwater catchments and subsurface drainage systems where the greatest annual [DOC] flux was measured during low flow (Bellmore et al., 2015; Wilson et al., 2013). Maximum [DOC] flux also coincided with the lower DO and higher specific conductivity concentrations present during low flow conditions. [DOC] was reduced to 32%-50% in summer, and to 76%-90% in winter, which supports the hypothesis that low temperatures and high flow conditions impair the efficiency of microbial biodegradation processes along the flow path from FF to LR.

Examination of DOM isolates in recharge waters sampled during the day (i.e., in shaded and unshaded stream channels) and at night revealed distinct diel differences in DOM quality. Non-photodegraded recharge from ECB (June 2014) contained abundant aromatic esters, amide

I, phenol, and polysaccharide macromolecular groups that were not present in the FF DOM isolate. FF recharge isolated at night (September 2013) was enriched in aliphatic ester, amide II, phenol, alkane, and polysaccharide groups relative to the isolate collected 12 hours earlier. Prior research found evidence of diel rhythms in surface water bodies, due to phytoplankton release of amino acids followed by nocturnal uptake by bacteria (e.g., Burney, 1994). The findings herein indicate that all macromolecular functional groups in stream DOM are subject to photodegradation, and that aromatic macromolecules are both easily photo-ionized and microbially transformed. The macromolecular composition of the photodegraded DOM isolates from FF were so similar to those from LR, that the extent to which DOM was turned over along the flow path was not obvious until fresh inputs (ECB) and additional sampling locations (JC) were considered. This portion of the research supports Hypothesis 1 and underscores the need to investigate groundwater recharge dynamics in more detail using continuous monitoring networks and high-resolution DOM characterization methods.

### 4.4.2 Hypothesis 2: Specific macromolecular indicators of DOM degradation exhibit decreasing IR absorbance with extended residence time and transport in the subsurface

Decomposition models proposed by Baldock et al (1992) and others (Kalbitz et al., 2003; Moorhead et al., 2006) for soil OM predict the preferential breakdown of proteins and carbohydrates during early stages of degradation, leaving lignin and alkyl C residues in partially decomposed OM, and finally the loss of lignin and accumulation of recalcitrant structures in the most decayed, smallest size fraction of OM. In this study, FTIR spectroscopy enabled the identification of specific macromolecular compounds in DOM isolates associated with DOM turnover by microbial activity. The most illuminating indication of DOM transformation along a relatively short section of the groundwater flow path is the transition of DOM macromolecular

structure in fresh ECB recharge to JC (Figure 4.7). From the sink point of ECB to the upstream access point in JC, DOM compositional structure became enriched in amide I, amide II, phenolic, and polysaccharide functional groups, whereas [DOC] declined by 11% (an estimated 7-hour transit time) which suggests that [DOC] is not always a representative surrogate for DOM quality. Macromolecular structural transformations between JC and LR included a nearly complete loss of amide I, phenols, and polysaccharides, with a decline in [DOC] of 18% (transit time of 16 – 22 hours) based on the velocity calculations from Chapter 3.

The behavior of amide I, phenols, and polysaccharides in the DOM isolate spectra from ECB to JC, and their absence downstream in the LR, regardless of the multiple in-feeders that contribute fresher DOM, indicated that these labile constituents were added during recharge through the epikarst and rhizosphere, and recycled relatively rapidly by microbial processing in the cave stream.

Statistical analyses indicated similarity between carboxyls, esters, and phenols, and dissimilarity to amide groups represent potentially quantifiable relationships between labile DOM quality and macromolecular structure despite the close association of macromolecules in DOM. Phenol:carboxyl ratios used to estimate terrigenous plant inputs were always high in the FF DOM isolate, and amide:carboxyl ratios were typically higher in LR, which suggested that lignin components were easily degraded by microorganisms in the cave stream Linear relationships between phenols, carboxyl groups, and alkanes suggested the progressive transformation of fresh plant OM to a semi-labile form, that reached a seasonal low in late summer, as demonstrated by aliphatic ester and alkane bands indicative of low bioavailability and bioreactivity. Thus, in this study, the loss of amide I along the flow path, and the prominence of alkanes and aliphatic esters in late summer, low flow DOM isolates were

indicative of highly degraded, semi-labile organic matter. With additional data, these OM changes could prove to be useful indicators of microbial processing in karst systems.

### 4.4.3 Hypothesis 3: Dissolved organic carbon-to-total-nitrogen ratios (OC:TN) decrease downstream coincident with microbial processing and by-product formation

Dissolved nitrogen content increased consistently throughout the cave system across all seasons and hydrologic conditions, and suggested that organic nitrogen compounds play an important role in the formation of semi-labile aquatic DOM. According to a recent literature review of carbon to nitrogen ratios from different locations and sources, including the Gulf of Mexico and selected rivers (13-29) versus bacteria and phytoplankton (3.7-6.6) (Maie et al., 2006), the decreasing OC:TN values along the flow path reflected the increased predominance of microbial DOM from FF and ECB to LR. Accumulating N content in DOM has also been observed in estuaries (Benner, 2002; Bronk, 2002; Hedges et al., 1997) and can be explained by a combination of several processes including autochthonous production (Thomas, 1997) and decomposition of bacterial necromass (McKnight et al., 1994), which have been shown to elevate the N concentration in organic acids. Polyphenols and proteinaceous compounds from aquatic plants have also been correlated with DON fluxes (D'Orazio et al., 2009; Maie et al., 2006), and may be protected from biotic consumption through some type of DOM encapsulation mechanism (Knicker et al., 1997; Nguyen et al., 2003)

Another explanation may be related to the ultra-low IR absorbance in nocturnal DOM isolates from LR from September 2013. During daylight hours, inputs from periphyton and plants were photodegraded and of lower quality, but at night the DOM in FF recharge was of high quality and had a non-photodegraded composition that was completely absent in the cave stream. This discrepancy could be indicative of an increase in microbial activity due to priming

effects (Kuzyakov, 2010; Kuzyakov et al., 2000), which may be driven by the fresh surface water inputs. Rhizo-depositional processes cycle on a diurnal basis (Kuzyakov, 2010), and also contribute pulses of highly labile DOM as root exudates that enhance soil OM degradation and leach excess ON to groundwater (Chen et al., 2008; Kuzyakov et al., 2000). The rapid transformation of DOM composition between ECB and JC may signal biochemical hotspots or "hot moments" in the critical zone, where localized biochemical processes are accelerated (e.g., McClain et al., 2003) due to priming effects in which labile OM interacts with more recalcitrant OM to enhance decomposition (Guenet et al., 2010). More data will be required to confirm this single observation, but it presents a venue for future research in the epikarst and near-surface groundwater systems that could fill in knowledge gaps about recharge mechanisms and other critical zone processes.

Finally, heterotrophic bacterial cells are highly efficient at taking up organic and inorganic nutrients, yet the small cells in oligotrophic systems have little intrinsic storage capacity and are adapted to low nutrient conditions. Downstream DOM at LR may reflect C-limited conditions where increased levels of ON exceed bacterial uptake capacity at end of the cave stream flowpath. The persistence of ON compounds in freshwater systems has been previously reported, and linked to both DOM recalcitrance (Kellerman et al., 2015; Roberts et al., 2006) and "leaks" in the food web (Neff et al., 2003).

## 4.5 Summary

Macromolecular functional groups indicative of OM decomposition were isolated from surface-derived recharge and cave stream DOM using a weak anion exchange resin (DEAE). The aim of this research was to refine a field-based protocol for tracing microbially-induced DOM transformations from recharge to discharge in an oligotrophic karst groundwater system,

and to incorporate carbon cycle processes into a hydro-ecological monitoring framework. Changes in the IR absorption intensities of carboxyl groups, esters, amides, alkanes, phenols, and polysaccharides in the DOM isolates were analyzed relative to hydrologic conditions, geochemistry, season, and location along the flow path from a sinking surface stream to the resurgence of a cave stream. The relative contribution of macromolecular functional groups varied with season, DOM freshness, and flow conditions; however, the most informative data were collected during summer, low-flow conditions under less surface water dilution from rainfall and snow melt, and longer water residence times. Late summer DOM isolates were aliphatic in character, as opposed to winter and late spring isolates, which were more aromatic. A statistically significant (P-value $<0.05$) decrease in DOC concentration between surface recharge and the downstream cave stream was documented during summer, low-flow conditions when water transit times through the cave were on the order of days to weeks.

Unmeasured OM recharge most likely masked rapid DOM turnover (as [DOC]) until non-photodegraded recharge from other sinking streams in the catchment was considered. Contributions from rhizo-deposition to DOM inputs along the flowpath may have been initially underestimated in this study, as inferred from sharp increases in amide I, phenols, and polysaccharides in recently recharged groundwater near the upstream end of the cave stream (early spring). DOC concentration was not a representative surrogate for high DOM quality in fresh recharge (upper cave); however, in the lower segment of the flow path, nearly 40% of DOC in fresh recharge was rapidly turned over in less than 24 hours, resulting in the loss of amide I, structural alterations of amide II, and 13% to 15% reductions in ester and phenol macromolecules.

The most extensively-degraded DOM (based on FTIR absorbance spectra) primarily contained alkanes, aliphatic ester groups, and organo-silicate compounds, which were interpreted as components of semi-labile, relatively low-quality DOM. The nearly complete degradation of DOM in nocturnal isolates indicated that cycles of higher microbial activity occurred, possibly driven by the priming effects of fresh, un-photodegraded DOM from the surface and root zone. This may be the first known report of possible priming effects in a karst groundwater system, and warrants additional future research. Organic carbon to nitrogen ratios decreased along the flow path during all seasons, from an average 7.7 on the surface to 2.7 in the cave stream. In addition to the progressive transformation and loss of amides, phenols, certain polysaccharides, the OC:TN and spectral signature of semi-labile DOM are potential bioindicators of microbial processing in groundwater that can be monitored over time and space in low-carbon groundwater systems.

## Chapter 4 Appendix

Table 4.1 Geochemical and physicochemical data from all samples.

| Sample Site | Date (year-month) | Temp (°C) | pH | Dissolved Oxygen | Alkalinity (as $CaCO_3$ ) | Cond. (µS $cm^{-1}$) | Cl | $SO_4^{2-}$ | $NO^{3-}$ | $Na^+$ | Mg+ | Ca+ | $K^+$ |
|---|---|---|---|---|---|---|---|---|---|---|---|---|---|
| Fort Falls (n = 11) | 12-Oct | 14.2 | 7.8 | 8.9 | 168.6 | 416 | 25.88 | 34.68 | 0.48 | 8.57 | 11.19 | 50.68 | 4.56 |
| | 12-Dec | 5.3 | 8.2 | 12.0 | | 248 | 9.48 | 34.59 | 1.78 | 9.71 | 7.86 | 25.83 | 2.61 |
| | 13-Feb | 4.8 | 6.6 | . | | 237 | 20.12 | 48.98 | 3.96 | 11.24 | 7.85 | 19.98 | 2.01 |
| | 13-May | 21.2 | 7.3 | 5.5 | 162.5 | 389 | 34.28 | 31.06 | 0.30 | 12.88 | 10.70 | 39.78 | 3.56 |
| | 13-Jun | 23.8 | 7.2 | 6.9 | | 376 | | | | | | | |
| | 13-Sep | 19.1 | 7.5 | 7.6 | 127.4 | 368 | 24.76 | 29.28 | | 8.78 | 9.50 | 42.78 | 3.82 |
| | 13-Oct | 16.8 | 7.7 | 9.3 | 125.4 | 325 | | | | | | | |
| | 14-Jan | 5.4 | 6.7 | 11.4 | | 178 | | | | 12.54 | 6.50 | 12.84 | 2.54 |
| | 14-Mar | 12.5 | 7.0 | | | 270 | | | | | | | |
| | 14-May | 27.9 | 7.6 | 5.0 | | 337 | | | | | | | |
| | 14-Jun | 26.2 | 7.2 | 2.7 | | 154 | | | | | | | |
| Mean | | 14.3 | 7.4 | 7.2 | 144.6 | 284 | 21.29 | 35.12 | 1.00 | 10.48 | 8.78 | 28.81 | 3.06 |
| Std.Dev | | 8.2 | 0.5 | 3.0 | 19.7 | 81 | 9.1 | 7.8 | 1.7 | 1.9 | 1.8 | 14.70 | 1.0 |
| ECB (n=1) | 14-Jun | 25.3 | 7.2 | 3.7 | | 355 | | | | | | | |
| Jones Cave (n=9) | 12-Oct | 14.2 | 8.1 | 10.1 | 122.4 | 405 | 24.84 | 32.84 | 1.11 | 7.45 | 11.15 | 50.85 | 4.06 |
| | 13-May | 12.8 | | | 121.0 | 269 | 22.85 | 20.7 | 0.34 | 10.47 | 10.53 | 40.47 | 2.37 |
| | 13-Jun | 18.4 | 7.0 | 7.4 | | 341 | | | | | | | |
| | 13-Sep | 17.9 | 7.5 | 7.5 | 110.3 | 326 | | | | 10.40 | 8.94 | 40.80 | 4.30 |
| | 13-Oct | 15.2 | 7.7 | 9.3 | 152.0 | 194 | | | | | | | |
| | 14-Jan | 5.2 | 7.4 | 11.9 | | 140 | | | | 8.44 | 4.24 | 7.45 | 1.83 |
| | 14-Mar | | | | | | | | | | | | |
| | 14-May | 15.9 | 7.3 | 5.9 | | 315 | | | | | | | |

Table 4.1
Cont.

| Sample Site | Date | Temp (°C) | pH | Dissolved Oxygen (mg $L^{-1}$) | Alkalinity (as $CaCO_3$ ) | Cond. (µS $cm^{-1}$) | Cl | $SO_4^{2-}$ | $NO^3$ | Na | Mg | Ca | K |
|---|---|---|---|---|---|---|---|---|---|---|---|---|---|
| Jones Cave | | | | | | | | | | | | | |
| Mean | | 13.5 | 7.5 | 7.99 | 125.5 | 280.4 | 23.83 | 26.07 | 0.61 | 9.10 | 8.17 | 28.12 | 2.95 |
| Std.Dev | | 3.8 | 0.32 | 2.13 | 15.5 | 83.8 | 1.41 | 8.59 | 0.54 | 1.49 | 3.13 | 18.92 | 1.23 |
| Lake Room | 12-Oct | 11.9 | 8.1 | 9.6 | 122.5 | 338 | 20.40 | 21.25 | 2.05 | 6.24 | 6.53 | 46.58 | 2.87 |
| | 12-Dec | 7.8 | 8.5 | 12.5 | | 227 | 4.83 | 20.16 | 1.29 | 7.69 | 6.16 | 28.48 | 2.30 |
| (n=11) | 13-Feb | 5.8 | 7.0 | n.a. | | 201 | 15.86 | 43.39 | 1.52 | 9.09 | 5.93 | 21.88 | 1.78 |
| | 13-May | 12.0 | 7.8 | 9.0 | 205.0 | 319 | 20.12 | 18.23 | 1.72 | 8.08 | 6.51 | 42.30 | 1.75 |
| | 13-Jun | 15.7 | 7.3 | 7.9 | | 310 | | | | | | | |
| | 13-Sep | 15.2 | 7.6 | 6.4 | 127.4 | 335 | 19.33 | 21.78 | 1.59 | 10.58 | 8.42 | 56.84 | 3.17 |
| | 13-Oct | 13.7 | 7.7 | 7.8 | 133.95 | 270 | 19.58 | 21.18 | 1.65 | 9.94 | 7.26 | 47.53 | 2.47 |
| | 14-Jan | 3.9 | 7.6 | 12.2 | | 160 | | | | | | | |
| | 14-Mar | 5.6 | 6.8 | n.a. | | 267 | | | | | | | |
| | 14-May | 13.8 | 7.9 | 6.4 | | 304 | | | | | | | |
| | 14-Jun | 15.5 | 7.0 | 4.8 | | 230 | | | | | | | |
| Mean | | 10.3 | 7.5 | 8.42 | 143.88 | 261.85 | 15,11 | 23.21 | 1.62 | 8.48 | 6.75 | 38.61 | 2.33 |
| Std. Dev. | | 4.1 | 0.47 | 2.54 | 33.61 | 20.51 | 0.17 | 0.42 | 0.42 | 0.45 | 0.82 | 6.59 | 0.49 |

Table 4.2 Inorganic and organic nutrient concentrations in the Cascade Cave system.

| Sample Site | Date | TIC | DIC | TOC | DOC | TN | DN | OC:TN |
|---|---|---|---|---|---|---|---|---|
| | 12-Dec | 32.42 | 32.08 | 2.55 | 2.38 | n.a. | n.a. | - |
| FF | 13-Feb | 19.34 | 19.29 | 2.47 | 2.05 | n.a. | n.a. | - |
| (n=6) | 13-May | 51.55 | 51.70 | 4.34 | 4.68 | 0.40 | 0.43 | 10.88 |
| | 13-Sep | 59.60 | 59.50 | 2.87 | 2.91 | 0.35 | 0.34 | 8.56 |
| | 14-Mar | 23.20 | 21.70 | 1.86 | 1.99 | 0.59 | 0.53 | 3.75 |
| | 14-Jun | 61.66 | 60.99 | 2.61 | 2.88 | 0.34 | 0.38 | 7.58 |
| | | (±18.67) | (±18.87) | (± 0.83) | (±0.99) | (±0.12) | (±0.08) | |
| ECB | 14-Jun | 74.51 | 73.97 | 1.86 | 1.95 | 0.28 | 0.22 | 8.86 |
| | 13-May | 49.96 | 51.28 | 2.93 | 1.75 | 0.41 | 0.54 | 3.24 |
| JC | 13-Sep | 55.72 | 55.07 | 2.85 | 2.85 | 0.56 | 0.55 | 5.18 |
| (n=3) | 14-Jun | 56.74 | 57.00 | 1.75 | 1.73 | 0.49 | 0.50 | 3.46 |
| | | (±3.66) | (±2.91) | (±0.66) | (±0.64 | (±0.08) | (±0.03) | |
| | 12-Dec | 36.28 | 34.34 | 2.33 | 1.81 | n.a. | n.a. | - |
| LR | 13-Feb | 24.13 | 24.10 | 2.03 | 1.78 | n.a. | n.a. | - |
| (n=6) | 13-May | 56.42 | 51.10 | 1.41 | 1.49 | 0.49 | 0.59 | 2.53 |
| | 13-Sep | 60.50 | 58.53 | 1.43 | 1.48 | 0.59 | 0.62 | 2.39 |
| | 14-Mar | 30.10 | 32.78 | 1.63 | 1.80 | 0.65 | 0.53 | 3.40 |
| | 14-Jun | 54.16 | 54.08 | 1.47 | 1.42 | 0.55 | 0.54 | 2.63 |
| | | (±15.34) | (±13.89) | (±0.38) | (±0.18) | (±0.07) | (±0.04) | |

All units in mg $L^{-1}$. n.a. = not analyzed Standard deviation shown in parentheses.

Figure 4.1. Photographs of field DOM isolation set-up on the surface at Fort Falls (left), and in Cascade Cave (center), with close-up of filter and stacked tubes (right).

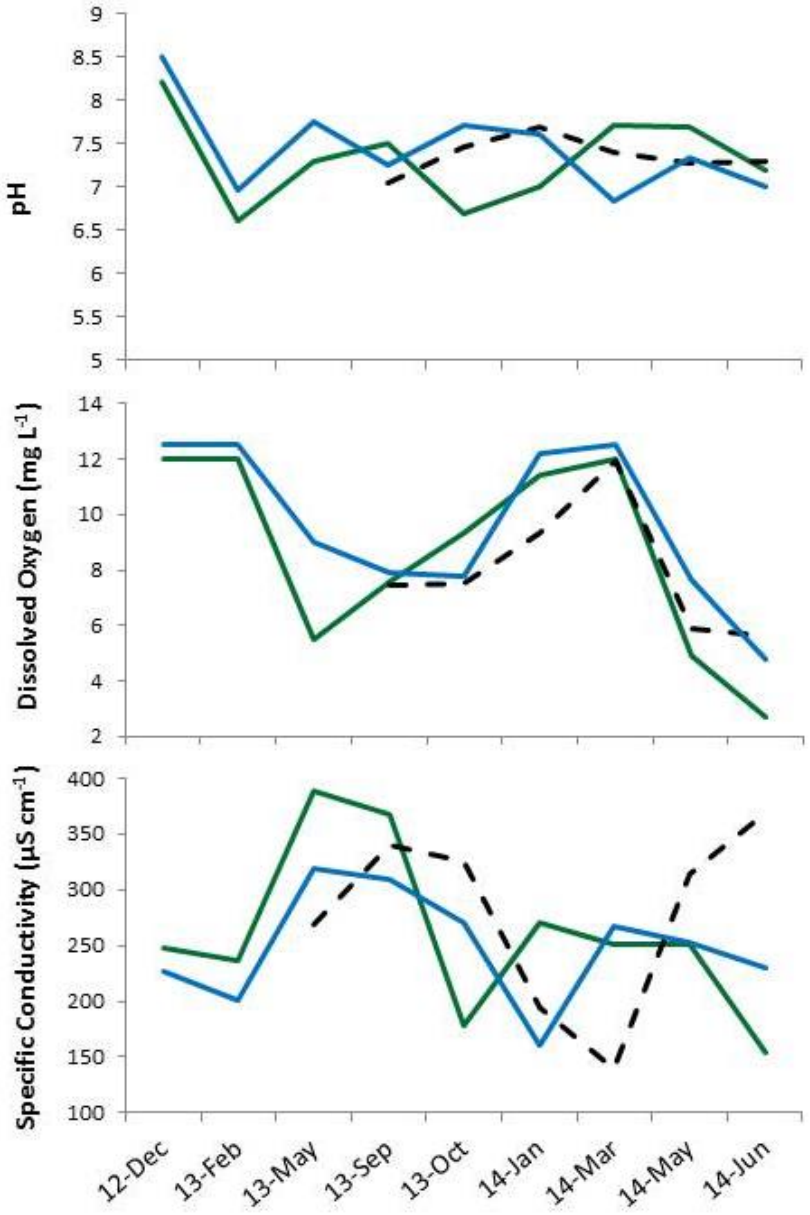


Figure 4.2. Time series plots, from top to bottom, of pH (semi-log), dissolved oxygen and specific conductivity (µS $cm^{-1}$) along the Cascade Cave system flow path. Green lines, water at the recharge point Fort Falls; dashed lines, water in Jones Cave; solid lines, water in the Lake Room of Cascade Cave.

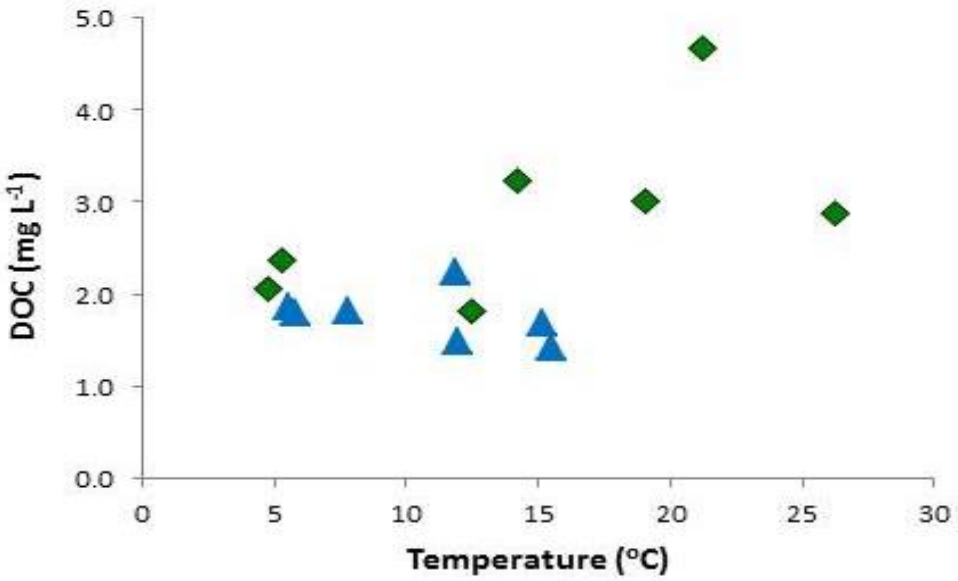


Figure 4.3. Seasonal relationships between DOC (units mg $^{-1}$) and temperature at the surface recharge point of Fort Falls (FF) (green diamonds) and at the Lake Room (LR) in Cascade Cave (blue triangles). Data from Oct. 2012 – June 2014.

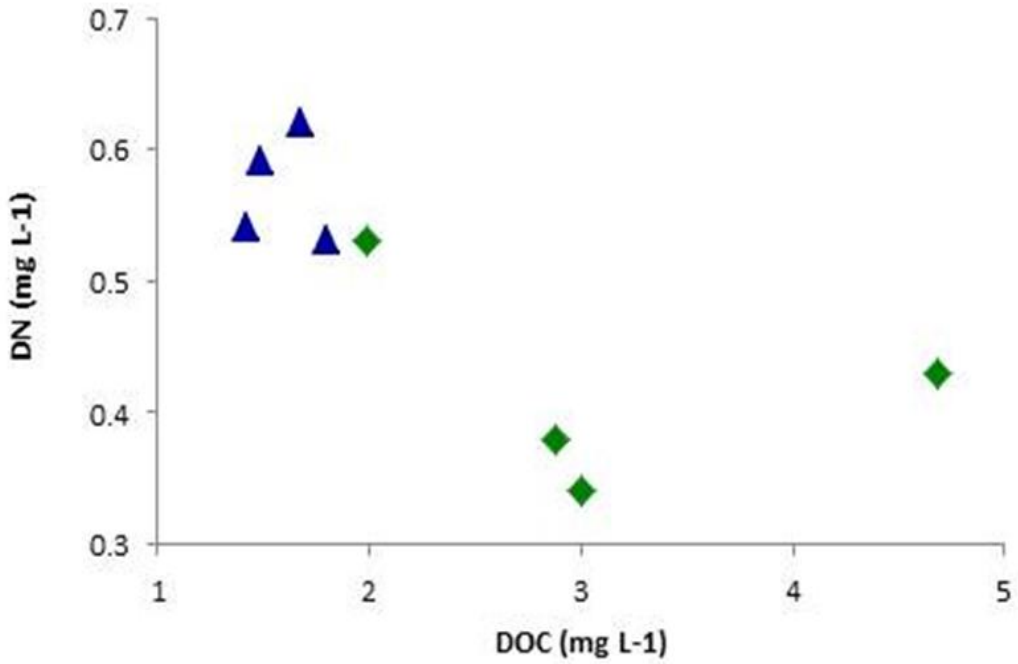


Figure 4.4. Seasonal relationships between DOC and DN (units mg $^{-1}$) at the surface recharge point of Fort Falls (FF) (green diamonds) and at the Lake Room (LR) in Cascade Cave (blue triangles) in 2013-2014.

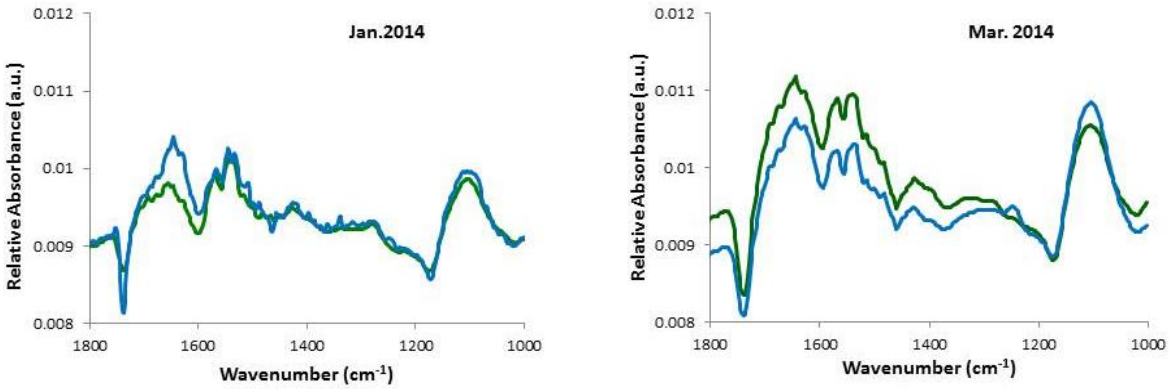


Figure 4.5. FTIR spectra of DOM isolates from Fort Falls (green) and Lake Room (blue) in early (left) and late (right) winter, and under high flow conditions (~ 0.006 $m^3 s^{-1}$ .

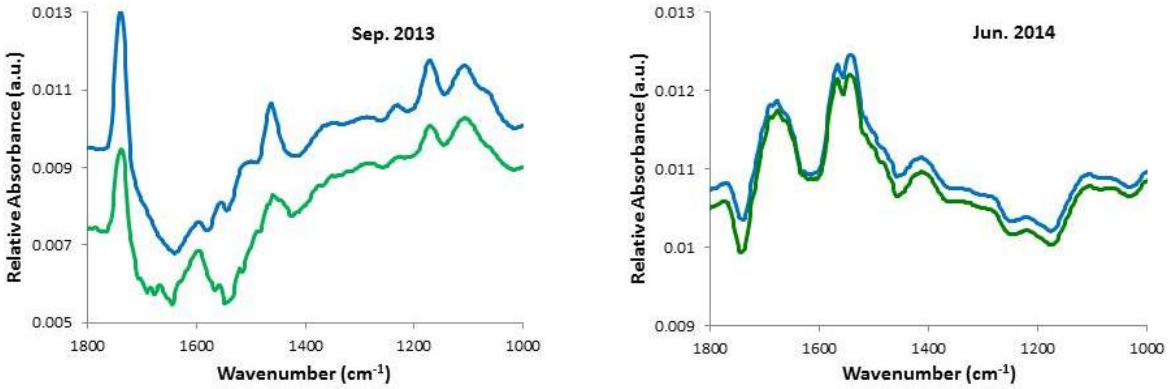


Figure 4.6. FTIR spectra of DOM isolates from Fort Falls (green) and the Lake Room (blue) in late (left) and early (right) summer to compare low flow conditions (~ 0.0006 $m^3 s^{-1}$).

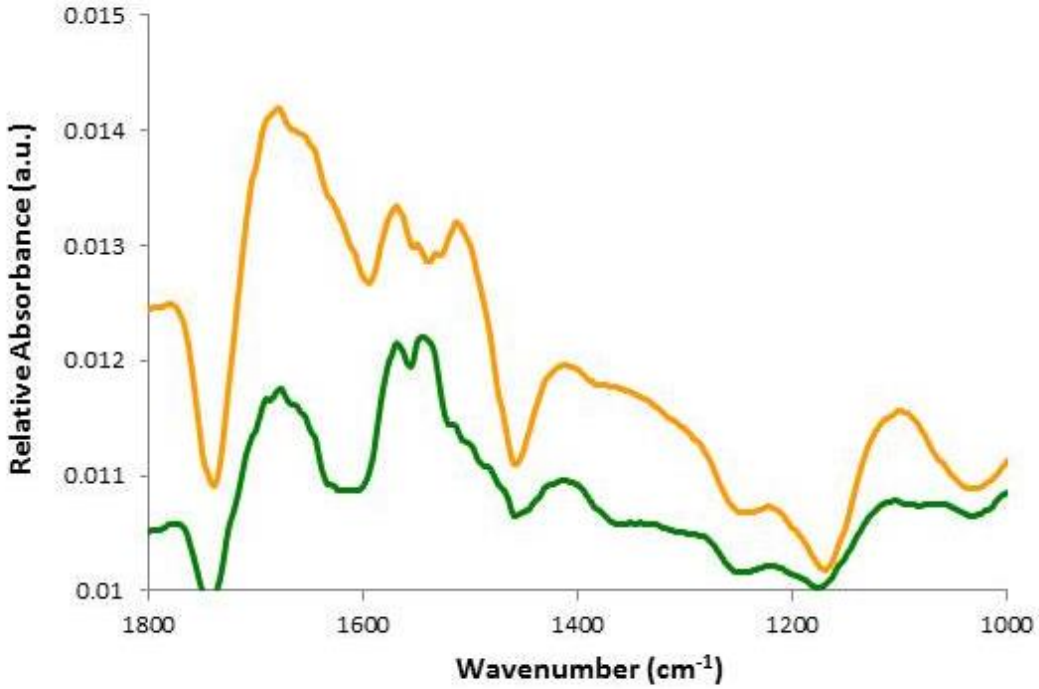


Figure 4.7. Comparison of FTIR spectra for DOM isolates from adjacent sinking stream inputs to the Cascade Cave system. Water samples from James Branch at Fort Falls (green) and Echo Canyon Branch (orange) were collected in daylight in June 2014.

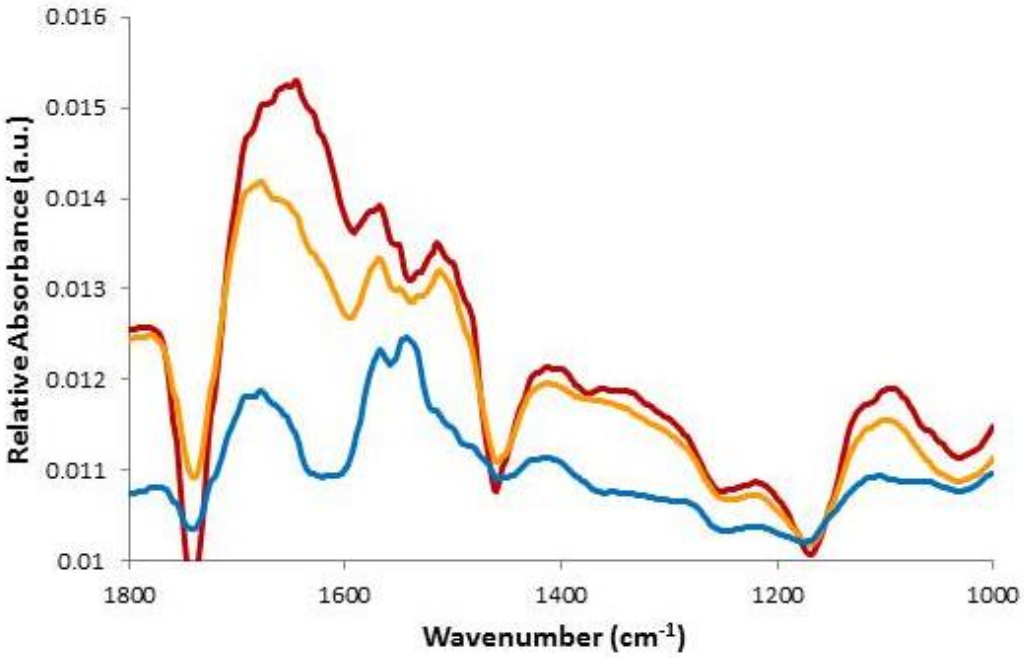


Figure 4.8. Change in DOM isolate spectra along the flow path from Echo Canyon Branch (orange) through Jones Cave (red) to the resurgence at the Lake Room (blue) in Cascade Cave. Water samples were collected during daylight in June 2014.

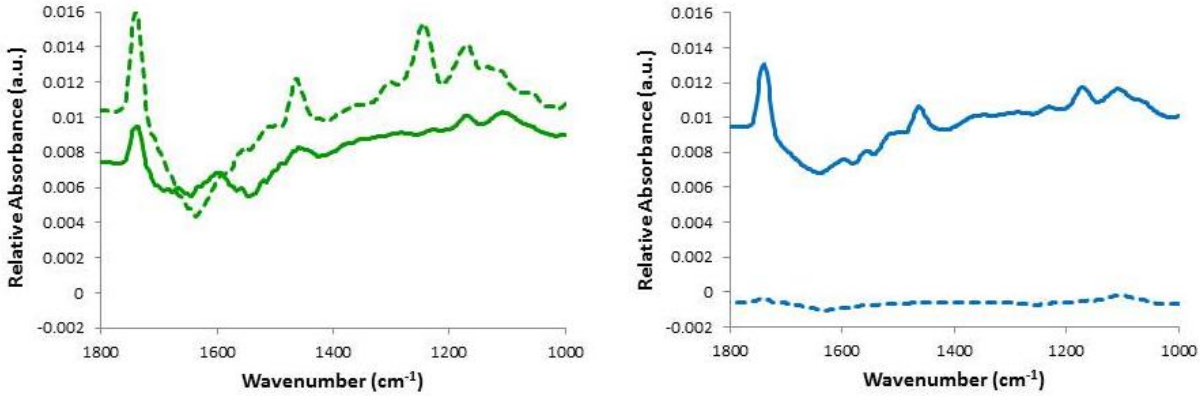


Figure 4.9. FTIR spectra of September 2013 DOM isolates: Left panel, Fort Falls at night (dashed) vs. day (solid); Right panel, Lake Room at night (dashed) vs. day (solid).

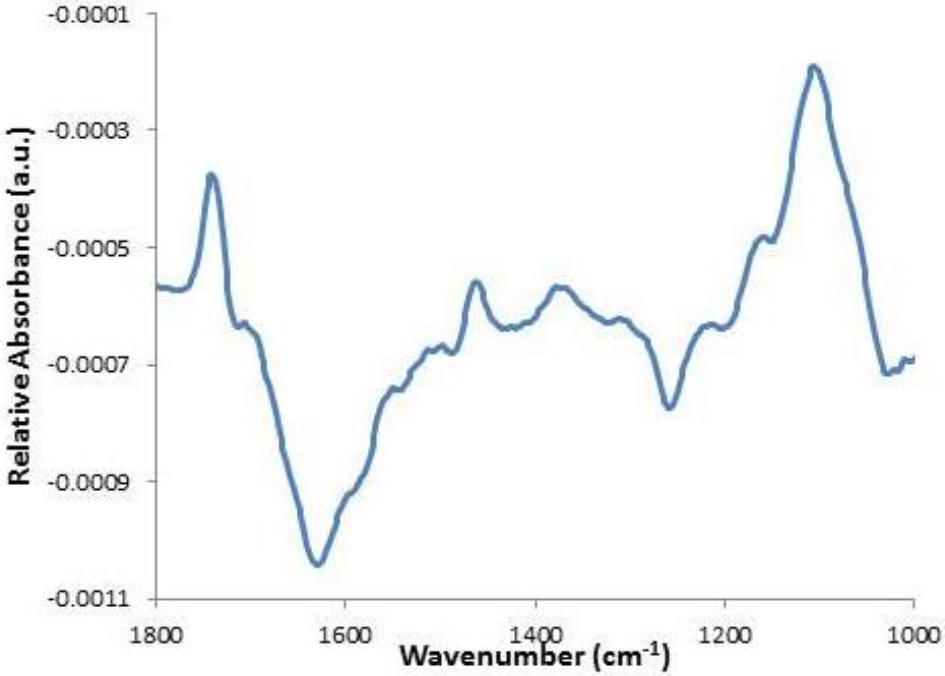


Figure 4.10. FTIR spectra of September 2013 DOM isolate from the Lake Room at night, expanded from Fig. 4.0.9 (above).

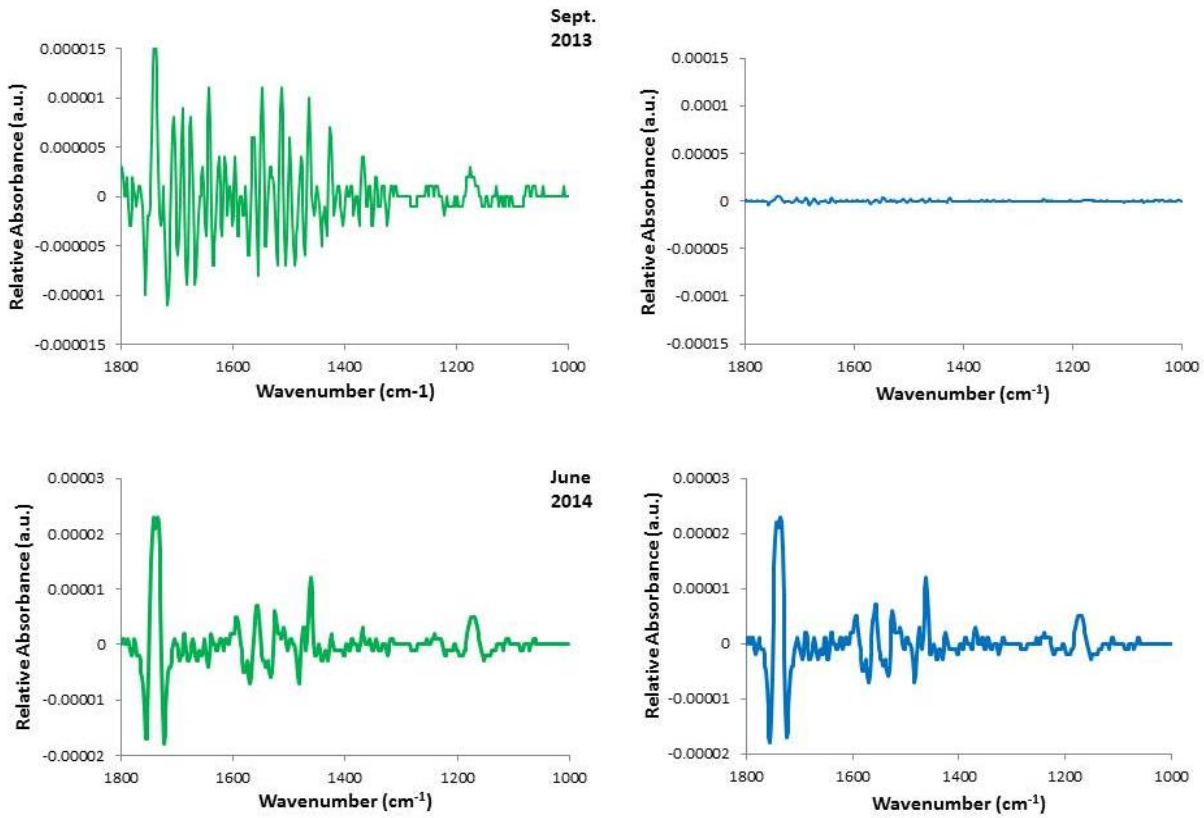


Figure 4.11. Second derivatives of DOM isolate FTIR spectra from James Branch at Fort Falls (green) and the Lake Room in Cascade Cave (blue).

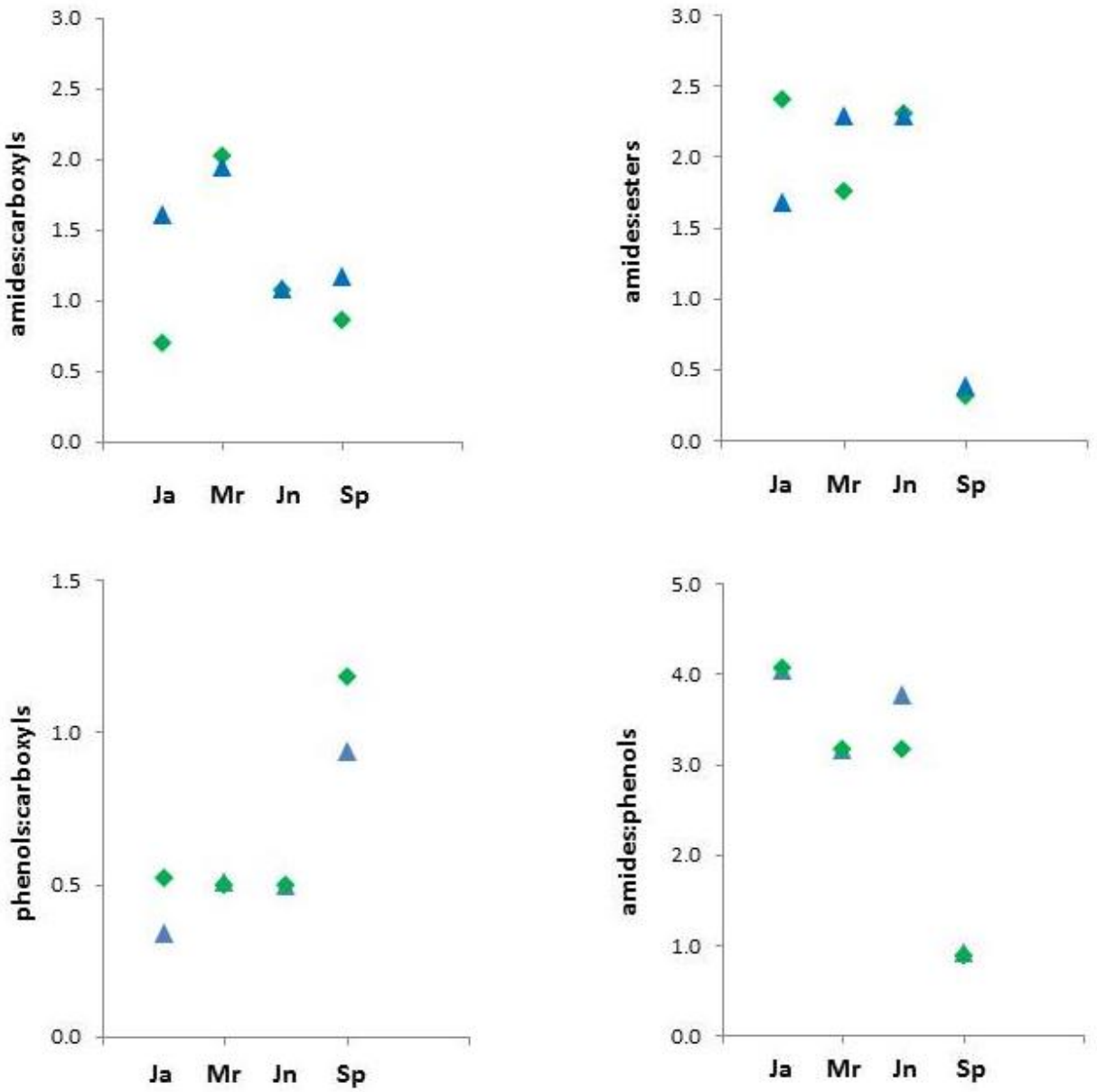


Figure 4.12. Functional group ratios for DOM isolates from surface recharge at Fort Falls (green) and the Lake Room (blue) in Cascade Cave for the four sample events.

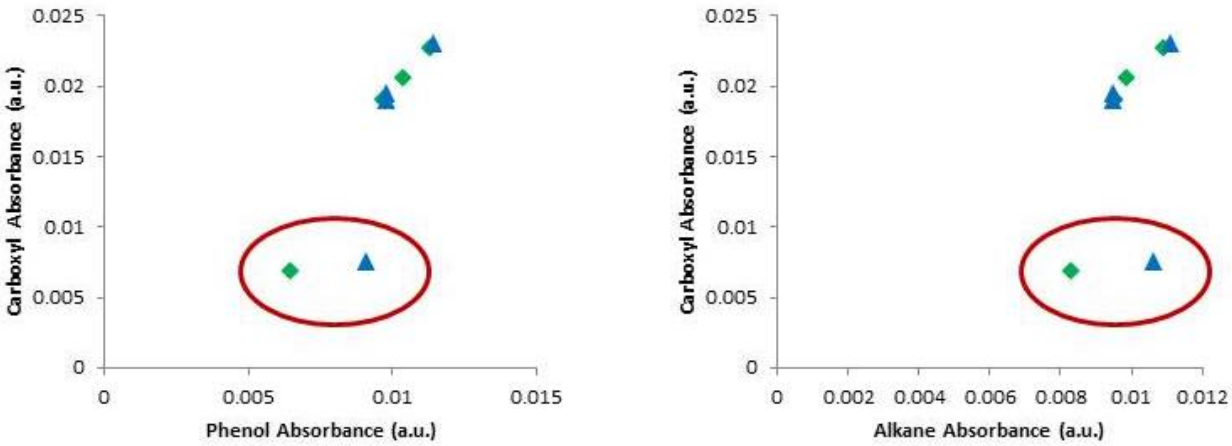


Figure 4.13. Relationship of DOM isolate carboxyl, phenolic, and alkane functional groups at Fort Falls (green) and the Lake Room (blue) in Cascade Cave. The Sept. 2013 DOM isolates are circled in red.

# Chapter 5. Lipid Biomarkers Revealed Rapid Microbial Community Response to Changing Environmental and Hydrological Conditions

## 5.0 Abstract

Phospholipid fatty acid (PLFA) profiles from the membrane lipids of filtered water (suspended) and sieved sediment (attached) samples in the Cascade Cave system indicated disparate configurations in the respective microbial communities. Biomass estimates were three orders of magnitude higher for the attached samples. The PLFA profiles revealed diverse microbial community structure although there is a strong Gram-negative ($Gram^-$) bacterial presence. The suspended community structure was dominated by monounsaturates, or $Gram^-$ bacteria, followed by polyunsaturated PLFA indicative of eukaryotic microorganisms (fungi, diatoms, algae, etc.) and terminally-branched saturated PLFA (Gram-positive bacteria ($Gram^+$). Meanwhile, the attached communities were dominated by monounsaturates, followed by mid-chain branched saturates and terminally-branched monounsaturated PLFA (sulfate- and metal- reducing bacteria and actinomycetes). A prominent difference in the $Gram^-$ community structure is the prevalence of 18-C monounsaturated PLFA in suspended fractions and the 16-C monounsaturated PLFA s in the attached fraction. The presence of eukaryotes (polyunsaturated PLFA) was prevalent in the suspended samples, and occurred in greater concentrations at Fort Falls prior to entering the cave (recharge).

The suspended microbial community exhibited elevated *trans*- to *cis*- and cyclopropane to precursor $Gram^-$ bacteria biomarker ratios for stress (transport, temperature) and nutrient limitation sensitive to groundwater recharge, flow velocities, and seasonal variations. These ratios plus the *iso*- to *anteiso*- ratios ($Gram^+$ bacterial biomarker) suggested microbial growth cycles and phases in suspended communities which may affect DOM transformation and degradation on a seasonal basis.

Attached communities were characterized by changes in the mid-chain branched

saturated and terminally-branched monounsaturated PLFA profiles with a predominance of Actinomycetes at the Fort Falls site during warm weather. Furthermore, increases in PLFA biomarkers indicative of anaerobic bacteria (sulfate and metal reducers) were associated with cooler temperatures and low flows in both the suspended and attached communities within this this bulk aerobic cave stream. This trend coincides with increases in sulfate concentrations. The attached samples cluster into two groups based on temperature.

PLFA biomarker ratios provided evidence for changes in cave stream microbial communities. Geochemical correspondence with certain PLFA classes suggest that the interaction of heterotrophy and chemoautotrophy in attached communities play an important role in nutrient cycling in surface water influenced groundwater systems.

## 5.1 Introduction

Microbial community structure in freshwater ecosystems is influenced by climate, land use, vegetation, and OM quality (e.g., Fierer et al., 2006; Martiny et al., 2006) along geochemical and environmental gradients (Findlay et al., 2008; Horner-Devine et al., 2004). Microorganisms have multiple mechanisms to adapt to rapidly changing environmental conditions, such as sudden fluctuations in temperature, water and nutrient availability, and exposure to toxic compounds, including their own metabolic by-products (Sigee, 2005). Most of these mechanisms involve transcriptional adjustments to the composition of a class of lipids, known as polar phospholipids, which are specialized structural components of cell membranes that can serve as biomarkers of certain prokaryotic and eukaryotic taxa, indicators of stress response, and that represent viable cells (Bossio et al., 1998; Tunlid et al., 1990).

Changes to the bacterial cell membrane lipid bilayer can reversibly alter cell membrane

rigidity and provide protection from dehydration, osmotic stress, and cold shock, etc. (Ramos et al., 2001). Such transformations can mirror shifts in microbial community structure that have been linked to the natural attenuation of petroleum contamination and explosive ordnance (e.g., Hazen et al., 2010; Ringelberg et al., 2008), fluctuating hydrologic conditions in salt marshes and estuaries (Hernandez et al., 2001; Keith-Roach et al., 2002); seasonal dynamics in forested/pristine catchments (Mosher et al., 2011; Schulze-Makuch et al., 2003; Schütz et al., 2009); and the strategies of microorganisms adapted to life in oligotrophic seawater (e.g.,Méjanelle et al., 2005). To this end, lipid biomarker analyses and phospholipid fatty acid (PLFAs) profiles offer a set of established, culture-independent methods to evaluate biochemical characteristics of microbial communities across environmental and geochemical conditions (Vestal et al., 1989; Volkman, 2006; White, 1995). PLFA are phenotypic analyses that provide a means to examine how microorganisms respond to disturbance and environmental stressors, have also been used to quantify living microbial biomass in seawater (Méjanelle et al., 2005; Volkman, 2006), estuaries (Guckert et al., 1985; Hernandez et al., 2001; White et al., 1977), groundwater (Onstott et al., 2006; Pfiffner et al., 2006), soils (Kaur et al., 2005; McKinley et al., 2005), sediments (Keith-Roach et al., 2002; White et al., 1979), and relatively impermeable sedimentary rocks (Fredrickson et al., 1997).

### 5.1.1 Definitions and Fatty Acid Biosynthesis

Lipids, as discussed here, are biomolecules composed of fatty acids that form *ester* linkages to glycerol (ether linkages associated with Archaea were not analyzed). As such, lipids are hydrophobic and insoluble in water. In nature, fatty acids are synthesized through the condensation of malonyl coenzyme A (CoA) by a fatty acid synthase complex, resulting in a carboxylic acid group attached to a straight or branched hydrocarbon chain commonly 12- to 22-

carbon atoms in length (Christie, 2015). Phospholipids are essential structural components of the cytoplasmic membranes that encapsulate cells and regulate the transmission of nutrients and metabolic byproducts. The cytoplasmic membrane is generally organized into a phospholipid bilayer interspersed with proteins (Figure 5.1), in which the glycerol-phosphate head groups of the fatty acids form hydrophilic outer regions, and the hydrocarbon tails comprise the hydrophobic inner region of the membrane (Madigan et al., 2012).

Fatty acids are either *saturated*, in which all carbon atoms are covalently bonded to hydrogen atoms, or *unsaturated*, where one or more double bonds are present between carbon atoms (Figure 5.2). Membrane lipids must maintain enough fluidity to allow diffusion and solute transport across the membrane, regardless of changing environmental conditions; thus, balanced fatty acid compositions are essential to the maintenance of appropriate membrane fluidity in dynamic environments (Kaneda, 1991; Ratledge et al., 1988). To accomplish this, certain fatty acids can rotate around the C-C bonds into a variety of configurations. Saturated fatty acids most often occur as straight chain structures, although branched-chain saturates (mostly associated with Gram$^+$ bacteria and mycobacteria) are also widely distributed in the environment. One or more double bonds (monounsaturated and polyunsaturated PLFAs) restrict the movement of the acyl chain, composed of oxygen double-bonded to hydrocarbons, so microorganisms have developed mechanisms to rapidly compensate for degrees of saturation in response to stressors, such as sudden changes in temperature, substrate quality, hydration state, or geochemistry (Gurr et al., 2002).

### 5.1.2 Fatty Acid Nomenclature

Lipid biochemistry has evolved from diverse disciplines of study, and formal, but complex, naming conventions have been established by the International Union of Pure and

Applied Chemistry (IUPAC) and the International Union of Biochemistry and Molecular Biology (IUBMB) (Gurr et al., 2002). Common names historically used in the literature have been replaced by more the specific systematic nomenclature, which describes the structure of lipids using carbon-chain length to establish root names, based on functional groups in the compounds. In systematic notation, carbon atoms are counted from the carboxylic acid end of the molecule, with the position of double bonds indicated with a z-notation, such as 9z-octadecenoic acid (IUBMB, 2015). Lipids have been named using the $\Delta^x$ (delta-x) system, in which double bond locations (counted from the carboxylic acid end) are indicated by the number x, and molecular configuration around the bond denoted by a *cis*- or *trans*- prefix, such as *cis, cis*-$\Delta^9$, $\Delta^{12}$octadecadienoic acid (Anneken et al., 2000). Literature on the nutritional and physiological effects of lipids typically used an n-x (n minus x), or ω-x, system for locating double bonds counted from the methyl end of the compound, such as the n-3 fatty acids with their double bonds located on the third carbon-carbon bond from the terminal methyl carbon (e.g.,Grey et al., 2014).

For the sake of simplicity, a common form of short-hand nomenclature is used here that identifies fatty acids by two numbers separated by a colon; the first number specifies carbon chain length, and the second denotes degree of unsaturation. Double bond positions following the symbol ω, denote the location of double bonds at certain carbon units counted from the methyl end of the molecule (Gurr et al., 2002). The position of the double bonds depends on the specific pathway of fatty acid biosynthesis, i.e., desaturation directed from the methyl end produces characteristic families of fatty acids (ω3, ω6, ω9) (Ruess et al., 2010). For example, 16:0 (hexadecanoate) is a saturated (no double bonds) fatty acid that is 16-carbon units in length, whereas 16:1 (hexadecenoate) is a monounsaturated (one double bond) fatty acid composed of

16-carbon units. Monounsaturate FAME may have a *cis* or *trans* configuration of the double bond, in which case the nomenclature would be expressed as 16:1ω7c or 16:1ωt, respectively. Mid-chain branched FAME are designated by a prefix, such as 10me16:0 (10-methyl hexadecanoate), where the first number indicates the location of the methyl branch. Terminally branched FAME have iso- or anteiso- designation depending on whether the methyl branch is located on the first or second carbon, respectively. Cyclopropyl FAME are designated with the prefix, cy.

### 5.1.3 Fatty Acid Classes and Biomarkers

More than 100 different fatty acids have been identified in natural lipids. Fatty acids are often grouped into classes based on their chemical structure and carbon chain length. PLFA classes can be associated with specific groups of organisms due to the particular enzyme complexes that carry out elongation reactions in fatty acid biosynthesis. Table 5.1presents the fatty acids commonly found in soils, sediments, and water, arranged by class and predominant biological source. Some fatty acids considered biomarkers for certain groups of organisms can occasionally be found, in minor amounts, in the lipids of other organisms (e.g., branched-chain and cyclopropyl fatty acids linked to $Gram^+$ and $Gram^-$ bacteria, respectively). Nonspecific PLFA, such as those in the normal saturates class, reflect the most common mechanisms of fatty acid metabolism among microorganisms and higher life forms, in which the carbon chain is elongated through the repetitive condensation of the primer, acetyl-CoA, by malonyl-CoA to produce hexadecanoate (16:0) as the main component of the lipid pool (Ratledge et al., 1988; Reilly, 2015; Ruess et al., 2010).

In addition to the quantification of PLFA classes to compare microbial community structure, higher resolution analyses are possible by focusing on individual fatty acids associated

with specific taxonomic groups (18:1ω8 for methanotrophs) and on potential biomarker fatty acid ratios (*trans/cis*) that reflect the physical state of cell membranes. This is because microorganisms respond to changing environmental conditions by rapidly adjusting their cell-membrane fluidity through alterations in phospholipid composition (Ramos et al., 2001). Ratios of the relative abundances of specialized fatty acids activated immediately during stress response can indicate microbial community structure, physiological status, and response to environmental conditions (Bossio et al., 1998; Guckert et al., 1986; Heipieper et al., 2010; Kieft et al., 1994).

The particular mechanisms employed in homeoviscous adaptations depend on the strain of microorganism and growth stage (Kieft et al., 1994). During the active growth phase, Gram$^-$ bacteria can convert unsaturated fatty acids to saturated fatty acids to protect the cell membrane from exposure to toxic solvents (Heipieper et al., 2010). Non-growing cells can also mimic unsaturated-to-saturated transformations in response to solvent, osmotic, or heat stress through the rapid (within 30 minutes) conversion of unsaturated fatty acids from *cis*- to *trans*- forms for greater membrane rigidity (Härtig et al., 2005; Maier et al., 2000). *Anteiso*-branched fatty acids respond similarly to unsaturated fatty acids by increasing in proportion relative to the *iso*-branched fatty acids during a drop in temperature, so community response to rising and falling temperatures may be reflected in the relative amounts of *iso*- and *antesio*- branched chain fatty acids. PLFA patterns of many bacteria and fungi (as well as other eukaryotes) show higher degrees of unsaturation in response to lower temperatures (and vice versa) in order to maintain adequate membrane fluidity (e.g.,Ruess et al., 2010).

In culture, cyclopropane fatty acids form enzymatically from *cis*- fatty acids over periods of several days and are thought to stabilize lipids from degradation and turnover during transition to stationary phase. The formation of cyclopropane fatty acids at the expense of monoenoic

precursor fatty acids has been used as an indicator for Gram$^-$ bacteria in starvation-survival mode (Bossio et al., 1998; Kieft et al., 1997). Cyclopropane formation, which is non-reversible, can also simulate increased saturation in response to rapidly increasing temperatures (Loffhagen et al., 2007), and is thought to improve the viability of slowly-growing cells in relatively harsh environments (Zhang et al., 2008).

### 5.1.4 PLFA Analysis Links Environment to DOM Quality

The results of Chapter 4 established that the active macromolecular groups in DOM include carboxyl groups, carbohydrates, amides, and esters, which also happen to be primary constituents of cellular membrane lipids in prokaryotes and eukaryotes. PLFA profiles are recognized as being highly sensitive to site-specific environmental conditions (Kieft et al., 1994; Ramos et al., 2001; D. C. White et al., 1998) and have recently been used to monitor stream quality (DeForest et al., 2016). Working in low-order streams draining forested catchments underlain by limestone and sandstone, Mosher and Findlay (2011) used PLFA analysis to correlate benthic microbial community structure with stream geochemistry and DOM quality, and found similar seasonal patterns in all streams. PLFA profiles from microbial communities in hyporheic zone sediments differed from those in nearby Columbia River (WA) waters, and also showed seasonal effects (Moser et al., 2003). Schütz et al. (2009) used PLFA analyses to better understand microbial degradation processes in the vadose zone of an artificial groundwater recharge facility adjacent to the Rhine River. Lane et al. (2013) used PLFA and $^{13}C$ labeling to determine that biofilms in oligotrophic limestone streams in the Ozarks were dominated by Gram$^-$ bacteria and were highly efficient processors of DOM. In this study, PLFA analyses were used as a rapid means of surveying microbial diversity across the respective surface stream and cave stream habitats, and enabled comparison of microbial community responses to

disturbance and stressors related to hydrologic conditions, geochemistry, and DOM quality. To my knowledge, this is the first application of PLFA profiling to the characterization of microbially-driven DOM transformations from surface water recharge to groundwater discharge in a cave system.

For the purposes of this research, relevant stress adaptive mechanisms in bacteria included *i*) changes in *trans/cis* isomerization of unsaturated fatty acids, *ii*) the formation of cyclic fatty acids containing cyclopropyl ring structures, and *iii*) changes in the *iso/anteiso* ratio of methyl branched fatty acids (e.g., Frostegård et al., 1993; Guckert et al., 1985; Kerger et al., 1986). PLFA analysis is a relatively rapid, inexpensive method that produces low rates of type-II errors (i.e., false negatives) in detecting differences in community structure compared with community-level profiling and DNA fingerprinting techniques (Ramsey et al., 2006). However, PLFA analyses do not provide the in-depth microbial identification associated with DNA methods. Overall, this research complements the isolation and analysis of dissolved organic matter (DOM) under high-flow and low-flow conditions to evaluate hydrologic influence on DOM source and quality, as well as how OM quality and structure are affected by biotic and abiotic transformations that occur along the subsurface flowpath, as described in Chapters 3 and 4 of this dissertation.

## 5.2 Objectives and Hypotheses

Freshwater ecosystems are recognized “hot spots” for nutrient cycling activity, especially at soil-water interfaces and surface water and groundwater regimes, where microorganisms are responsible for nutrient recycling but organic matter (OM) fluxes are largely unknown (Cole et al., 2007). The purpose of this research was to characterize the structure and physiology of

microbial communities at surface and subsurface sites in the James Branch – Cascade Cave study area, where sinking streams contribute terrigenous OM to the karst groundwater system, often with minimal filtration or retardation. PLFA analysis was performed to estimate suspended and attached microbial biomass quantitatively, to obtain fingerprints of the microbial community structure for comparison over space and time, and to identify seasonal indicators of microbial stress. PLFA profiles were used to discern community differences between sites (i.e., surface/upstream vs. cave/downstream) and types of samples, such as suspended (i.e., planktonic) and attached (i.e., benthic). Two main hypotheses were tested in this research.

First, Hypothesis 1 stated that suspended microbial communities would be dominated by eukaryotic organisms (e.g., plants, fungi, algae) and Gram$^-$ bacteria (e.g., r-strategists) on the surface; whereas, attached communities in the more nutrient-limited environment in the cave stream would be dominated by Actinobacteria, sulfate-reducing bacteria, and Gram$^+$ bacteria (e.g., k-strategists). Secondly, Hypothesis 2 stated that surface microbial communities would exhibit comparatively higher levels of stress indicators (*trans*-to-*cis* fatty acids and cyclopropyl to monenoic precursors) in the suspended fractions due to seasonal temperature extremes, transport and flow conditions, and other environmental factors. Conversely, bacterial adaptations in the attached communities would indicate stationarity and starvation relative to suspended communities, with the cave environment being the least variable. Finally, PLFA profiles and biomarker ratios were analyzed with respect to geochemistry, DOC concentration, DOM quality, season, and flow regime to elucidate relationships between microbial community status and structure in the dynamic karst system.

## 5.3 Methods

### 5.3.1 Water and Sediment Sampling

Water and sediment samples were collected seasonally from late 2012 through mid-2014 in the James Branch-Cascade Cave system, which was described in Chapter 1. Water and sediment samples from the surface stream, James Branch at Fort Falls (FF), and the cave stream of Cascade Cave, in the Lake Room (LR), were collected concurrently with the DOM isolation effort described in Chapter 4. Water was pumped directly from the source using a Geotech peristaltic pump with polyethylene tubing and filtered to 0.2 µm through 142 mm diameter Millipore (EMD Millipore, Merck KGaA, Germany) sterile polyvinylidene fluoride (PVDF) filters attached to a pre-sterilized polycarbonate in-line filter holder (Geotech Environmental Equipment, Denver, Colorado, USA). The suspended fraction of OM lipids was extracted from the filters, which were collected and placed in Whirl-pak® bags, labeled with source name/date/volume filtered, and frozen on a mixture of water ice and dry ice for transport to the laboratory.

The attached fraction of OM lipids was extracted from stream sediment samples, collected in duplicate at FF and LR (and at ECB and JC in June 2014). Sediments were scooped from the stream beds using solvent-rinsed, presterilized (by muffling at 450$^{o}$C for 6 hours) stainless steel spoons and were wet-sieved on-site in pre-sterilized sieves to retain the 90 µm - 500 µm size fraction of fine- to medium-grained sand. Sieved samples were transferred to sterile 50 mL Falcon tubes, placed in labeled Whirl-pak® bags, and frozen on a mixture of water ice and dry ice for transport to the laboratory. Both filters and sediments were stored at -80$^{o}$C until PLFA extraction.

### 5.3.2 PLFA Extraction and Analysis

In preparation for PLFA extraction, filters were thawed at room temperature in darkness, then aseptically cut in half, and transferred to glass 250 mL centrifuge bottles. All glassware used in extraction procedures was cleaned according to an intensive washing protocol and baked in a muffle oven at 450ºC for 6 hours (D. White et al., 1998). Frozen sediments were lyophilized in the dark (Labconco Model 7753000 FreeZone6 Freeze Dry System, Labconco Corporation, Kansas City, Missouri, USA), homogenized, weighed (to 25 g), and transferred to baked glass 250 mL centrifuge bottles. A known volume (50 µL) of the intact polar lipid, 1,2-dinonadecanoly-*sn*-glycero-3-phosphocholine in chloroform (Matreya LLC, State College, Pennsylvania, USA) was added as an internal standard for quality control to gauge the recovery efficiency of the extraction process for the FAME, nonadecanoate (19:0) (Keith-Roach et al., 2002).

Total lipids were extracted using a modified first-phase chloroform:methanol:aqueous buffer (2.0:1.0:0.8) method (Bligh et al., 1959; White et al., 1979) with high purity grade (Burdick & Jackson, Inc. Solvents for Gas Chromatography, $GC^2$) or equivalent solvents (Fisher Scientific). Extracts were incubated in the dark for 4 hours, separated via centrifugation, and decanted into 250 mL separatory funnels (sediment extracts) or 50 mL test tubes (filter extracts). Additional chloroform and HPLC grade water (chloroform extracted) were added and the containers were shaken vigorously. The organic phase was allowed to separate from the aqueous phase overnight (Figure 5.3a), and drained (or pipetted) into 250 mL round-bottom flasks. Solvents were removed by rotary evaporation (Rotovapor Re-121, Büchi Laboratoriums-Technik, Flawil, Switzerland) at < 37ºC under a stream of nitrogen gas, and the dried total lipids were re-suspended in chloroform and transferred to 15 mL test tubes (Figure 5.3.b). Total lipids were separated into neutral lipid, glycolipid, and polar lipid classes by silicic acid column

chromatography using 0.5 g 100-200 mesh silicic acid powder (Unisil, Clarkson Chemical Co., South Williamsport, PA) (Guckert et al., 1985) and three solvents of increasing polarity (chloroform, acetone, and methanol) at respective volumes (mL) of 5:5:10 (Figure 5.3.c).

The polar lipid fractions were trans-esterified to FAMEs by a mild alkaline methanolysis reaction (Guckert et al., 1985), and blown down under nitrogen gas. FAMEs were re-suspended in hexane, transferred to GC vial inserts, and dried under nitrogen. The samples were re-suspended in 30 µL hexane containing the FAME, methy-eicosanoate (22:0) as an external standard for quantification (D. White et al., 1998). The FAMEs were separated, quantified, and identified using an Agilent 6890 series gas chromatograph interfaced to an Agilent 5973 mass selective detector with a 60 m non-polar cross-linked methyl silicone column (0.25 mm I.D., 0.25 µm film thickness)(RTX-1, Restek). The following linear temperature program was employed (D. White et al., 1998): 60 $^{o}$C for 2 minutes then ramped at a rate of 10$^{o}$C min$^{-1}$to 150$^{o}$C, next ramped at 3$^{o}$C min$^{-1}$ to 312$^{o}$C . Injector temperature was 270$^{o}$C and detector temperature was 290$^{o}$C during a total run time of 65 min. The PLFA standards, Bacterial Acid Methyl Esters CP Mixture (1114), and Polyunsaturated FAME Mixtures, PUFA-2(1081) and PUFA-3(1177) (Matreya LLC, State College, Pennsylvania, USA) were included in each sample run to calibrate retention times, and peak identification was enhanced through the use of Agilent MSD ChemStation Data Analysis Software F.01.00 along with the NIST11 compound library. Extraction efficiencies were calculated based on internal standard peak area of sample divided by peak area of the internal standard in the buffer control x 100.

### 5.3.3 Quantification and Statistical Analysis

Data were compiled, aligned, and reduced in Microsoft Excel, and abundances of PLFAs were calculated from peak intensity ratios to the external standard fatty acid. The data were

normalized as picomole (pmol) PLFA per gram dry weight of sediment, or as pmol PLFA per mL filtered water, and expressed as mole percentages of the total PLFAs. For the biomass estimates, microorganisms with similar lipids and biochemical characteristics were grouped together as *a priori* functional groups (Dobbs et al., 1988a, 1988b), primarily for the purpose of differentiating between microeukaryotes and prokaryotes. Based on an assumption that half of the PLFA contribution from eukaryotes are polyenoic, microeukaryotic biomass can be calculated as 1/2 the sum of polyenoic PLFA (Findlay et al., 1993). Prokaryotic biomass can then be calculated at the difference between total microbial biomass and microeukaryotic biomass. In this study, the Findlay and Dobbs approach was modified by calculating microeukaryote biomass as described above, eliminating ubiquitous normal saturated fatty acids (Table 5.1), and calculating prokaryotic biomass as the sum of the following "biomarker" fatty acids (Frostegård et al., 1996): i15:0, a15:0, 15:0, i16:0, 16:1ω9, 16:1ω7t, i17:0, a17:0, 17:0, cy17:0, 18:1ω5, and cy19:0. Relative biomass estimates for bacteria were calculated using a conversion factor for average cell sizes (24,000 cells/pmol) ( Balkwill et al., 1988; Frostegård et al., 1993; D. White et al., 1998).

PLFA analyses may generate large data sets, with high variability between duplicate samples attributed to the heterogeneity of microbial communities, especially in soils and sediments (Keith-Roach et al., 2002). The PLFA concentrations from duplicate samples were, therefore, averaged for statistical analysis. PLFAs were grouped into 7 classes (Table 5.1) for preliminary statistical analyses. For some analyses, the two least abundant groups - mid-chain branched saturates (MBS) and terminally-branched monounsaturates (BM) were combined into a single class.

Significant differences between sample locations (i.e., sites) and sample types (i.e., sediment biofilms, colloids filtered from water) were determined by comparing the means of

each variable using a Completely Randomized Design (CRD) split-split repeated measures ANOVA in a SAS/STAT (Version 9.4) generalized linear mixed model with an unstructured matrix (GLIMMix Procedure) (Littell et al., 2006). PLFA abundance data were transformed (arc-sin square-root) to lower the block-by-treatment effects (Littell et al., 2006), and to ensure that all statistical assumptions in the model were met based on a 95% confidence interval, with significance determined by $P<0.05$. PLFA data from three sampling times (December 2012, February 2012, and September 2013) were log-transformed to resolve resolution differences attributed to GC maintenance in early 2014. Variation about the mean was calculated as the standard deviation divided by the square root of the sample size, which was divided by the mean and converted to relative standard error (%).

Individual PLFAs were summed or ratioed, and presented as time-series plots of: *trans/cis* PLFA = (∑16:1ω9t+18:1ω9t+18:1ω7t+20:1ω9t)/(∑16:1ω9c+18:1ω9c+18:1ω7c+20:1ω9c); iso/anteiso PLFA = (∑i15:0+i17:0)/(∑a15:0+a17:0); saturated/monounsaturated PLFA = (terminally-branched saturates+mid-chain branched saturates)/(monounsaturates+branched monounsaturates); me18:0/me16:0 = 10me18:0/10me16:0 or sum of me16:0s; and cyclopropyl/precursors = (∑cy17:0+cy19:0)/(∑ 16:1ω7c+18:1ω7c). Ratios of prokaryotes to eukaryotes were determined from the biomass calculations, as described above. Differences between means of sample site and sample types were calculated in Excel using a one-tailed -test, with significance determined as $P<0.05$.

Principal components analysis (PCA) is a multivariate multiple regression method commonly used to visualize relationships between multiple interacting parameters and to examine relationships between microbial community structure and physiological status to environmental conditions (A. Ellison et al., 2004). PCA models were performed in CANOCO

(Version 5.0) on 42 individual PLFAs from 24 samples and 8 environmental variables or ion concentrations, including water temperature, [DOC] , and dissolved sulfate, chloride, magnesium, sodium, calcium, potassium concentrations. The data were log-transformed: Y' = log (100 x Y + 1.00) due to the compositional nature of the data as mole percentages of a total sample (ter Braack et al., 2012). PLFAs were plotted as 'species' against environmental variables to produce ordination diagrams (biplots) with arrows radiating out from the center. Vector length and direction are proportional to the steepest increase in numerical values, and angles between vectors indicate the closest correspondence between environmental variables and PLFA classes and or ratios. Axes 1 and 2 were labeled according to the percent of explained variance (ter Braack et al., 2012).

## 5.4 Results

### 5.4.1 Water Chemistry

Water temperatures on the surface ranged from a summer high of nearly 28ºC to approximately 5ºC in winter; whereas, water temperatures in the cave stream ranged between around 16ºC and 4ºC during the same period. Average pH was 7.4 and 7.5 at FF and LR, respectively, and alkalinities at both sites ranged around 145 mg $L^{-1}$. Both the surface stream and the cave stream environments were highly oxygenated (dissolved oxygen > 7.0 mg $L^{-1}$), and had DOC concentrations < 5.0 mg $L^{-1}$. Hydrochemistry was discussed in Chapter 4 and the data for each sample presented in Chapter 4 Appendix Table 4.1 and Table 4.2).

.

### 5.4.2 Total Bacterial and Microeukaryotic Biomass

Total biomass in the attached community was 1 to 2 orders of magnitude more abundant than in the suspended community at both FF and LR over most seasons and flow conditions, except for two apparent bloom events in the suspended fractions during March and June 2014 (Figure 5.4). Biomass in the suspended community peaked during warmer seasons and was lowest at both sites in December and January, varying by 50% at LR and by a much greater margin at FF (Table 5.2). In the attached community, biomass abundance at FF consistently exceeded that at LR, and both varied by 41% and 36% respectively over all seasons and flow conditions (Table 5.3). Total microbial biomass (as PLFA concentrations) ranged from nearly 0.01 pmol $mL^{-1}$ in the suspended fractions, to more than 9500 pmol $g^{-1}$ in the attached fractions (Table 5.2 and Table 5.3). The contribution of bacterial PLFA and microeukaryotic PLFA to total biomass are compared in Figure 5.5and indicate that prokaryotes dominate in suspended communities at both surface and subsurface sample sites, but that microeukaryotes were disproportionally higher in the attached community at Fort Falls.

The PLFA extraction process, calculated as extraction efficiencies, recovered 60% of the internal standard for filter samples and averaged 40% for sediment samples. Lower recoveries for the sediment samples were most likely due to the fine-fraction clay residuals in the sieved sediments that remained suspended during the separation phase and did not settle into the organic fraction.

### 5.4.3 PLFA Classes by Sample Type

Analysis of the average PLFA composition of all samples by class indicates significant differences in microbial community structure between sample types and sites (Figure 5.6). Monounsaturates dominated all sites and sample types. Most notably, mid-chain branched

saturated and branched monounsaturated PLFA comprised approximately 20% of the attached community, and were 10 times more abundant than in the suspended fraction PLFA. Overall, monounsaturates and terminally-branched saturates were more abundant at LR in both fractions, and polyunsaturated and normal saturated PLFA decreased between FF and LR in both community types.

### 5.4.4 PLFA Profiles for Attached and Suspended Fractions

Figure 5.7 reveals details about PLFA differences between suspended and attached microbial communities. Forty-one individual PLFAs were detected in the suspended fraction, including 8 *cis* and *trans* isomers of monounsaturates, and 6 iso and anteiso FAMEs each of terminally-branched saturates and terminally-branched monounsaturates. The most abundant PLFAs in the suspended fractions were 16:0, 16:1ω7*c*, 18:1ω9*t*, 18:1ω9*c*, and 16:1ω5. 16:1ω7*c* is a precursor for cyclopropyl fatty acids while 18:1ω9*c* and 18:1ω9*t* are precursors to polyenoic PLFA (Gurr et al., 2002). Additionally, the suspended fractions had greater relative abundances of the polyunsaturates, 18:3ω3, 18:4ω3, and 18:2ω6, indicative of eukaryotes such as cyanobacteria, algae, higher plants, and fungi (Frostegård et al., 1993; Zelles, 1997).

Forty-two individual PLFA were identified in the attached fraction, which contained more mid-chain branched saturates, specifically, 12me14:0, 11me16:0, and 12me16:0, and a very low abundance of 10me16:0 fatty acids. The most abundant PLFAs in the attached fractions were 16:0, 16:1ω9*t*, 16:1ω7*t*, 18:1ω9*c*, and 18:1ω5. Attached communities at both FF and LR contained a greater proportion of the polyunsaturated PLFA, 18:3ω3, than the suspended communities (Figure 5.7).

### 5.4.5 Biomarker Ratios through Time

Selected ratios of individual PLFA previously used as biomarkers of nutritional status and physiological stress were plotted as time series for all sample events (Figure 5.8). Ratio statistics for both suspended and attached fractions are summarized in Table 5.4. The *trans/cis* ratios, biomarkers for physiological adjustments in response to temperature fluctuations and mechanical stress in Gram$^-$ bacteria (Härtig et al., 2005), show a significant 5-fold increase in the suspended communities, with respect to the attached communities, and may indicate nutrient limitation. The sum of cyclopropyl PLFA (cy17:0 + cy 19:0) ratioed to their precursor PLFA were also exhibited significantly elevated and more variable in the suspended communities. Cyclopropyl/precursor ratios varied inversely between sites, and the highest values occurred during cold season, high flow conditions at FF, and during warm season, low flow events at LR. Both PLFA fractions and sites exhibited similar median values of iso/anteiso ratios, biomarkers for temperature response in Gram$^+$ bacteria, with more variability in the suspended community. The greatest divergence between sites and fractions occurred in warm season, low flow conditions suggestive of a temperature response mechanism in the suspended community.

The 10me18:0/10me16:0 (∑me16:0 for the attached fraction) showed dynamic changes at FF in both communities relative to LR. 10me18:0 is a biomarker for Actinomycetes, while 10me16:0 is a biomarker for metal- and sulfate-reducing bacteria. Due to the low abundance of 10me16:0 in the attached fraction, indicative of some metal- or sulfate-reducers, 10me16:0 was combined with 11me16:0, and 12me16:0 (∑me16:0) for ratio analyses. These ratio results suggest that the proportion of Actinomycetes in the attached communities at both sites increased during warm season, low flow conditions, and dropped relative to the proportions of sulfate reducers and other anaerobic bacteria in cold, high flow conditions. However, ratio values were

consistently < 0.5 at LR, indicating that anaerobes formed an important component of both suspended and attached communities in the cave stream environment.

Additional differences in microbial community structure were highlighted by the ratios of saturated/monounsaturated PLFA (Table 5.4). Proportions of $Gram^+/Gram^-$ bacteria were significantly higher at FF in the suspended community, whereas, downstream in the cave stream, proportions of $Gram^+/Gram^-$ bacteria were significantly higher in the attached community (data not shown).

### 5.4.6 Multivariate Analysis

Figure 5.9 depicts PLFA vectors associated with sample-time and sample-type in an unconstrained PCA model of all PLFA profiles, showing the 22 most highly-weighted FAMEs. The first ordination axis of the model explained 29.74% of the variance, and the second ordination axis explained 16.32 % of the total variance. Attached and suspended samples discretely separated to the left- or right- halves of the graph, respectively. The first cluster of attached samples in the upper left quadrant of the graph were collected during the earliest two events in the study under cold, high flow conditions. These samples (Dec 2012 and Feb 2013) correspond closely with mid-chain branched saturates, terminally-branched monounsaturates, and cyclopropyls, which align in the opposite direction of temperature, and are indicative of sulfate-reducing bacteria and stressed physiological status. The second cluster of attached samples, primarily associated with warmer conditions, are centered in the lower, left-hand quadrant of the graph. These samples correlated with a different set of mid-chain branched saturates (Actinomycetes) and terminally-branched monounsaturates, and their position may have been influenced by the strong vector for the terminally-branched saturate, *a*15:0, indicative of $Gram^+$ bacteria. The attached communities had higher relative abundances of 16 carbon

monounsaturates.

The suspended samples clustered more loosely along the positive end of Axis 1, with no clear differentiation between sample times. Suspended samples at both sites were closely associated with the fungal/cyanobacterial indicator, 18:2ω6, polyunsaturated precursors, 18:1ω9, and monounsaturates, 18:1ω7, characteristic of Gram$^-$bacteria, as well as two terminally-branched saturates (*i*16:0 and *i*17:0) affiliated with Gram$^+$ bacteria.

Environmental and geochemical parameters were considered in the PCA model in Figure 5.10, which was run with 42 individual PLFA by subtracting the eight samples that lacked ion data (June 2013, January 2014, March 2014, and June 2014)(Table 4.1). In this version of the model, showing the 35 most heavily-weighted FAME, the first ordination axis explained 41.21% of the variance, and the second canonical axis explained 23.29 % of the total variance. The suspended and attached samples occupied opposite ends of Axis 1, compared to the Figure 4.9 without environmental variables, but still plotted on discrete halves of the graph. Sulfate and pH weakly corresponded with cy17:0 and sulfate-reducing bacteria (10me16:0) in the upper left-hand quadrant, and inversely corresponded with aqueous concentrations of DOC and other ions, as well as temperature (lower right-hand quadrant). The distinct separation of Gram$^-$ communities (based on carbon length) between suspended and attached samples is more apparent on Fig. 5.10 due to the larger number of monounsaturates displayed.

## 5.5 Discussion

The capacity for freshwater ecosystems to adapt to more frequent, extreme weather events, and ultimately long-term climate change, in a given region may depend on the fluidity with which microorganisms can respond to diel and annual/seasonal fluctuations in light,

temperature, discharge, and DOM quality. This research examined microbial community structure, biomass, and physiological status with the aims of: a) evaluating the configuration and dynamics of microbial communities dependent upon OM in the Cascade Cave system, and b) identifying parameters informative for the development of hydro-biomonitoring strategies in oligotrophic karst groundwaters.

The environmental dynamics of the surface stream and cave stream varied widely, as illustrated by marked fluctuations in suspended community biomass at Fort Falls compared to the relatively stable biomass in the cave stream suspended community, and in the attached communities at both sites. Attached community biomass was consistently more abundant at FF, where primary production could take place, but was often highest in the cave stream during warm weather, low flow conditions with lowest [DOC] and varying DOM quality. This suggests that the cave stream communities expressed their metabolic efficiency for taking up nutrients from a very limited DOM pool while actively growing in the low-flow environment.

PLFA ratios were most useful in the determination of significant differences between the configuration of suspended and attached microbial communities and their responses to environmental stressors. Hypothesis 1 predicted that the surface suspended community would be dominated by Gram$^-$ bacteria and eukaryotes (algae, fungi, and other photoautotrophs) due to the photic environment, but that the attached community would contain greater proportions of Actinomycetes and Gram$^+$ bacteria in the darkness of the cave stream. Indeed, the abundance of eukaryotes decreased along the flow path in the suspended community, similar to trends seen in soil profiles with depth (Bossio et al., 1998; Fierer et al., 2003; Schütz et al., 2009). However, contrary to the first hypothesis, Gram- bacteria dominated in all samples, and Actinomycetes, anaerobes, and Gram$^+$ bacteria comprised significantly greater proportions of the attached

communities. Brannen and Engel (2015) also worked in the Cascade Cave system and found that certain bacteria in recharge waters from FF colonized attached communities in the cave stream over time. In this research, the abundance of both anaerobes and $G^+$ bacteria increased in the cave stream attached communities, suggesting that both groups partition from suspended to attached form as they are transported through the cave. It has also been shown that growing cells can adjust to rising temperatures by increasing saturated fatty acid production (Gurr et al., 2002; Heipieper et al., 2010), so these results may reflect a physiological response of part of the microbial community rather than a compositional difference. As modeled by the PCA, however, attached communities at both sites corresponded to 16-carbon monounsaturates indicative of sulfate-reducing and/or metal-reducing bacteria.

Even though the Cascade Cave system is a highly oxygenated environment, PLFA profiles and ratios suggest the presence of a stable anaerobic population in the cave stream attached community, as well as in the subsurface suspended community. Anaerobic bacteria have been documented in biofilms in deep mines (Pfiffner et al., 2006), oxygenated hyporheic zones in river systems (Moser et al., 2003), and attached to suspended particulate matter in a phreatic cave system (Moss et al., 2011), which may lend credence to the suggestion (Chapter 4) that OM could also be transported in aggregation with particulate matter. In this study, PCA highlighted the correspondence of mid-chain branched saturate PLFA with sulfate and pH (and inversely with [DOC]) indicating that they may be facultative anaerobic sulfate-reducing bacteria. The PCA model suggested close associations between $G^-$ bacteria and fungi in the suspended fraction that could also be linked to OM sorption and transport on inorganic colloids (Chanudet et al., 2007).

Hypothesis 2 focused on microbial homeostasis, and predicted that suspended microbial

communities would exhibit higher levels of stress response indicators relative to microorganisms living in the comparatively stable attached environment. High stress response has previously been correlated with microbial transport through soils and in groundwater recharge events (Balkwill et al., 1988; Schütz et al., 2009). Three PLFA ratios, *trans-/cis*- isomers, iso-/anteiso-isomers, and cy17:0+cy19:0/precursors were evaluated as biomarkers for growth phase/stress, temperature response, and starvation, respectively. *Trans/cis* ratios > 0.1 have been used as indices of stress response in cell cultures and environmental samples (Guckert et al., 1986; Kaur et al., 2005). *Trans*-monounsaturates are only observed in non –growing cells, and reflect a rapid response to suddenly changing environmental conditions (Härtig et al., 2005; Heipieper et al., 2010). The continuously elevated *trans/cis* ratios in the suspended communities may reflect a constant defense against natural antimicrobial agents, nutrient limitation, diurnal response to sunlight (FF) or reaction to an aphotic environment in the subsurface (LR).

Gram$^+$ bacteria activate iso-branched fatty acids at high temperatures to maintain membrane fluidity, and use anteiso-branched fatty acids similarly to unsaturated PLFA during dropping temperatures (Kaneda, 1991), so community response to rising and falling temperatures may be reflected in the relative amounts of iso- and antesio-branched chain fatty acids. These trends were most prominently observed in the suspended communities, and are interpreted as representative of seasonality in the community response to environmental conditions. The sampling interval was not small enough to detect sudden changes in temperature, however, anteiso-branched fatty acids have been shown to be especially important for bacterial growth at low temperature and alkaline pH (Giotis et al., 2007), which may explain their nearly equal abundance between sites, and low variability at LR over time.

For Gram$^-$ bacteria communities, cyclopropyl/precursor ratios were consistently very low

in the attached communities fractions relative to the suspended communities. This ratio suggests that, during the warm season, suspended communities begin form cyclopropyls as they are transported from the surface via groundwater recharge and physiologically adjust to slower growth conditions, cooler temperatures, and lower nutrient levels. Attached communities, on the other hand are far more stable and show fewer signs of physiological adjustment over time. Cyclopropyl formation is irreversible but accumulation in LR was not observed during winter, high-flow conditions, presumably due to dilution effects. Stress response in the suspended communities also corresponded with insignificant [DOC] utilization along the flow path under high flow conditions.

Previous studies have observed seasonality in the structure of microbial communities in surface waters (Mosher et al., 2011), and PLFA analyses have been linked to stream water chemistry quality and seasonal fluctuations (DeForest et al., 2016; Moser et al., 2003) Elucidating the effects of DOM quality on microbial community structure, and the microbial degradation of that DOM in the environment have been more difficult. This research detected strong seasonality in suspended microbial communities transported with DOM along the flow path, but relatively little response to DOM quality in the attached communities, based on PLFA biomarker ratios. With additional samples from fall and winter, low flow conditions, on smaller sampling intervals, such relationships may become more apparent.

## 5.6 Conclusion

The complex, dynamic interchange between surface and subsurface flow and between attached and free-living microbial communities reveal strategies for survival in low-nutrient cave environments, and inform conceptual models of OM transformation and degradation. Suspended

microbial communities exhibit markedly different stress responses during different seasons; whereas, the relative stability of the attached communities could be interpreted as being due to finely-tuned interactions between various community members in order to adjust to ever-changing, often adverse environmental conditions in the karst ecosystem. Inclusion of cellular biomarker analysis in hydrogeological investigations will add new dimensions to our current understanding of microbial community resilience and response to the short- and long-term impacts of climate change on karst aquifers.

## Chapter 5 Appendix

Table 5.1. Phospholipid fatty acid markers characteristic of certain groups of organisms

| PLFAs | Class | Primary Biological Source |
|---|---|---|
| 14:0, 15:0, 16:0, 17:0, 18:0, 20:0 | Normal Saturates | Ubiquitous |
| i14:0, i15:0, a15:0, i16:0, i17:0, a17:0 | Terminally-branched Saturates | $Gram^+$ bacteria, Bacillus, Arthrobacter |
| 12me14:0, 10me16:0, 11me16:0, 12me16:0, 10me18:0 | Mid-chain branched Saturates | Actinomycetes<br>Metal or Sulfate Reducers |
| i14:1, i15:1, a15:1, i16:1, a16:1, i17:1, a17:1, i18:1, a18:1 | Terminally-branched Monounsaturates | Bacteria |
| n14:1-n20:1, 16:1ω9c, 16:1ω9t, 16:1ω7c, 16:1ω7t, 16:1ω5c, 16:1ω5t, 18:1ω9c, 18:1ω9t, 18:1ω7c, 18:1ω7t, 20:1ω9c, 20:1ω9t | Monounsaturates | $Gram^-$ bacteria |
| cy17:0, cy19:0 | Cyclopropyls | $Gram^-$ or $Gram^+$ bacteria<br>(stress or physiological status) |
| 16:3, 18:3, 20:3, 18:4ω3, 18:3ω6, 18:2ω6, 18:3ω3, 20:4, 20:4ω6, 20:2ω6, 20”5, 20:5ω3, 22:6 | Polyunsaturates | Eukaryotic influence<br>(algae, plants, fungi, protozoa, diatoms) |

“c” = *cis* fatty acids “t” = *trans* fatty acids

(from Federle et al., 1986; Wood, 1988; Vestal and White, 1989; Wilkinson, 1988; Mirza et al., 1991; Frostegård et al., 1993; Dunstan et al., 1994; Bardgett et al., 1996; Zelles, 1997,1999; Kieft et al., 1997; Bååth, 2003; Ruess and Chamberlain, 2010)

Table 5.2. PLFA classes in the suspended fraction from Fort Falls (top row) and Lake Room (bottom row). All data in mol %, unless otherwise indicated.

| Class | 12Dec | 13Jun | 13Sep | 14Jan | 14Mar | 14Jun | Mean | Std. Dev. | RSE(%)[1] |
|---|---|---|---|---|---|---|---|---|---|
| Normal | 42.06 | 41.24 | 32.25 | 16.04 | 29.42 | 27.26 | 29.94 | 9.68 | 13 |
| Saturates * | 33.17 | 25.38 | 22.93 | 14.02 | 21.01 | 18.29 | 21.69 | 6.55 | 12 |
| Terminally-Branched | 8.93 | 5.72 | 5.60 | 11.08 | 8.06 | 11.29 | 8.13 | 2.49 | 12 |
| Saturates | 11.94 | 16.48 | 6.21 | 6.90 | 7.98 | 7.03 | 8.83 | 4.02 | 19 |
| Mid-chain Branched | 1.08 | 1.22 | 0.78 | 4.42 | 0.60 | 0.13 | 0.84 | 1.54 | 75 |
| Saturates * | 1.99 | 2.35 | 1.02 | 4.85 | 1.52 | 0.85 | 1.76 | 1.46 | 34 |
| Terminally-Branched | 0.37 | 0.40 | 0.39 | 0.64 | 0.44 | 0.63 | 0.47 | 0.12 | 11 |
| Monounsaturates * | 0.64 | 1.16 | 1.14 | 0.36 | 0.76 | 0.70 | 0.79 | 0.31 | 17 |
| Monounsaturates * | 45.10 | 38.64 | 48.77 | 56.57 | 44.39 | 46.34 | 46.33 | 5.91 | 5 |
| | 47.37 | 45.04 | 61.62 | 63.00 | 54.75 | 62.39 | 55.20 | 7.96 | 6 |
| Cyclopropyls* | 1.45 | 0.64 | 0.94 | 5.42 | 1.08 | 0.53 | 1.18 | 1.86 | 65 |
| | 2.15 | 2.46 | 1.52 | 6.60 | 2.95 | 5.89 | 3.12 | 2.12 | 28 |
| Polyunsaturates * | 1.22 | 12.14 | 11.27 | 5.83 | 16.02 | 13.84 | 7.75 | 5.51 | 29 |
| | 2.74 | 7.11 | 5.56 | 7.39 | 10.96 | 4.98 | 5.93 | 2.77 | 19 |
| Total PLFAs | 0.54 | 4.31 | 1.82 | 2.28 | 12,271 | 17,036 | 35.56 | 7742 | 8850 |
| (pMol $mL^{-1}$) | 1.1.3 | 6.41 | 0.76 | 5.31 | 1.33 | 1.47 | 1.96 | 24.58 | 50 |
| Estimated Relative Biomass[2] | 1.36E+04 | 1.08E+05 | 4.54E+04 | 5.70E+04 | 1.35E+05 | 3.78E+05 | 7.60E+04 | 1.32E+05 | |
| (Cells $mL^{-1}$) | 2.83E+04 | 1.60E+05 | 1.90E+04 | 1.33E+05 | 3.32E+04 | 3.67E+04 | 4.91E+04 | 6.15E+04 | - - |

* Statistically significant differences between sites ($p < 0.5$)
[1] Variance about the mean as Relative Standard Error (%)
[2] Conversion factor for average cell size: 25,000 cells $pmol^{-1}$

Table 5.3. PLFA classes extracted from the attached fraction at Fort Falls (top row) and Lake Room (bottom row). All data presented in mol %, unless otherwise indicated.

| Class | 12Dec | 13Feb | 13Jun | 13Sep | 14Mar | 14Jun | Mean | Std. Dev. | RSE[1] (%) |
|---|---|---|---|---|---|---|---|---|---|
| Normal* Saturates | 17.57<br>16.38 | 19.75<br>14.68 | 6.97<br>14.30 | 5.97<br>7.81 | 3.57<br>7.05 | 22.99<br>6.10 | 10.29<br>10.24 | 8.26<br>4.54 | 33<br>18 |
| Terminally-Branched Saturates | 9.15<br>10.53 | 10.28<br>11.82 | 9.71<br>10.71 | 7.44<br>11.82 | 6.08<br>9.38 | 9.68<br>11.36 | 8.58<br>10.90 | 1.62<br>0.94 | 8<br>4 |
| Mid-chain Branched Saturates | 10.77<br>14.23 | 8.41<br>10.83 | 6.95<br>16.14 | 9.96<br>11.22 | 6.16<br>12.25 | 7.48<br>11.14 | 8.29<br>12.25 | 2.07<br>2.34 | 10<br>8 |
| Terminally-Branched Monounsaturates | 0.36<br>0.68 | 0.36<br>0.54 | 25.02<br>BDL | 18.17<br>18.50 | 15.98<br>14.14 | 8.54<br>14.43 | 4.50<br>1.05 | 10.09<br>8.43 | 97<br>227 |
| Monounsaturates | 48.94<br>46.45 | 52.62<br>52.71 | 45.95<br>55.25 | 46.27<br>44.85 | 56.98<br>51.68 | 35.32<br>49.28 | 47.17<br>49.91 | 7.35<br>3.94 | 6<br>3 |
| Cyclopropyls | 5.25<br>5.74 | 2.60<br>3.63 | 0.50<br>BDL | 0.47<br>0.25 | BDL<br>0.56 | 3.99<br>1.27 | 0.71<br>0.58 | 2.16<br>2.29 | 124<br>162 |
| Polyunsaturates* | 7.96<br>5.99 | 5.97<br>5.79 | 4.90<br>3.59 | 11.14<br>5.11 | 11.09<br>4.84 | 12.08<br>6.11 | 8.39<br>5.16 | 3.01<br>0.95 | 15<br>8 |
| Total PLFAs (pMol $g^{-1}$) | 9,500<br>2,522 | 6083<br>3,318 | 1,219<br>380 | 1,663<br>927 | 1,882<br>884 | 5,747<br>3,018 | 3290<br>1410 | 3,304<br>1,258 | 41<br>36 |
| Estimated Relative Biomass[2]* (Cells $g^{-1}$) | 2.38E+08<br>6.30E+07 | 1.52E+08<br>8.30E+07 | 3.05E+07<br>9.52E+06 | 4.16E+07<br>2.32E+07 | 4.71E+07<br>2.21E+07 | 1.44E+08<br>7.54E+07 | 7.47E+07<br>3.89E+07 | 8.60E+07<br>2.96E+07 | - - |

* Statistically significant differences between sites ($p < 0.05$)
[1] Variance about the mean as Relative Standard Error (%)
[2] Conversion factor for average cell size: 25,000 cells $pmol^{-1}$

Table 5.4. Summary of specific marker PLFA for groups of organisms and physiological status.

| PLFA Ratio | Biomarker | Suspended Fraction | Attached Fraction | Significant Difference by Type |
|---|---|---|---|---|
| Monoenoics/Polyenoics | Prokaryotes/Eukaryotes | LR* | LR* | √ |
| *trans*/*cis* isomers | Growth phase, stress | FF* | FF | √ |
| i15:0+ i17:0/a15:0+ a17:0 | G+, temperature response | LR | LR | |
| Saturates/Monounsaturates | G+ vs G- bacteria | FF* | LR* | √ |
| Cy 17:0+ Cy19:0/Precursors | G-, stress, starvation | LR* | FF | √ |
| 10me18:0/∑me16:0 | Actinomycetes/Anaerobes | FF* | FF* | √ |

* Significantly greater between sites ($P < 0.05$)

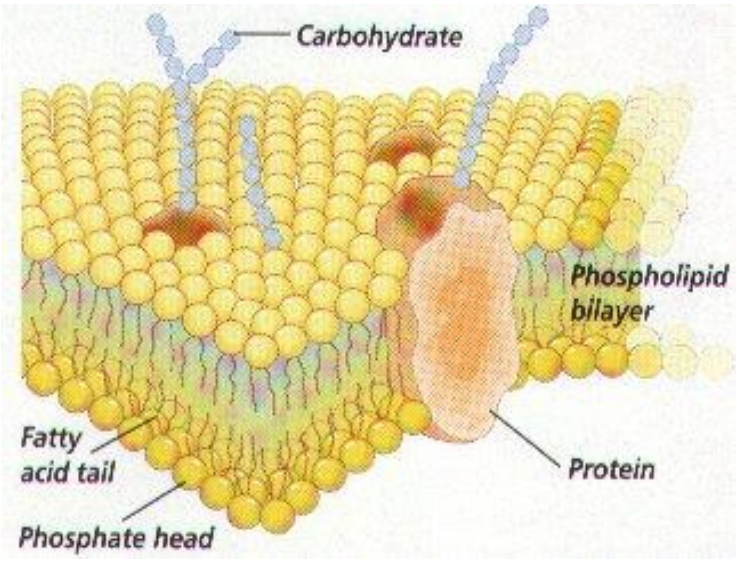


Figure 5.1 Structure of the cytoplasmic membrane of a cell.
(http://www.biologyjunction.com/cell%20%20notes%20bi.htm)

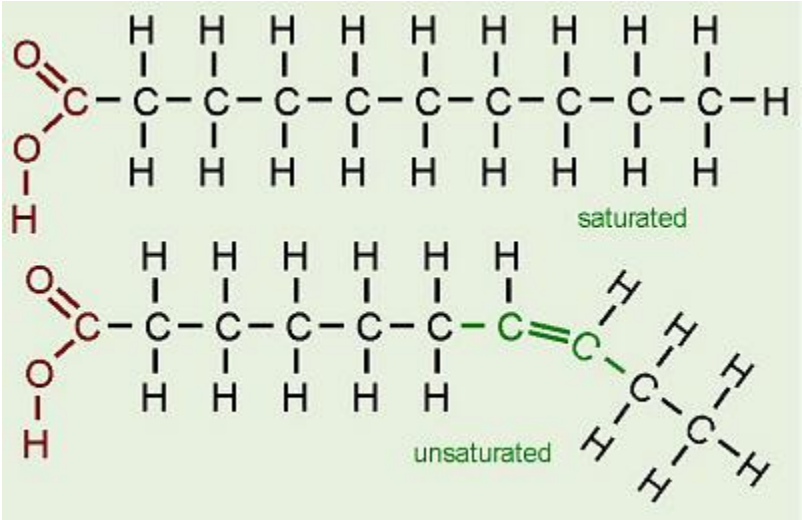


Figure 5.2 Generalized structure of saturated (top) and unsaturated (bottom) fatty acids. (http://homepage.smc.edu/wissmann_paul/humanbiology/lipids.html)

Figure 5.3. Separatory funnels (a), rotary evaporation (b), and silicic acid column (c) chromatography steps in the modified Bligh Dyer PLFA extraction process

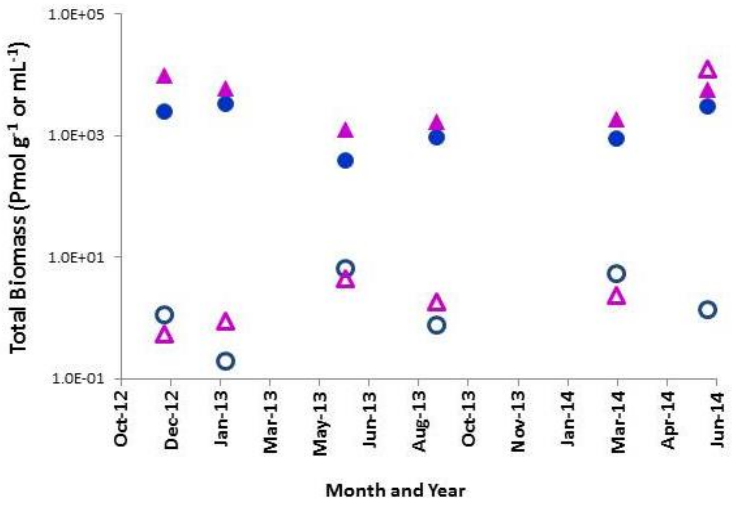


Figure 5.4 Seasonal total microbial biomass in the suspended community (open symbols) as pmol PLFA $mL^{-1}$, and in the attached community (closed symbols) as pmol PLFA $g^{-1}$ for the surface stream at Fort Falls (pink triangles) and the Lake Room (blue circles).

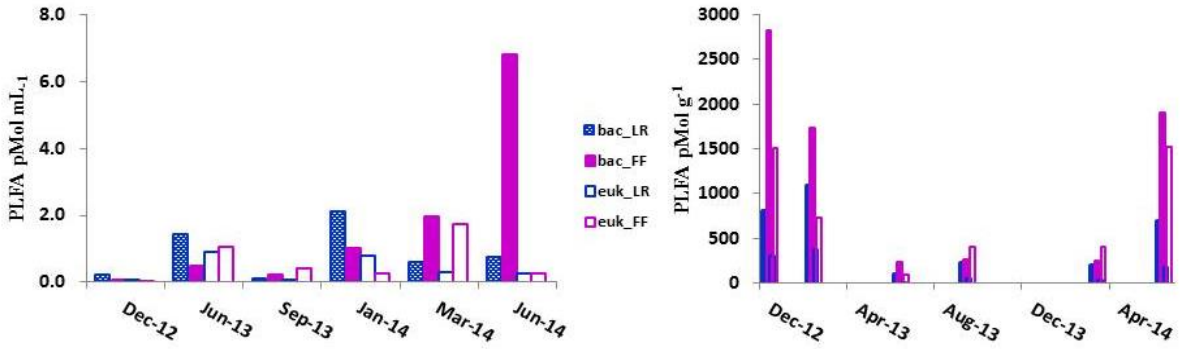


Figure 5.5 Concentration of PLFA characteristic of prokaryote (bac-) and eukaryote (euk-) contributions to total biomass in suspended and attached fractions from FF (pink) and LR (blue).

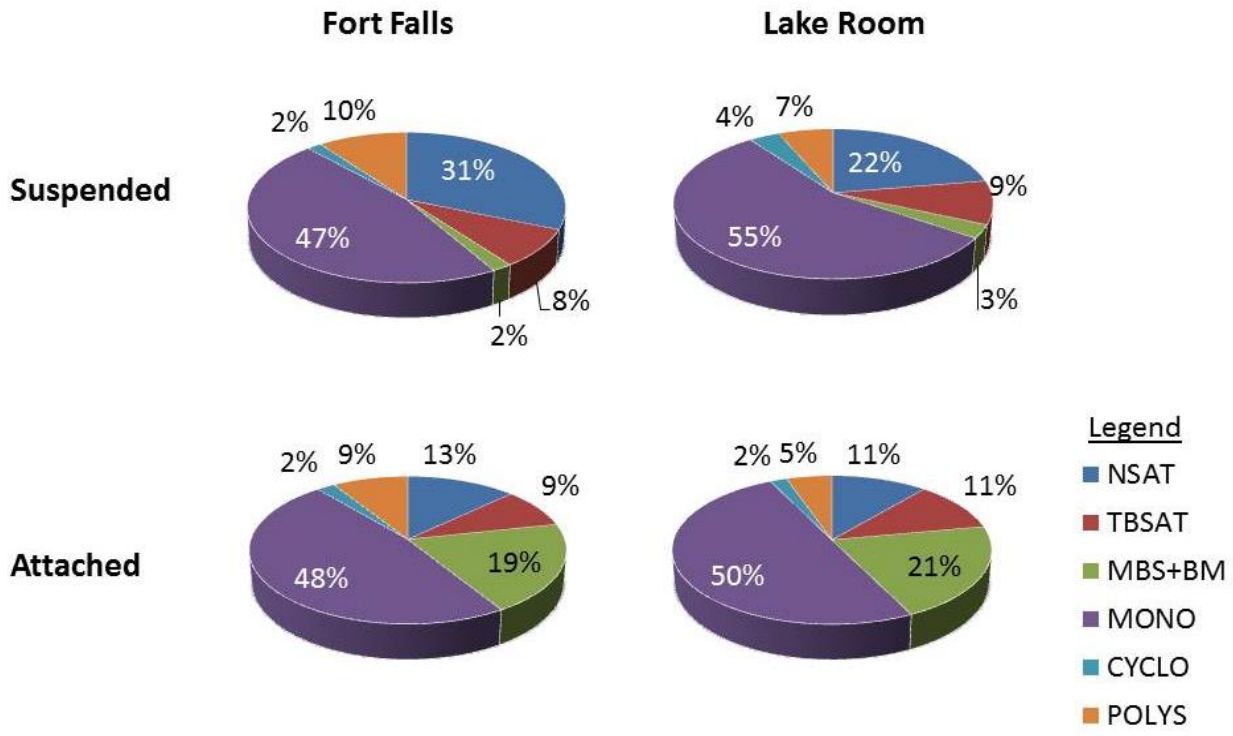


Figure 5.6 Comparison of average PLFA class distributions by sample type for each site.

(NSAT = normal saturates; TBSAT = terminally-branched saturates; MBS+BM = mid-chain branched saturates plus branched monounsaturates; MONO = monounsaturates; CYCLO=cyclopropranes; POLYS = polyunsaturates).

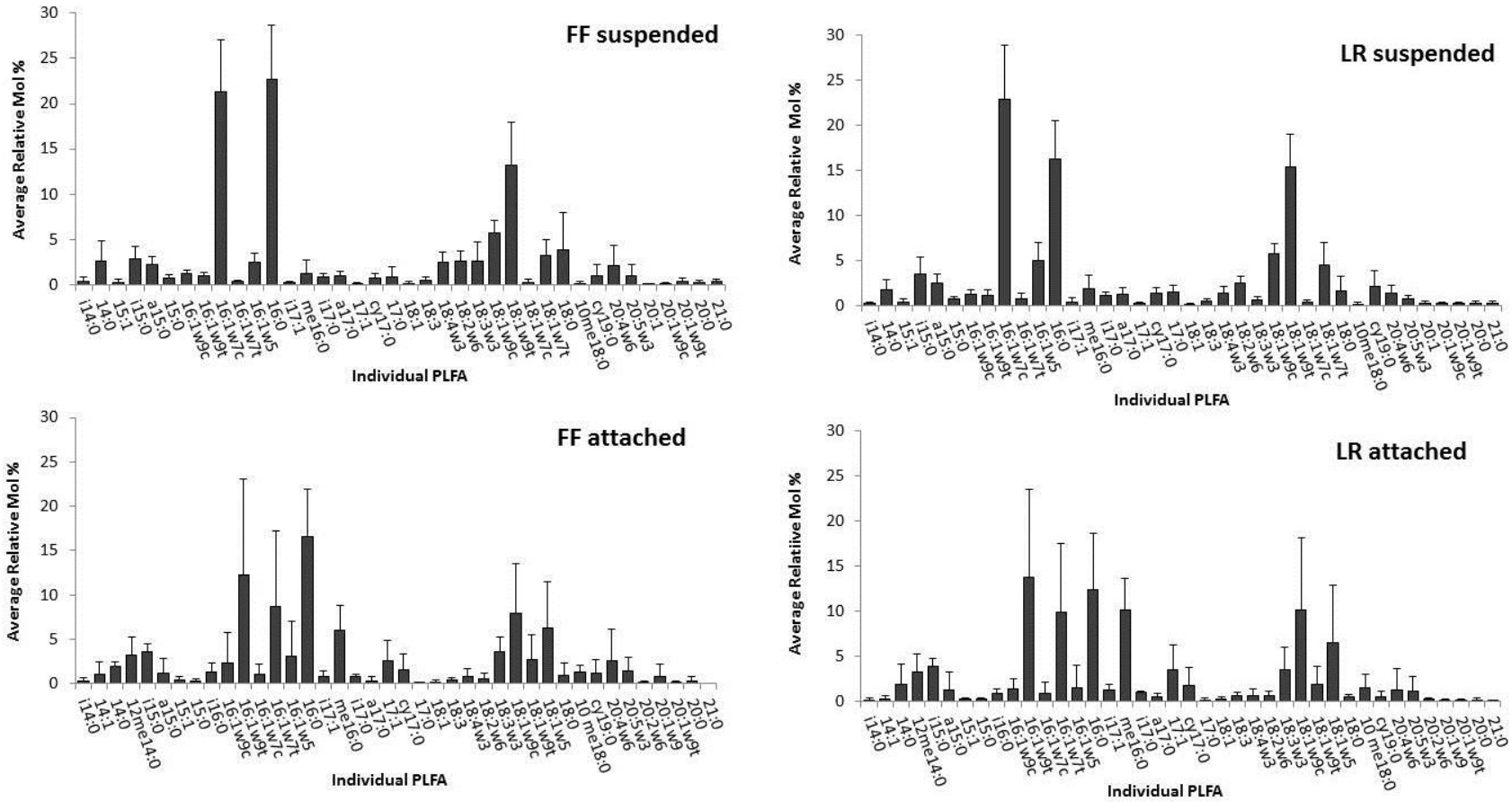


Figure 5.7 Comparison of PLFA profiles averaged over all sample events for suspended (A) and attached (B) fractions at Fort Falls, and for suspended (C) and attached (D) fractions at Lake Room. Error bars represent one standard deviation.

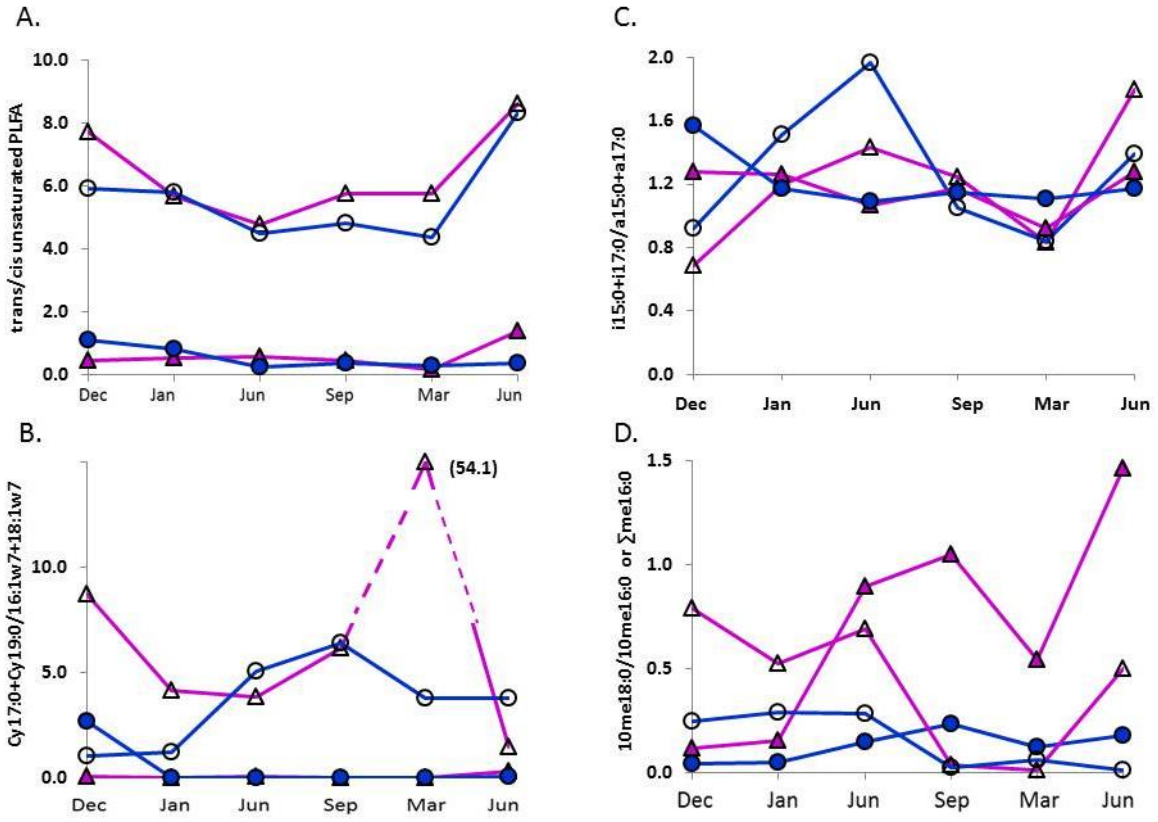


Figure 5.8 Time series analysis of biomarker PLFA ratios from suspended (open) and attached (solid) fractions at FF (pink) and LR (blue): A. *trans/cis* unsaturated PLFA, B. cyclopropyls/precursor PLFA, C. *iso/anteiso* terminally-branched saturates, D. Actinomycetes/sulfate-reducing bacteria.

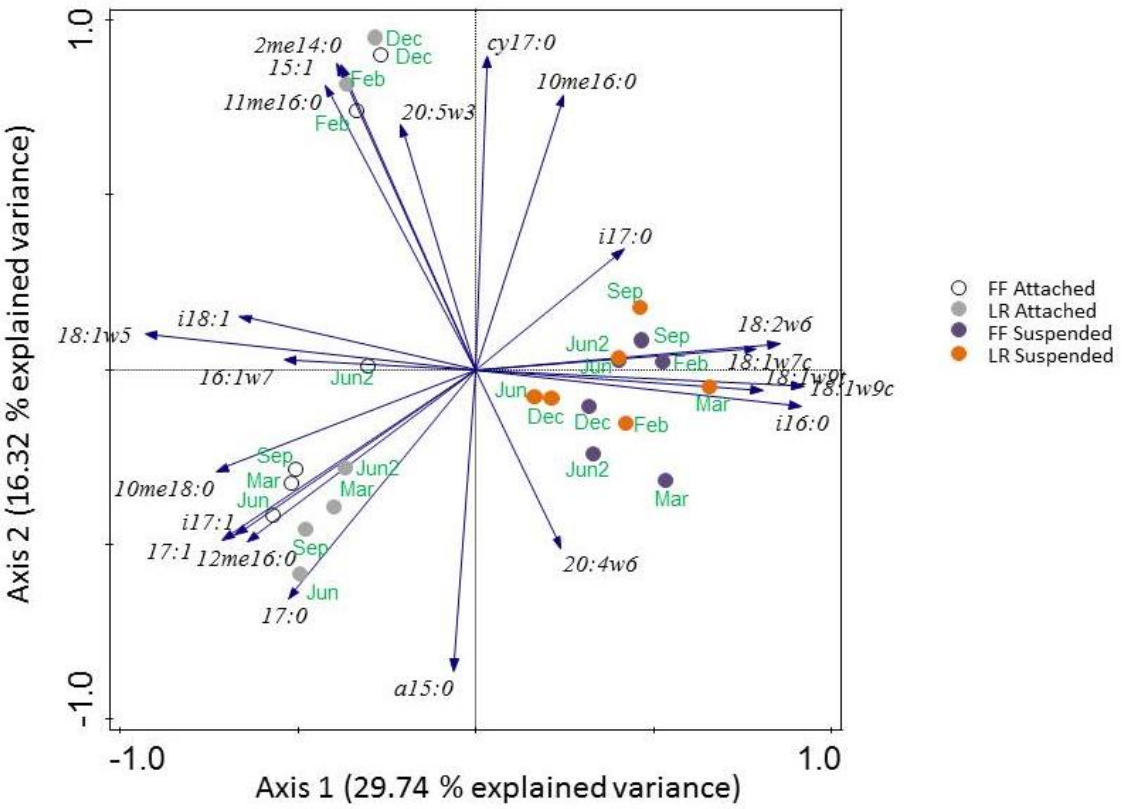


Figure 5.9 Principle components analysis (PCA) of the complete PLFA data set (42 individual PLFA) for the 12 filter samples (suspended) and 12 sediment samples (attached), using PLFA as species. For clarity, only the PLFA with the longest vector lengths (greatest weighs) are shown. Specific sample events are depicted as open and closed circles related to sample type.

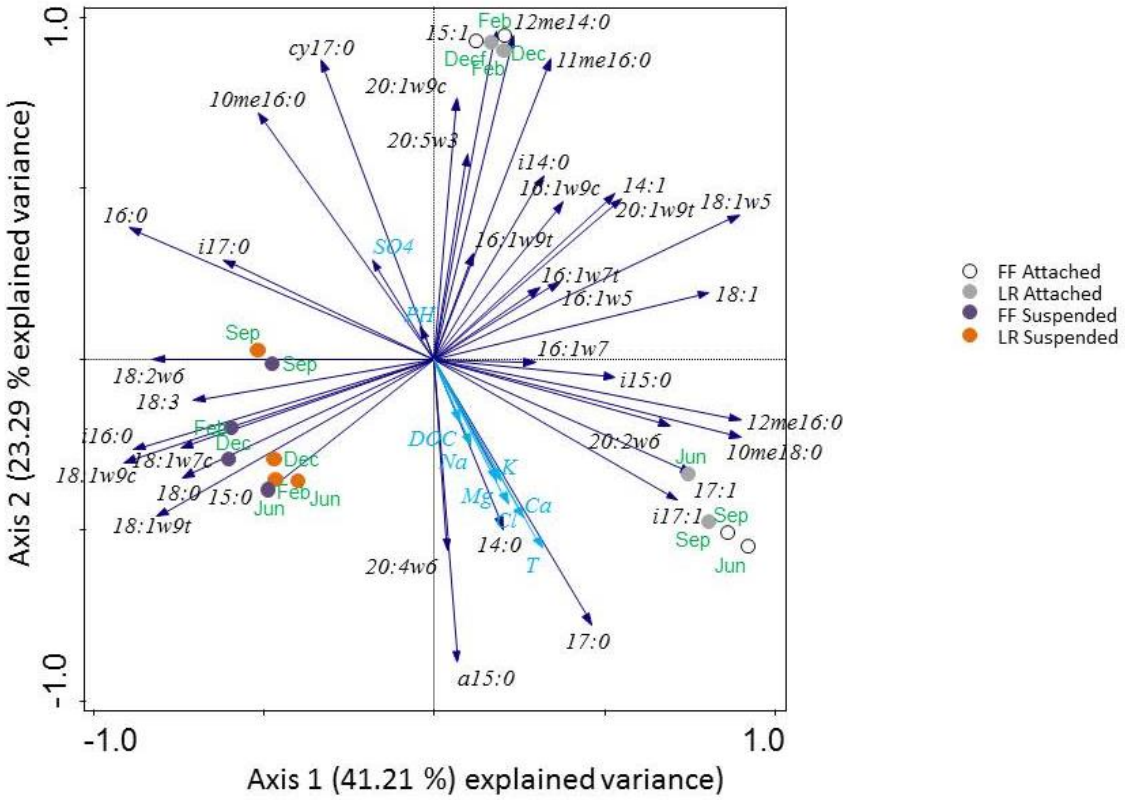


Figure 5.10 Principle components analysis (PCA) of the complete PLFA data set (42 individual PLFA) for the 12 filter samples (suspended) and 12 sediment samples (attached), using PLFA as species with 8 environmental variables.

# Chapter 6. Dissertation Conclusions

The objectives of this dissertation research were to investigate the seasonal dynamics of microbially-driven OM degradation in a karst groundwater system that was influenced by surface water, and to identify patterns and biomarkers of carbon cycle processes useful for monitoring long-term hydroecological trends in the Appalachian region. Through the use of a combination of approaches focused on macromolecular functional groups, bulk OM was isolated and concentrated in the field (Chapter 2, Chapter 4) for spectroscopic characterization (Ch. 4) and affiliation with microbial community structure and response (Chapter 5) under seasonally-variable environmental and flow conditions (Chapter 3).

The results provided evidence that DOM quality varied across the catchment diurnally, which affects the timing and location of DOM quality monitoring and impacts subsequent to interpretations of carbon cycle processes. Rapid macromolecular transformation (<7 hours) of labile DOM was documented along short segments (<300 m) of the upper cave stream that suggested a priming effect on the activity of attached microbial communities. Dissolved organic nitrogen accumulated in the cave stream, indicative of microbial recycling, re-working, and utilization of DOM, and was coincident with decreasing DOC concentrations.

Lipid profiles revealed different microbial community structures in suspended and attached fractions, both on the surface and in the cave stream, and reflected relative stability and successful adaptation in the attached community compared to the highly stressed status of suspended bacteria in transit through the cave system. Other researchers have shown that biofilms in oligotrophic streams have exceptionally high carbon and nutrient use efficiencies (Dodds et al., 2008; Lane et al., 2013), which was supported here for the subsurface segment of the flow path. The archaeal community was not characterized, however, the Gram+ component

of the attached prokaryotic community was consistently more anaerobic than suspended fractions, and was particularly persistent in the colder, non-photic cave environment.

Global estimates of $CO_2$ evasion (outgassing) from inland surface waters have been recently revised on the basis of stream slope, surface area, latitude, and water chemistry (Raymond et al., 2013; Wehrli, 2013). The new estimates support the concept of streams and rivers as bioprocessing pipelines and indicate that lower order, headwater streams are disproportionally large emitters of $CO_2$, consistent with their ecological role as hotspots for gaseous and nutrient exchange. The groundwater/hyporheic contribution to OM processing remains elusive; however, carbon cycle investigations in model karst systems, such as the Cascade Cave system, may help reconcile stream-based ideas about natural OM heterotrophic processing, i.e., the River Continuum Concept (Vannote et al., 1980), and evolving soil/vadose zone models (Marin-Spiotta et al., 2014; Simon et al., 2007; Simon et al., 2010). Despite the lack of deep soil cover, the Cascade Cave system was a highly efficient biodegradation route for natural OM, which suggests that additional significant decomposition capacity may lie with microbial degraders attached to reactive surfaces in the inaccessible epikarst zone. The association of viable anaerobic bacteria and semi-labile macromolecules in the suspended fraction suggests that aggregation and protection on colloidal particulate matter may play an important role in transporting nutrients to downstream springs and discharge points (Tranvik et al., 2010), where the complexes would be photodegraded and bound nutrients released to consumers upon re-entering the photic environment (Marin-Spiotta et al., 2014). Therefore, future carbon cycle studies in the Cascade Cave catchment should also focus on the fate of DOM as it is re-introduced to the photic zone as groundwater recharge.

The hydrogeologic and metabolic processes at work during subsurface transport in karst systems can be considered analogous to those occurring in the hyporheic zones at the interface between streams and shallow, alluvial aquifers (e.g., Boulton et al., 1998; Valett et al., 2009; Vinson et al., 2007). Hyporheic ecotones are sites of solute and nutrient exchange with surface water, floodplains, and groundwater along biochemically active corridors in unconsolidated sediments (Baker et al., 2000; Stanford et al., 1993). In comparison, groundwater in many epigenic karst systems flows along preferential flow paths that have been dissolutionally etched into relatively impermeable consolidated matrices (Ford et al., 2007). Although the mechanisms of groundwater-surface water interactions and DOM transformations differ between surface-influenced cave streams and hyporheic zones, the expanded use of weak-anion exchange SPE to isolate hydrophilic DOM in other karst systems, as well as different geologic settings, may reveal similarities in microbial bioprocessing in interconnected surface stream/groundwater systems that can ultimately be quantified and scaled up to inform regional climate and carbon cycle models.

International efforts to link biogeography and hydrochemistry with environmental data for aquifers and their recharge areas have presented substantial challenges related to scaling and complexity. Effective implementation of these novel programs is limited by a lack of knowledge about groundwater-surface water interactions (Battin et al., 2008b), sparse microbial and faunal data for uncontaminated sites (Goldscheider et al., 2006), and low natural concentrations of carbon and nutrients (Griebler et al., 2010). The development of low-cost, portable, and sensitive DOM characterization techniques for oligotrophic aquifers, as demonstrated here for the Cascade Cave system, could greatly advance the ecological assessment of groundwater systems.

These results highlight the importance of addressing both OM quality and microbial community structure as ecosystem properties that must be incorporated in comprehensive biomonitoring strategies to track long-term regional trends in groundwater recharge and water quality. Quantifying direct linkages between macromolecular DOM transformations and microbial community status in complex aquatic systems remains a challenge because seasonal patterns in DOM quality and microbial processing can be over-printed by environmental variables such as local climate, hydrologic conditions, vegetation and land use. The key may be to investigate DOM transformations in stable, nearly pristine systems at the critical zone interface and reach scale processes at shorter (monthly or less) sampling intervals, especially during low flow conditions during all seasons, which was not done here. Furthermore, including total nitrogen, organic phosphorus, and inorganic ligands, such as silica and iron, into geochemical parameter analysis (in addition to flow data) may facilitate the integration of environmental and microbiological factors in a more comprehensive assessment of water quality trends.

## References

Abdulla, H., Minor, E., Dias, R., & Hatcher, P. (2010). Changes in compound classes of dissolved organic matter along an estuarine transect: A study using FTIR and $^{13}C$ MNR. *Geochimica et Cosmochimica Acta, 74*, 3815-3838.

Aiken, G.R., McKnight, D.M., Thorn, K., & Thurman, E.M. (1992). Isolation of hydrophilic organic acids from water using nonionic macroporous resins *Organic Geochemistry, 18*(4), 567-573.

Alberts, J.J., & Takács, M. (2004). Total luminescence spectra of IHSS standard and reference fulvic acids, humic acids and natural organic matter: comparison of aquatic and terrestrial source terms. *Organic Geochemistry, 35*(3), 243-256.

Alexander, S.C. (2005). *Spectral deconvolution and quantification of natural organic material and fluorescent tracer dyes.* Paper presented at the Sinkholes and the Engineering and Environmental Impacts of Karst (2005).

Aley, Thomas J. (1999). *Groundwater Tracing Handbook.* Protem, MO: Ozark Underground Laboratory.

Aley, TJ. (1999). The Ozark underground laboratory's groundwater tracing handbook: Ozark Underground Laboratory. *Protem, Missouri*.

Allison, S.D., Chacon, S.S., & German, D.P. (2014). Substrate concentration constraints on microbial decomposition *Soil Biology & Biochemistry, 79*, 43-49.

Amelung, W., Brodowski, S., Sandhage-Hofmann, A., & Bol, R. (2008). Combining biomarker with stable isotope analysis for assessing the transformation and turnover of soil organic matter. *Advances in Agronomy, 100*, 155-250.

Amery, F, Vanmoorleghem, C, & Smolders, E. (2009). Adapted DAX-8 fractionation method for dissolved organic matter (DOM) from soils: development, calibration with test

components and application to contrasting soil solutions. *European journal of soil science, 60*(6), 956-965.

Amon, Rainer MW, & Benner, Ronald. (1996). Bacterial utilization of different size classes of dissolved organic matter. *Limnology and Oceanography, 41*(1), 41-51.

Anneken, D. J., Both, S., Christoph, R., Fieg, G., Steinberner, U., & Westfechtel, A. (2000). Fatty Acids *Ullmann's Encyclopedia of Industrial Chemistry*: Wiley-VCH Verlag GmbH & Co. KGaA.

ASTM, International. (2015). *ASTM D5176-08* West Conshohocken, PA: Association for Standards and Testing of Materials International Retrieved from www.astm.org.

Baker, A., & Genty, D. (1999). Fluorescence wavelength and intensity variations in cave waters. *Journal of Hydrology, 217*, 19-34.

Baker, A., & Inverarity, R. (2004). Protein-like fluorescence intensity as a possible tool for determining river water quality. *Hydrological Processes, 18*(15), 2927-2945.

Baker, A., & Lamont-Black, J. (2001). Fluorescence of dissolved organic matter as a natural tracer of ground water *Ground Water, 39*(5), 745-750.

Baker, M.A., Valett, A.M., & Dahm, C.N. (2000). Organic carbon supply and metabolism in a shallow groundwater ecosystem. *Ecology, 81*(11), 3133-3148.

Balkwill, D.L., Leach, F.R., Wilson, J.T., McNabb, J.F., & White, D.C. (1988). Equivalence of microbial biomass measures based on membrane lipid and cell wall components, adenosine triphosphate, and direct counts in subsurface sediments. *Microbial Ecology, 16*, 73-84.

Battin, T., Kaplan, L., Findlay, S., Hopkinson, C., Marti, E., Packman, A., . . . Sabater, F. (2008a). Biophysical controls on organic carbon fluxes in fluvial networks. *Nature Geoscience, 1*, 95-100.

Battin, T., Kaplan, L., Findlay, S., Hopkinson, C., Marti, E., Packman, A., . . . Sabater, F. (2008b). Biophysical controls on organic carbon fluxes in fluvvial networks. *Nature Geoscience, 1*, 95-100.

Bellmore, R.A., Harrison, J. A., Needoba, J. A., Brooks, E. S., & Kent, K. C. (2015). Hydrologic control of dissolved organic matter concentration and quality in a semiarid artificially drained agricultural catchment. *Water Resources Research, 51*(10), 8146-8164.

Benner, R. (Ed.). (2002). *Chemical composition and reactivity* San Diego: Academic Press.

Benner, R. (Ed.). (2003). *Molecular indicators of the bioavalability of dissolved organic matter*. San Diego: Academic Press.

Benner, R., & Opsahl, S. (2001). Molecular indicators of the sources and transformations of dissolved organic matter in the Mississippi River plume. *Organic Geochemistry, 32*, 597-611.

Berggren, Martin, Laudon, Hjalmar, & Jansson, Mats. (2009). Hydrological control of organic carbon support for bacterial growth in boreal headwater streams. *Microbial ecology, 57*(1), 170-178.

Bianchi, T.S., & Canuel, E.A. . (2011). Lignins, Cutins, and Suberins *Chemical Biomarkers in Aquatic Ecosystems* (pp. 417). Princeton, NJ: Princeton University Press.

Birdwell, J., & Engel, A.S. (2009). Variability in terrestrial and microbial contributions to dissolved organic matter fluorescence in the Edwards Aquifer, central Texas *Journal of Cave and Karst Studies, 71*, 144-156.

Birdwell, J., & Engel, A.S. (2010). Characterization of dissolved organic matter in cave and spring waters using UV-Vis absorbance and fluorescence spectroscopy *Organic Geochemistry, 41*, 270-280. doi: 10.1016/j.orggeocgem.2009.11.002

Bligh, E.G., & Dyer, W.J. (1959). A rapid method of total lipid extraction and purification *Canadian Journal of Biochemistry and Physiology, 37*, 911-917.

Bossio, D.A., & Scow, K.M. (1998). Impacts of carbon and flooding on soil microbial communities: Phopholipid fatty acid profiles and substrate utilization patterns. *Microbial Ecology, 35*, 265-278.

Boult, S, Jugdaohsingh, R, White, K, Smith, B, & Powell, J. (2001). Evidence that polysaccharide and humic and fulvic acids are co-extracted during analysis but have different roles in the chemistry of natural waters. *Applied geochemistry, 16*(9), 1261-1267.

Boulton, A.J., Findlay, S., Marmonier, P., Stanley, E.H., & Valett, H.M. (1998). The functional significance of the hyporheic zone in streams and rivers. *Annual Review of Ecological Systems, 29*, 59-81.

Brady, N.C., & Weil, R.R. (2008). *The Nature and Properties of Soils*. Upper Saddle River, NJ: Pearson Prentice-Hall.

Brannen-Donnelly, K., & Engel, A.S. (2015). Bacterial diversity differences along an epigenic cave stream reveal evidence of community dynamics, succession, and stability *Frontiers in Microbiology 6*, 729. doi: 10.3389/fmicb.2015.00729

Brannen, K., Engel, A.S., & Birdwell, J. (2009). *Tracing the origins of chromophoric dissolved organic matter in karst aquifers* Paper presented at the 15th International Congress of Speleology Kerrville, TX.

Bronk, D.A. (Ed.). (2002). *Dynamics of DON*. San Diego: Academic Press.

Brooks, P.D., McKnight, D.M., & Bencala, K.E. (1999). The relationship between soil heterotrophic activity, soil dissolved organic carbon (DOC) leachate, and catchment-scale DOC export in headwater catchments. *Water Resources Research, 35*(6), 1895-1902.

Brown, T.L., Engel, A.S., Brannen, K., & Birdwell, J. (2011). *Estimating aquifer contributions to carbon cycle budgets based on dissolved organic matter characterization in karst aquifers.* Paper presented at the Carbonate Geochemistry: Reactions and Processes in Aquifers and Reservoirs Billings, MT.

Brown, T.L., Jones, S.W., & McKay, L.D. (2009). *Fluorescence characterization of carbonate aquifers.* Paper presented at the 15th International Congress of Speleology, Kerrville, TX.

Buffam, I, Galloway, JN, Blum, LK, & McGlathery, KJ. (2001). A stormflow/baseflow comparison of dissolved orgnaic matter concentrations and bioavailablity in an Appalachian stream. *Biogeochemistry, 53,* 269-306.

Burney, C.M. (1994). Seasonal and diel changes in particulate and dissolved organic matter. *The biology of particulates in aquatic systems. Lewis, Florida*, 97-135.

Cabaniss, S.E. (1991). Carboxylic acid content of a fulvic acid determined by potentiometry and aqueous Fourier transform infrared spectrometry *Analytica Chimica Acta, 1,* 23-30.

Cabaniss, S.E., & McVey, I.F. (1995). Aqueous infrared carboxylate absorbances: aliphatic monocarboxylates. *Spectrochimica Acta Part A: Molecular and Biomolecular Spectroscopy, 51*(13), 2385-2395.

Chanudet, V., & Fillela, M. (2007). Submicron organic matter in a peri-alpine, ultra-oligotrophic lake. *Organic Geochemistry, 38,* 1146-1160.

Chen, C.R., & Xu, Z.H. (2008). Analysis and behavior of soluble organic nitrogen in forest soils. *Journal of Soils and Sediments, 8*(6), 363-378. doi: 10.1007/s11368-008-0044-y

Chin, Y-P., Aiken, G.R., & Danielsen, K.M. (1997). Binding of pyrene to aquatic and commercial humic substances: the role of molecular weight and aromaticity. *Environmental Science & Technology, 31*(6), 1630-1635.

Christie, WW. (2015). The Lipid Home. from http://www.lipidhome.co.uk/lipids/basics/whatlip/index.htm

Ciais, P., Sabine, C., Bala, G., Bopp, L., Brovkin, V., Canadell, J., . . . Heimann, M. (2014). Carbon and other biogeochemical cycles *Climate Change 2013: The Physical Science Basis. Contribution of Working Group I to the Fifth Assessment Report of the Intergovernmental Panel on Climate Change* (pp. 465-570): Cambridge University Press.

Clifford, M., & McGeer, J.C. . (2010). Development of a biotic ligand model to predict the acute toxicity of cadmium to Daphnia pulex. *Aquatic Toxicology, 98*(1), 1-7.

Coble, P. (1996). Characterization of marine and terrestrial DOM in seawater using excitation-emission matrix spectroscopy. *Marine Chemistry, 51,* 325-346.

Cole, JJ, Prairie, YT, Caraco, NF, McDowell, WH, Tranvik, LJ, Striegl, RG, . . . Middelburg, JJ. (2007). Plumbing the global carbon cycle: integrating inland waters into the terrestrial carbon budget. *Ecosystems, 10*(1), 172-185.

Company, Rohm and Haas. (2000). Amberlite XAD Polymeric Adsorbents

Cory, R.M., & McKnight, D.M. (2005). Fluorescence spectroscopy reveals ubiquitous presence of oxidized and reduced quinones in dissolved organic matter. *Environmental Science and Technology, 39*(21), 8142-8149.

Cozzolino, A, Conte, P, & Piccolo, A. (2001). Conformational changes of humic substances induced by some hydroxy-, keto-, and sulfonic acids. *Soil Biology and Biochemistry, 33*(4), 563-571.

Crawford, Nicholas. (1996). *The Karst Hydrogeology of the Cumberland Plateau Escarpment of Tennessee: Subterranean stream invasion, conduit cavern development, and slope retreat in the Lost Creek Cove area, White County, Tennessee*: Tennessee Department of Conservation, Division of Geology.

Cronan, C.S. (2009). Major Cations (Ca, Mg, Na, K, Al). In G. E. Likens (Ed.), *Encyclopedia of Inland Waters* (pp. 354-360). San Diego: Academic Press.

Croue, J.-P. (2004). Isolation of humic and non-humic NOM fractions: Structural characterizations *Environmental Monitoring and Assessment, 92*, 193-207.

D'Orazio, V., & Senesi, N. (2009). Spectroscopic properties of humic acids isolated from the rhizosphere and bulk soil compartments and fractionated by size-exclusion chromatography. *Soil Biology & Biochemistry, 41*, 1775-1781.

Daignault, SA, Noot, DK, Williams, DT, & Huck, PM. (1988). A review of the use of XAD resins to concentrate organic compounds in water. *Water research, 22*(7), 803-813.

DeForest, J.L., Drerup, S.A., & Vis, M.L. (2016). Using fatty acids to fingerprint biofilm communiti4es: a means to quickly and accurately assess stream quality *Environmental Monitoring and Assessment, 188*(277), 1-9. doi: 10.1007/s10661-016-5290-7

Delpla, I., Jung, A.-V., Baures, E., Clement, M., & Thomas, O. (2009). Impacts of climate change on surface water quailty in relation to drinking water production. *Environment International, 35*, 1225-1233.

Dobbs, F.C., & Guckert, J.B. (1988a). *Callianassa trilobita* (Crustacea: Thalassinidea) influences abundance of meiofauna and biomass, composition, and physiolgic state of microbial communities within its burrow *Marine Ecology Progress Series, 45*, 69.

Dobbs, F.C., & Guckert, J.B. (1988b). Microbial food resources of the macrofaunal-deposit feeder *Ptychodera bahamensis* (Hemichordata: Enteropnuesta) *Marine Ecology Progress Series, 45*, 127.

Docherty, K.M., & Gutknecht, J.L.M. . (2012). The role of environmental microorganisms in ecosystem responses to global change: current state of research and future outlooks. *Biogeochemistry, 109*, 1-6. doi: 10.1007/s10533-011-9614-y

Dodds, WK, & Oakers, RM. (2008). Headwater influences on downstream water quality. *Environmental Management, 41*, 367-377.

Eaton, A.D. (2005). *Standard Methods for the Examination of Water and Wastewater* (21 ed.). Washington, D.C.: American Public Health Association, American Waterworks Association, Water Environment Foundation.

Egli, T. (2010). How to live at very low substrate concentration. *Water Research, 44*, 4826-4837.

Eimers, C.M., Watmough, S.A., & Buttle, J.A. (2008). Long-term trends in dissolved organic carbon concentration: a cautionary note. *Biogeochemistry, 87*, 71-81. doi: 10.1007/s10533-007-9168-1

Einseidl, F., Hertkorn, N., Wolf, M., Frommberger, M., Schmitt-Kopplin, P., & Koch, B. (2007). Rapid biotic molecular transformation of fulvic acids in a karst aquifer *Geochimica et Cosmochimica Acta, 71*, 5474-5482.

Ellison, A.M., & Gotelli, N.J. (2004). A primer of ecological statistics. *Sinauer, Sunderland, Massachusetts, USA.*

Ellison, AM, & Gotelli, NJ. (2004). *A primer of ecological statistics*.

Engel, A.S., & Engel, S.A. (2009, 2009). *A field guide for the karst of Carter Caves State Resort Park and the surrounding area, northeastern Kentucky* [Karst Waters Institute Special Publication ]. Select Field Guides to Cave and Karst Lands of the United States (15).

Englund, K.J. (Cartographer). (1976). Geologic Map of the Grahn Quadrangle, Carter County, KY.

Ettensohn, F.R., Rice, C.L., Dever, G.R., Jr., & Chesnut, D.R., Jr. . (1984). *Slade and Paragon Formations: New Stratigraphic Nomenclature for Mississippian Rocks Along the Cumberland Escarpment in Kentucky*. U.S. Geological Survey Bulletin (1605-B).

Farnleitner, A.H., Wilhartitz, I., Ryzinska, G., Kirschner, A.K.T., Stadler, H., Burtscher, M.M., . . . Mach, R.I. (2005). Bacterial dynamics in spring water of alpine karst aquifers indicate the presence of stable autochthonous microbial endokarst communities *Environmental Microbiology, 71*, 3003-3015.

Farnworth, JJ. (1995). Comparisons of the sorption from solution of a humic acid by Supelite DAX-8 and by XAD-8 resins. *IHSS Newsletter, 13*, 8-9.

Field, Malcolm S, Wilhelm, Ronald G, Quinlan, James F, & Aley, Thomas J. (1995). An assessment of the potential adverse properties of fluorescent tracer dyes used for groundwater tracing. *Environmental Monitoring and Assessment, 38*(1), 75-96.

Fierer, N., & Jackson, R.B. (2006). The diversity and biogeography of soil bacterial communities. *Proceedings of the National Academy of Sciences of the United States of America, 103*(3), 626-631.

Fierer, N., Schimel, J.P., & Holden, P.A. (2003). Variations in microbial community composition through two soil depth profiles. *Soil Biology and Biochemistry, 35*(1), 167-176.

Filella, M. (2009). Freshwaters: which NOM matters? *Environmental chemistry letters, 7*(1), 21-35.

Filella, M. (2014). Understanding what we are measuring: Standards and quantification of natural organic matter. *Water Research 50*, 287-293.

Fimmen, R.L., Cory, R.M., Chin, Y.P., Trouts, T.D., & McKnight, D.M. (2007). Probing the oxidation-reduction properties of terrestrially and microbially derived dissolved organic matter. *Geochimica et Cosmochimica Acta, 71*, 3003-3015.

Findlay, R.H., & Dobbs, F.C. (1993). Quantitative description of microbial communities using lipid analyses In P. F. Kemp, B. F. Sherr, E. C. Sherr & J. Cole (Eds.), *Handbook of Methods in Aquatic Microbial Ecology* (pp. 271-284). Boca Raton: Lewis.

Findlay, RH, Yeates, C, Hullar, MAJ, Stahl, DA, & Kaplan, LA. (2008). Biome-level biogeography of streambed microbiota. *Applied and Environmental Microbiology, 74*(10), 3014-3021.

Finzi, A.C., Austin, A.T., Cleland, E.E., Frey, S.D., B.Z., Houlton., & Wallenstein, M.D. (2011). Responses and feedbacks of coupled biogeochemical cycles to climate change: examples from terrestrial ecosystems. *Frontiers in Ecology and the Environment, 9*(1), 61-67.

Fisher, S.G., & Likens, G.E. (1973). Energy flow in Bear Brook, New Hampshire: an integrative approach to stream ecosystem metabolism *Ecological Monographs, 43*, 421-439.

Fontaine, S., Mariotti, A., & Abbadie, L. (2003). The priming effect of organic matter: a question of microbial competition? *Soil Biology and Biochemistry, 35*(6), 837-843.

Ford, D., & Williams, P. (1994). *Karst Geomorphology and Hydrology*. London: Chapman & Hall.

Ford, D.C., & Williams, P.W. (2007). *Karst Hydrogeology and Geomorphology*. New York: Wiley.

Fram, M.S., Fujii, R., Weishaar, J.L., Bergamaschi, B.A., & Aiken, G.R. (1999). *How DOC composition may explain the poor correlation between specific trihalomethane formation potential and specific UV absorbance* Charleston, S.C. .

Fredrickson, JK, McKinley, JP, Bjornstad, BN, Long, PE, Ringelberg, DB, White, DC, . . . Lehman, RM. (1997). Pore-size constraints on the activity and survival of

subsurface bacteria in a late cretaceous shale-sandstone sequence, northwestern New Mexico. *Geomicrobiology Journal, 14*(3), 183-202.

Friedlingstein, P., Cox, P., Betts, R., Bopp, L., Von Bloh, W., Brovkin, V., . . . Zeng, N. . (2006). Climate-carbon cycle feedback analysis: results from the $C^4$MIP model intercomparison. *Journal of Climatology, 19*, 3337-3353.

Frimmel, F.H. (1998). Characterization of natural organic matter as major constituents in aquatic systems. *Journal of Contaminant Hydrology, 35*(1), 201-216.

Frostegård, Å, Bååth, E, & Tunlio, A. (1993). Shifts in the structure of soil microbial communities in limed forests as revealed by phospholipid fatty acid analysis. *Soil Biology and Biochemistry, 25*(6), 723-730.

Frostegård, Å, Tunlid, A., & Baath, E. (1996). Changes in microbial community structure during long-term incubation in  two soils experimentally contaminated with metals. *Soil Biology and Biochemistry, 28*(1), 55-63.

Garip, S., Gozen, A., & Severcan, F. (2009). Use of Fourier transform infrared spectrsocopy for rapid comparative analysis of *Bacillus* and *Micrococcus* isolates. *Food Chemistry, 113*, 1301-1307.

Gibert, J. (1986). Ecologie d'un systeme karstique jurassien. Hydrogeologie, derive anaimale, transits de matieres, dynamique de la population de *Niphargus* (Crustace Amphipode). *Memoires de Biospeologie, 13*(1-379).

Giotis, E.S. , McDowell, D.A., Blair, I.S, & B.J., Wilkinson. (2007). Role of branched-chain fatty acids in pH stress toolerance in *Listeria monocytogenes Applied and Environmental Microbiology, 73*(3), 997-1001.

Glover, C.N., Sharma, S.K., & Wood, C.M. (2005). Heterogeneity in physicochemical properties explains differences in silver toxicity amelioration by natural organic matter to Daphnia magna. *Environmental toxicology and chemistry, 24*(11), 2941-2947.

Goldscheider, N., Hunkeler, D., & Rossi, P. (2006). Review: microbial biocenoses in pristiine aquifers and an assessment of investigative methods. *Hydrogeology Journal, 14*, 926-941.

Goldscheider, Nico, Meiman, Joe, Pronk, Michiel, & Smart, Christopher. (2008). Tracer tests in karst hydrogeology and speleology. *International Journal of Speleology, 37*(1), 3.

Göppert, Nadine, & Goldscheider, Nico. (2008). Solute and Colloid Transport in Karst Conduits under Low-and High-Flow Conditions. *Groundwater, 46*(1), 61-68.

Graening, G.O., & Brown, A.V. (2003). Ecosystem dynamics and pollution effects in an Ozark cave stream. *Journal of the American Water Resources Association, 39*, 497-505.

Green, R.T., Painter, S.L., Sun, A., & Worthington, S.R.H. (2006). Groundwater contamination in karst terranes. *Water, Air and Soil Pollution, 6*, 157-170.

Grey, A., & Bolland, M. (2014). CLinical trial evidence and use of fish oil supplements. *JAMA Internal Medicine, 174*(3), 460-462. doi: 10.1001/jamainternmed.2013.12765

Griebler, C., Stein, H., Kellermann, C., Berkhoff, S., Brielmann, H., Schmidt, S., . . . Hahn, H. J. (2010). Ecological assessment of groundwater ecosystems - Vision or illusion? *Ecological Engineering, 36*(9), 1174-1190. doi: 10.1016/j.ecoleng.2010.01.010

Grube, M., Lin, J.G., Lee, P.G., & Kokorevicha, S. (2006). Evaluation of sewage sludge-based compost by FT-IR spectroscopy. *Geoderma, 130*(3-4), 324-333.

Guckert, J.B., Antworth, C.P., Nichols, P.D., & White, D.C. (1985). Phospholipids, ester-linked fatty acid profiles as reproducible assays for changes in prokaryotic community structure of estuarine sediments. *FEMS Microbiology Ecology, 31*, 147-158.

Guckert, JB, Hood, MA, & White, DC. (1986). Phospholipid ester-linked fatty acid profile changes during nutrient deprivation of Vibrio cholerae: increases in the trans/cis ratio and proportions of cyclopropyl fatty acids. *Applied and environmental microbiology, 52*(4), 794-801.

Guenet, B., Danger, M., Abbadie, L., & Lacroix, G. (2010). Priming effect: bridging the gap between terrestrial and aquatic ecology. *Ecology, 91*(10), 2850-2861.

Gurr, M.I., Harwood, J.L., & Frayn, K.N. (2002). *Lipid Biogeochemistry: An Introduction* (5th ed.). Oxford: Blackwell Science, Ltd.

Hansell, D.A., Carlson, C.A., Repeta, D.J., & Schlitzer, R. (2009). Dissolved organic matter in the ocean: A controversy stimulates new insights. *Oceanography, 22*(4), 202-211.

Harlow, Jr., G.E., Orndorff, R.C., Nelms, D.L., Weary, D.J. , & Moberg, R.M. (2005). *Hydrogeology and ground-water availability in the carbonate aquifer system on Frederick County, Virginia* Reston.

Härtig, C., Loffhagen, N., & Harms, H. (2005). Formation of trans fatty acids is not involved in growth-linked membrane adaptation of Pseudomonas putida. *Applied and environmental microbiology, 71*(4), 1915-1922.

Hattenschwiler, S., & Vitousek, P.M. (2000). The role of polyphenols in terrestrial ecosystem nutrient cycling. *TREE, 15*(6), 238-243.

Hay, M.B., & Myneni, S.C.B. (2007). Structural environments of carboxyl groups in natrual organic molecules from terrestrial systems. Part I: Infrared spectroscopy. *Geochimica et Cosmochimica Acta, 71*, 3518-3532.

Hazen, TC, Dubinsky, EA, DeSantis, TZ, Andersen, GL, Piceno, YM, Singh, N, . . . Fortney, JL. (2010). Deep-sea oil plume enriches indigenous oil-degrading bacteria. *Science, 330*(6001), 204-208.

Hedges, J.I., Keil, R.G., & Benner, R. (1997). What happens to terrestrial organic matter in the ocean? *Organic Geochemistry, 27*(5-6), 195-212.

Heipieper, H.J., & Fischer, J. (2010). Bacterial Solvent Responses and Tolerance: *Cis-Trans* Isomerization. In K. N. Timmis (Ed.), *Handbook of Hydrocarbon and Lipid Microbiology* (pp. 4204-4211). Heidelberg: Springer-Verlag.

Hejzlar, J, Szpakowska, B, & Wershaw, RL. (1994). Comparison of humic substances isolated from peatbog water by sorption on DEAE-cellulose and Amberlite XAD-2. *Water Research, 28*(9), 1961-1970.

Hernandez, ME, Mead, R, Peralba, C, & Jaffé, R. (2001). Origin and transport of n-alkane-2-ones in a subtropical estuary: potential biomarkers for seagrass-derived organic matter. *Organic Geochemistry, 32*(1), 21-32.

Hessen, D., & Tranvik, L..J. (2013). *Aquatic humic substances: ecology and biogeochemistry* (Vol. 133): Springer Science & Business Media.

Hornberger, G.M., Raffensperger, J.P., Wiberg, P.L., & Eshleman, K.N. (1998). *Elements of Physical Hydrology*. Baltimore: The John Hopkins University Press.

Horner-Devine, MC, Lage, M, Hughes, JB, & Bohannan, BJM. (2004). A taxa–area relationship for bacteria. *Nature, 432*(7018), 750-753.

Ibrahim, MBM, Moursy, AS, Bedair, AH, & Radwan, EK. (2008). Comparison of DAX-8 and DEAE for isolation of humic substances from surface water. *J Environ Sci Technol, 1*, 90-96.

IUBMB, International Union of Pure And Applied Chemistry (IUPAC)-International Union of Biochemistry and Molecular Biology. (2015). Lipid Nomenclature. from http://www.chem.qmul.ac.uk/iupac/

Jaffe, R., McKnight, D.M., Maie, N., Cory, R.M., McDowell, W.H., & Campbell, J.L. (2008). Spatial and temporal variations of DOM composition in ecosystems: the importance of long-term monitoring of optical properties *Journal of Geophysical Research 113*(G4032).

Janoš, P. (2003). Separation methods in the chemistry of humic substances. *Journal of Chromatography A, 983*(1), 1-18.

Jardine, P.M., Mayes, M.A., Mulholland, P.J., Hanson, P.J., Tarver, J.R., Luxmoore, R.J., . . . Wilson, G.V. (2006). Vadose zone flow and transport of dissolved organic carbon at multiple scales in humid regions. *Vadose Zone Journal, 5*, 140-152.

Jiao, N., Herndl, G.J., Hansell, D.A., Benner, R., Kattner, G, Wilhelm, S.W., . . . Azam, F. (2010). Microbial production of recalcitrant dissolved organic matter: long-term carbon storage in the global ocean. *Nature Reviews/Microbiology, 8*, 593-599.

Jobbagy, E.G., & Jackson, R.B. (2000). The vertical distribution of soil organic carbon and its relation to climate and vegetation. *Ecological Applications 10*, 423-436.

Judd, Kristin E, Crump, Byron C, & Kling, George W. (2006). Variation in dissolved organic matter controls bacterial production and community composition. *Ecology, 87*(8), 2068-2079.

Kacurakova, M, Capek, P, Sasinkova, V, Wellner, N, & Ebringerova, A. (2000). FT-IR study of plant cell wall model compounds: pectic polysaccharides and hemicelluloses. *Carbohydrate polymers, 43*(2), 195-203.

Kaiser, K., & Guggenberger, G. . (2005). Storm flow flushing in a structured soil changes the composition of dissolved organic matter leached into the subsoil *Geoderma, 127*, 177-187.

Kaiser, Klaus, & Guggenberger, Georg. (2000). The role of DOM sorption to mineral surfaces in the preservation of organic matter in soils. *Organic geochemistry, 31*(7), 711-725.

Kalbitz, K., Schmerwitz, J., Schwezig, D., & Matzner, E. . (2003). Biodegradation of soil-derived dissolved organic matter as related to its properties. *Geoderma, 113*(3-4), 273-291.

Kaneda, T. (1991). Iso-and anteiso-fatty acids in bacteria: biosynthesis, function, and taxonomic significance. *Microbiological reviews, 55*(2), 288-302.

Kaplan, L.A., & Newbold, J.D. (2003). The role of monomers in stream ecosystem metabolism. In S. E. G. a. S. Findlay, R.L. (Ed.), *Aquatic Ecosystems: Intersactivity of Dissolved Organic Matter* (pp. 97-119). Boston: Academic Press.

Käss, W, Behrens, H, Himmelsbach, T, Hötzl, H, Hunkeler, D, Leibundgut, CH, . . . Stober, I. (1998). *Tracer technique in geohydrology*. Rotterdam: Balkema.

Kass, W. (1998). *Tracing Technique in Geohydrology*. Rotterdam: A.A. Balkema.

Kaur, A., Chaudhary, A., Kaur, A., Choudhary, R., & Kaushik, R. (2005). Phospholipid fatty acid - A bioindicator of environment monitoring and assessment in soil ecosystem. *Current Science, 89*(7), 1103-1112.

Keith-Roach, MJ, Bryan, ND, Bardgett, RD, & Livens, FR. (2002). Seasonal changes in the microbial community of a salt marsh, measured by phospholipid fatty acid analysis. *Biogeochemistry, 60*(1), 77-96.

Kellerman, AM, Kothawala, DN, Dittmara, T, & Tranvik, LJ. (2015). Persistence of dissolved organic matter in lakes related to its molecular characteristics. *Nature Geoscience, 8*, 454-459.

Kerger, B.D., Nichols, P.D., Antworth, C.P., Sand, W., Bock, E., Cox, J.C., . . . White, D.C. (1986). Signature fatty acids in the polar lipids of acid-producing Thiobacillus spp.: Methoxy, cyclopropyl, alpha-hydroxy-cyclopropyl and branched and normal monoenoic fatty acids. *FEMS microbiology letters, 38*(2), 67-77.

Kieft, Thomas L, Wilch, Ellen, O'connor, Kristina, Ringelberg, David B, & White, David C. (1997). Survival and phospholipid Fatty Acid profiles of surface and subsurface bacteria in natural sediment microcosms. *Applied and Environmental Microbiology, 63*(4), 1531-1542.

Kieft, TL, Ringelberg, DB, & White, DC. (1994). Changes in ester-linked phospholipid fatty acid profiles of subsurface bacteria during starvation and desiccation in a porous medium. *Applied and Environmental Microbiology, 60*(9), 3292-3299.

Klaine, S.J., Alvarez, P.J.J., Batley, G.E., Fernandes, T.F., Handy, R.D., Lyon, D.Y., . . . Lead, J.R. . (2008). Nanomaterials in the environment: Behavior, fate, bioavailability, and effects *Environmental Toxicology and Chemistry, 27*(9), 1825-1851.

Kleber, M., Nico, P.S., Plante, A., Filleys, T., Kramer, M., Swanston, C., & Sollins, P. (2011). Old and stable organic matter is not necessarily chemically recalcitrant:

implications for modeling concepts and temperature sensitivity. *Global Change Biology, 17*, 1097-1107.

Knicker, H., & Hatcher, P. (1997). Survival of protein in an organic-rich sediment: possible protection by encapsulation in organic matter. *Natursissenschaften, 84*(6), 231-234.

Korshin, G.V., Li, C., & Benjamin, M.N. (1997). Monitoring the properties of natural organic matter through UV spectroscopy: a consistent theory *Water Research, 31*(7), 1787-1795.

Kuzyakov, Y. (2010). Priming effects: Interactions between living and dead organic matter *Soil Biology & Biochemistry, 42*, 1363-1371.

Kuzyakov, Ya, Friedel, JK, & Stahr, K. (2000). Review of mechanisms and quantification of priming effects. *Soil Biology and Biochemistry, 32*(11), 1485-1498.

Lakowicz, J.R. (2013). *Principles of fluorescence spectroscopy*: Springer Science & Business Media.

Lam, B., Baer, A., Alaee, M., Lefebvre, B., Moser, A., Williams, A., & Simpson, A.J. (2007). Major structural components in freshwater dissolved organic matter. *Environmental Science & Technolology, 41*, 8240-8247.

Lane, C.S., Lyon, D.R., & Ziegler, S.E. (2013). Cycling of two carbon substrates of constrasting lability by heterotrophic biofilms across a nutrient gradient of headwater streams. *Aquatic Sciences, 75*, 235-250.

Lavelle, P., & Spain, A. (2001). *Soil Ecology*: Springer Science and Business Media.

Leenheer, J.A. (1981). Comprehensive approach to preparative isolation and fractionation of dissolved organic carbon from natural waters and wastewaters *Environmental Science & Technology, 15*(5), 578-587.

Leenheer, J.A. (2009). Systematic approaches to comprehensive analyses of natural organic matter. *Annals of Environmental Science 3*, 1-130.

Leenheer, J.A., & Croue, J.-P. (2003). Characterizing aquatic dissolved organic matter. *Environmental Science & Technology, 37*, 18A-26A.

Leenheer, J.A., Wershaw, R.L., & Reddy, M.M. (1995). Strong-acid, carboxyl-group structures in fulvic acid from the Suwannee River, Georgia: 1. Minor structures. *Environmental Science & Technology, 29*(2), 393-398.

Lierman, T., Ettensohn, F., & Mason, C. (2011). Geology of the Carter Caves Area. In M. Smith (Ed.), *Field Trip Guide* (pp. 50). Lexington, KY: American Institute of Professional Geologists-Kentucky Section

Littell, R.C., Stroup, W.W., Milliken, G.A., Wolfinger, R.D., & Schabenberger, O. (2006). *SAS for mixed models*: SAS institute.

Loaiciga, H.A. (2009). Long-term climate change and sustainable groundwater resources management *Environmental Research Letters, 4*, 1-11.

Loffhagen, N, Härtig, C, Geyer, W, Voyevoda, M, & Harms, H. (2007). Competition between cis, trans and cyclopropane fatty acid formation and its impact on membrane fluidity. *Engineering in Life Sciences, 7*(1), 67-74.

Macalady, D.L., & Walton-Day, K. (2011). Redox chemistry and natural organic matter (NOM): Geochemists' dream, analytical chemists' nightmare. In P. T. e. al. (Ed.), *Aquatic*

*Redox Chemistry, ACS Symposium Series* (pp. 85-111). Washington, D.C.: American Chemical Society.

MacCarthy, P. (1976). A proposal to establish a reference collection of humic materials for interlaboratory comparisons. *Geoderma, 16*, 179-181.

Madigan, M.T., Martinko, J.M., Stahl, D.A., & Clark, D.P. (2012). *Brock Biology of Microorganisms* (13 ed.). San Franscisco: Pearson Education, Inc.

Maie, N., Parish, K.J., Watanabe, A., Knicker, H., Benner, R., Abe, T., . . . Jaffé, R. (2006). Chemical characteristics of dissolved organic nitrogen in an oligotrophic subtropical coastal ecosystem. *Geochimica et Cosmochimica Acta, 70*(17), 4491-4506.

Maier, R.M., & Pepper, I.L. (2000). Terrestrial Environments. In R. Maier, I. Pepper & C. Gerba (Eds.), *Environmental Microbiology* (pp. 61-89). San Diego: Academic Press.

Marin-Spiotta, E., Gruley, K.E., Crawford, J., Atkinson, E.E., Mieswel, J.R., Greene, S., . . . Spencer, R.G.M. (2014). Paradigm shifts in soil organic matter research affect interpretations of aquatic carbon cycling: transcending disciplinary and ecosystem boundaries *Biogeochemistry, 117*, 279-297.

Martiny, JBH, Bohannan, BJM, Brown, JH, Colwell, RK, Fuhrman, JA, Green, JL, . . . Kuske, CR. (2006). Microbial biogeography: putting microorganisms on the map. *Nature Reviews Microbiology, 4*(2), 102-112.

Mason, R.P. (2013). *Trace Metals in Aquatic Systems*: John Wiley & Sons.

Maurice, P.A., Pullin, M.J., Cabaniss, S.E., Zhou, Q., Namjesnik-Dejanovic, K., & Aiken, G.R. (2002). A comparison of surface water natural organic matter in raw filtered water samples, XAD, and reverse osmosis isolates. *Water Research, 36*(9), 2357-2371.

Max, J-J., & Chapados, C. (2004). Infrared spectroscopy of aqueous carboxylic acids: Comparison between different acids and their salts. *The Journal of Physical Chemistry A, 108*(16), 3324-3337.

McCarthy, J.F., Williams, T.M., Liang, L., Jardine, P.M., Jolley, L.W., Taylor, D.L., . . . Cooper, L.W. (1993). Mobility of natural organic matter in a sandy aquifer *Environmental Science & Technology, 27*, 667-676.

McClain, M.E., Boyer, E.W., Dent, C.L, Gergel, S.E., Grimm, N.B., Groffman, P.M., . . . Mayorga, E. (2003). Biogeochemical hot spots and hot moments at the interface of terrestrial and aquatic ecosystems. *Ecosystems, 6*(4), 301-312.

McDonald, S., Bishop, A.G., Prenzler, P.D., & Robards, K. (2004). Analytical chemistry of freshwater humic substances. *Analytica Chimica Acta, 527*, 105-124.

McGuire, K.L., & Treseder, K.K. (2010). Microbial communities and their relevance for ecosystem models: decomposition as a case study *Soil Biology & Biochemistry, 42*, 529-535.

McKinley, VL, Peacock, AD, & White, DC. (2005). Microbial community PLFA and PHB responses to ecosystem restoration in tallgrass prairie soils. *Soil Biology and Biochemistry, 37*(10), 1946-1958.

McKnight, D.M., Andrews, E.D., Spaulding, S.A., & Aiken, G.R. (1994). Aquatic fulvic acids in algal-rich Antarctic ponds. *Limnology and Oceanography, 39*(8), 1972-1979.

McKnight, D.M., Boyer, E.W., Westerhoff, P.K., Doran, P.T., Kulbe, T., & Andersen, D.T. (2001). Spectrofluorometric characterization of dissolved organic matter for indication of precursor organic material and aromaticity. *Limnology and Oceanography, 46*, 38-48.

McKnight, Diane M, Harnish, Richard, Wershaw, Robert L, Baron, Jill S, & Schiff, Sherry. (1997). Chemical characteristics of particulate, colloidal, and dissolved organic material in Loch Vale Watershed, Rocky Mountain National Park. *Biogeochemistry, 36*(1), 99-124.

Méjanelle, L., Laureillard, J., & Rassoulzadegan, F. (2005). Polar lipid biomarkers of free-living bacteria from oligotrophic marine waters. *Biogeochemistry, 72*(3), 365-383.

Miles, C.J., Tuschall Jr, J.R., & Brezonik, P.L. (1983). Isolation of aquatic humus with diethylaminoethylcellulose. *Analytical Chemistry, 55*(2), 410-411.

Minor, E., Swenson, M.M., Mattson, B.M., & Oyler, A.R. (2014). Structural characterization of dissolved organic matter: a review of current techniques for isolation and analysis *Environmental Science Processes & Impacts, 16*, 2064-2079.

Moorhead, D.L., & Sinsabaugh, R.L. (2006). A theoretical model of litter decay and microbial interaction. *Ecological Monographs 76*, 151-174.

Moser, D., Fredrickson, J.K., Geist, D.R., Arntzen, E.V., Peacock, A.D., Li, S.M.W., . . . McKinley, J.P. (2003). Biogeochemical processes and microbial characteristics across groundwater-surface water boundaries of the Hanford reach of the Columbia River. *Environmental Science & Technology, 37*, 5127-5134.

Mosher, J.J, & Findlay, R.H. (2011). Direct and indirect influence of parental bedrock on streambed microbial community structure in forested streams. *Applied and Environmental Microbiology, 77*(21), 7681-7688.

Moss, J.A., Nocker, A., & Snyder, R.A. (2011). Microbial characteristics of a submerged karst cave system in Northern Florida. *Geomicrobiology Journal, 28*(8), 719-731.

Mostofa, KMG, Yoshioka, T, Konohira, E, & Tanoue, E. (2007). Dynamics and characteristics of fluorescent dissolved organic matter in the groundwater, river and lake water. *Water, air, and soil pollution, 184*(1-4), 157-176.

MRCC. (2014). Midwestern Regional Climate Center. mrcc.isws.illinois.edu

Mulholland, P.J., & Hill, W.R. (1997). Seasonal patterns in stream-water nutrient and dissolved organic carbon concentrations: separating catchment flow path and in-stream effects. . *Water Resources Research, 33*, 1297-1306.

Murdock, J.N., & Wetzel, D.L. (2009). FT-IR microspectroscopy enhances biological and ecological analysis of algae. *Applied Spectroscopy Reviews, 44*(4), 335-361.

Nebbioso, A., & Piccolo, A. (2013). Molecular characterization of dissolved organic matter (DOM): a critical review. *Analytical & Biolanalytical Chemistry, 405*, 109-124.

Neff, J.C., Chapin III, F.S., & Vitousek, P.M. (2003). Breaks in the cycle: dissolved organic nitrogen in terrestrial ecosystems. *Frontiers in Ecology and the Environment, 1*(4), 205-211.

Neilson, A.H.; Allard, A-S. (2008). *Environmental Degradation and Transformation of Orgnaic Chemicals*. Boca Raton, FL: CRC Press.

Newson, M, Baker, A, & Mounsey, S. (2001). The potential role of freshwater luminescence measurements in exploring runoff pathways in upland catchments. *Hydrological Processes, 15*(6), 989-1002.

Nguyen, H. V-M., Lee, M-L., Hur, J., & Schlautman, M.A. (2013). Variations in spectroscopic characteristics and disinfection byproduct formation potentials of dissolved organic matter for two contrasting storm events *Journal of Hydrology 481*, 132-142.

Nguyen, R.T., Harvey, H.R., Zang, X., van Heemst, J.D.H., Hetényi, M., & Hatcher, P.G. (2003). Preservation of algaenan and proteinaceous material during the oxic decay of Botryococcus braunii as revealed by pyrolysis-gas chromatography/mass spectrometry and 13 C NMR spectroscopy. *Organic Geochemistry, 34*(4), 483-497.

Nimmo, John R, Horowitz, Charles, & Mitchell, Lara. (2015). Discrete-Storm Water-Table Fluctuation Method to Estimate Episodic Recharge. *Groundwater, 53*(2), 282-292.

NOAA. (2015). National Centers for Environmental Information. www.ncdc.noaa.gov/cdo-web

NRCS. (2014). *Custom Soil Resources Report for Carter County, KY* Retrieved from websoilsurvey.sc.egove.usda.gov/App/HomePage.htm.

O'Dell, G. (2015). [Morehead State University].

Onstott, TC, Lin, L-H, Davidson, M, Mislowack, B, Borcsik, M, Hall, J, . . . Lippmann-Pipke, J. (2006). The origin and age of biogeochemical trends in deep fracture water of the Witwatersrand Basin, South Africa. *Geomicrobiology Journal, 23*(6), 369-414.

Paul, E.A., Collins, H.P., & Leavitt, S.W. (2001). Dynamics of resistant soil carbon of midwestern agricultural soils measured by naturally-occurring C-14 abundance. *Geoderma, 104*, 239-256.

Perakis, S.S., & Hedin, L.O. (2002). Nitrogen loss from unpolluted South American forests mainly via dissolved organic compounds. *Nature, 415*, 416-419.

Perdrial, J.N., McIntosh, J., Harpold, A., Brooks, P.D., Zapata-Rios, X., Ray, J., . . . Chorover, J. (2014). Stream water carbon controls in seasonally snow-covered mountain

catchments: impact of inter-annual variability of water fluxes, catchment aspect and seasonal processes. *Biogeochemistry, 118*, 273-290.

Perdue, E.M. (2009). Natural organic matter. In G. E. Likens (Ed.), *Encyclopedia of Inland Waters* (Vol. 2, pp. 806-819). Oxford: Elsevier.

Petrone, K.C., Richards, J.S., & Grierson, P.F. (2009). Bioavailability and composition of dissolved organic carbon and nitrogen in a near coastal catchment of south-western Australia. *Biogeochemistry, 92*, 27-40.

Pettersson, C., Ephraim, J., & Allard, B. (1994). On the composition and properties of humic substances isolated from deep groundwater and surface waters *Organic Geochemistry, 21*(5), 443-451.

Peuravuori, J., Koivikko, R., & Pihlaja, K. (2002). Characterization, differentiation and classification of aquatic humic matter separated with different sorbents: synchronous scanning fluorescence spectroscopy *Water Research, 35*, 4552-4562.

Peuravuori, J., Monteiro, A., Eglite, L., & Pihlaja, K. (2005). Comparative study for separation of aquatic humic-type organic constituents by DAX-8, PVP, and DEAE sorbing solids and tangential ultrafiltration: elemental composition, size-exclusion chromatography, UV-vis and FT-IR *Talanta, 65*, 408-422.

Peuravuori, J., Pihlaja, K., & Välimäki, N. (1997). Isolation and characterization of natural organic matter from lake water: two different adsorption chromatographic methods. *Environment international, 23*(4), 453-464.

Pfiffner, S.M., Cantu, J.M., Smithgall, A., Peacock, A.D., White, D.C., Moser, D.P., . . . van Heerden, E. (2006). Deep subsurface microbial biomass and community structure in Witwatersrand Basin mines. *Geomicrobiology Journal 23*, 431-442.

Phillips, Brian L, Casey, William H, & Karlsson, Magnus. (2000). Bonding and reactivity at oxide mineral surfaces from model aqueous complexes. *Nature, 404*(6776), 379-382.

Plummer, S. (2014). [Park Naturalist].

Potter, BB, & Wimsatt, JC. (2005). Method 415.3. Determination of total organic carbon and specific UV absorbance at 254 nm in source water and drinking water. *US Environmental Protection Agency, Cincinnati*.

Pronk, Michiel, Goldscheider, Nico, & Zopfi, Jakob. (2009). Microbial communities in karst groundwater and their potential use for biomonitoring. *Hydrogeology Journal, 17*(1), 37-48.

Pronk, Michiel, Goldscheider, Nico, Zopfi, Jakob, & Zwahlen, François. (2009). Percolation and particle transport in the unsaturated zone of a karst aquifer. *Groundwater, 47*(3), 361-369.

Quinlan, J.F., Davies, G.J., Jones, S.W., & Huntoon, P.W. (1996). The applicability of numerical models to adequately characterize ground-water flow in karstic and other triple-prosity aquifers. In J. D. R. J. O. Rumbaugh (Ed.), *Subsurface Fluid-flow (Groundwater and Vadose Zone ) Modeling* (Vol. ASTM STP 1288, pp. 115-133): American Society for Testing and Materials.

Quinlan, J.F., & Ewers, R.O. (1989). Subsurface drainage in the Mammoth Cave area In W. B. White & E. L. White (Eds.), *Karst Hydrology: Concepts from the Mammoth Cave Area* (pp. 65-103). New York: Van Nostrand Reinhold.

Ramos, Juan L, Gallegos, MT, Marqués, S, Ramos-González, MI, Espinosa-Urgel, M, & Segura, A. (2001). Responses of Gram-negative bacteria to certain environmental stressors. *Current opinion in microbiology, 4*(2), 166-171.

Ramsey, PW, Rillig, MC, Feris, KP, Holben, WE, & Gannon, JE. (2006). Choice of methods for soil microbial community analysis: PLFA maximizes power compared to CLPP and PCR-based approaches. *Pedobiologia, 50*(3), 275-280.

Ratledge, C., & Wilkinson, S.G. (1988). *Microbial lipids* (Vol. 1): Academic Press London.

Ratpukdi, T., Rice, J., Chilom, G., Bezbaruah, A., & Khan, E. (2009). Rapid fractionation of natural organic matter in water using a novel solid-phase extradction technique. *Water Environment Research 81*, 2299-2308.

Raymond, P. A., Hartmann, J., Lauerwald, R., Sobek, S., McDonald, C, Hoover, M., . . . Humborg, C. (2013). Global carbon dioxide emissions from inland waters. *Nature, 503*(7476), 355-359.

Reckhow, D.A., Singer, P., & Malcolm, R.L. (1990). Chlorination of humic materials: Byproduct formaiton and chemical interpretations. *Environmental Science and Technology, 24*(11), 1655-1664.

Reckhow, D.A.; Singer, P.; Malcolm, R.L. (1990). Chlorination of humic materials: Byproduct formaiton and chemical interpretations. *Environmental Science and Technology, 24*(11), 1655-1664.

Reilly, P. (2015). Biosynthesis of Fatty Acids AOCS Lipid Library. Urbana, IL: The American Oil Chemists Society. Retrieved from lipidlibrary.aocs.org.

Ringelberg, D., Richmond, M., Foley, K., & Reynolds, C. (2008). Utility of lipid biomarkers in support of bioremediation efforts at army sites. *Journal of Microbial Methods, 74*, 17-25.

Ritchie, J.D., & Perdue, E.M. (2003). Proton-binding study of standard and reference fulvic acids, humic acids, and natural organic matter. *Geochimica et Cosmochimica Acta, 67*(1), 12.

Ritchie, J.D., & Perdue, E.M. (2008). Analytical constraints on acidic functional groups in humic substances. *Organic Geochemistry, 39*, 17. doi: 10.1016/j.orggeochem.2008.03.003

Roberts, B.J., & Howarth, R.W. (2006). Nutrient and light availability regulate the relative contribution of autotrophs and heterotrophs to respiration in freshwater pelagic systems *Limnology and Oceanography, 51*(1), 288-298.

Rosario-Ortiz, F.L., Snyder, S.A., & Suffet, I.A. (2007). Characterization of dissolved organic matter in drinking water sources impacted by multiple tributaries. *Water Research, 41*, 4115-4128.

Ruess, L., & Chamberlain, P.M. (2010). The fat that matters: soil food web analysis using fatty acids and their carbon stable isotope signature. *Soil Biology and Biochemistry, 42*(11), 1898-1910.

Sandford, A.E., Nelms, D.L., Pope, J.P., & Selnick, D.L. (2012). *Quanitfying components of the hydrologic cycle in Virginia using chemical hydrograph separation and multiple regression analysis* Reston, VA.

Sandford, W.E., Nelms, D.L., Pope, J.P., & Selnick, D.L. (2012). *Quantifying components of the hydrologic cycle in Virginia using chemical hydrograph separation and multiple regression analysis*. (Scientific Investigation Report 2011-5198).

Schmidt, F., Elvert, M., Koch, B.P., Witt, M., & Hinrichs, K.-U. (2009). Molecular characterization of dissolved organic matter in pore water of continental shelf sediments *Geochimica et Cosmochimica Acta, 73*, 3337-3358.

Schmidt, M.W.I., Torn, M.S., Abiven, S., Dittmar, T., Guggenberger, G., Janssens, I.A., . . . Trumbore, S.E. . (2011). Persistence of soil organic matter as an ecosystem property. *Nature 478*, 49-56.

Schmitt, J., Nivens, D., White, D.C., & Flemming, H-C. (1995). Changes of biofilm properties in response to sorbed substances-an ATR-FTIR study. *Water Science and Technology, 32*(8), 149-155.

Schulze-Makuch, Dirk, Goodell, Philip, Kretzschmar, Thomas, & Kennedy, John F. (2003). Microbial and chemical characterization of a groundwater flow system in an intermontane basin of southern New Mexico, USA. *Hydrogeology Journal, 11*(3), 401-412.

Schumacher, M., Christl, I., Vogt, R.D., Barmettler, K., Jacobsen, C., & Kretzschmar, R. (2006). Chemical composition of aquatic dissolved organic matter in five boreal forest catchments sampled in spring and fall seasons. *Biogeochemistry, 80*, 263-275.

Schütz, Kirsten, Nagel, Peter, Vetter, Walter, Kandeler, Ellen, & Ruess, Liliane. (2009). Flooding forested groundwater recharge areas modifies microbial communities from top soil to groundwater table. *FEMS microbiology ecology, 67*(1), 171-182.

Shuman, M.S. . (1990). Carboxyl acidity of aquatic organic matter: does XAD extraction introduce systematic error? . In E. M. Perdue & E. T. Gjessing (Eds.), *Organic Acids in Aquatic Ecosystems: Dahlem Konferenzen* (pp. 97-109). Chichester: Wiley.

Sigee, D.C. (2005). *Freshwater Microbiology: Diversity and Dynamic Interactions of Microorganisms in the Aquatic Environment*. Chichester: John Wiley & Sons.

Simjouw, J.-P., Minor, E.C., & Mopper, K. (2005). Isolation and characterization of estuarine dissolved organic matter: Comparison of ultrafiltration and C18 solid-phase extraction techniques. *Marine Chemistry, 96*, 219-235.

Simon, K.S., & Benfield, E.F. (2001). Leaf and wood breakdown in cave streams. *Journal of the North American Benthological Society 482*, 31-39.

Simon, K.S., Benfield, E.F, & Macko, S.A. (2003). Food web structure and the role of epilithic biofilms in cave streams. *Ecology, 84*(9), 2395-2406.

Simon, K.S., Pipan, T., & Culver, D. (2007). A conceptual model of the flow and distribution of organic carbon in caves. *Journal of Cave and Karst Studies, 69*, 279-284.

Simon, K.S., Pipan, T., Ohno, T., & Culver, D.C. (2010). Spatial and temporal patterns in abundance and character of dissolved organic matter in two karst aquifers. *Fundamental and Applied Limnology, 177*(2), 81-92.

Simpson, M.J., & Simpson, A.J. (2012). The chemical ecology of soil organic matter molecular constituents *Journal of Chemical Ecology, 38*, 768-784.

Sinsabaugh, S.E.G. , & Findlay, R.L. (2003). Dissolved organic matter: Out of the black box into the mainstream. In S. Findlay & S. E. G. Sinsabaugh (Eds.), *Aquatic Ecosystems:*

*Interactivity of Dissolved Organic Matter* (pp. 479-498). Amsterdam: Academic Press.

Sirotkina, I.S., Varshal, G.M., Lure, Y.Y., & Stepanova, N.P. (1974). Use of cellulose sorbents and sephadexes in systematic analysis of organic matter in natural-water. *Journal of Analytical Chemistry of the USSR, 29*(8), 1403-1408.

Skoog, D.A., Holler, F.J., & Crouch, S.R. (2007). *Principles of Instrumental Analysis* (6th ed.). Belmont, CA: Thomson Higher Education.

Sleighter, R., & Hatcher, P. (2008). Molecular characterization of dissolved organic matter (DOM) along a river to ocean transect of the lower Chesapeake Bay by ultrahigh resolution electrospray ionization Fourier transform ion cyclotron resonance mass spectrometry *Marine Chemistry, 110*(3-4), 140-152.

Smart, C, & Karunaratne, K. (2002). Characterisation of fluorescence background in dye tracing. *Environmental Geology, 42*(5), 492-498.

Smith, B., & Moody, P. (1991). The use of DEAE cellulose to extract anionic organic material from groundwaters. *British Geological Survey Technical Report WE/91/9*, 42.

Society, International Humic Substances. (2016). Isolation of IHSS samples. from www.humicsubstances.org/isolation.html

Stanford, J.A., & Ward, J.V. (1993). An ecosystem perspective of alluvial rivers: Connectivity and the hyporheic corridor *Journal of the North American Benthological Society, 12*, 48-60.

Steinberg, C.E.W., Kamara, S., Prokhotskaya, V.Y., Manusadzianas, L., Karasyova, T.A., Timofeyev, M.A., . . . Menzel, R. (2006). Dissolved humic substances-ecological

driving forces from the individual to the ecosystem level? . *Freshwater Biology, 51*, 1189-1210. doi: 10.111/j.1365-2427.2006.01571.x

Steinberg, C.E.W., Timofeyev, M.A., & Menzel, R. (2009). Dissolved Humic Substances: Interactions with Organisms. In G.E.Likens (Ed.), *Biogeochemistry of Inland Waters. A Derivative of Enclyclopedia of Inland Waters* (pp. 457-463). Amsterdam: Academic Press.

Stevenson, F.J. (1994). *Humus chemistry: genesis, composition, reactions*: John Wiley & Sons.

Sun, L, Perdue, EM, Meyer, JL, & Weis, J. (1997). Use of elemental composition to predict bioavailability of dissolved organic matter in a Georgia river. *Limnology and Oceanography, 42*(4), 714-721.

Sun, L., Perdue, E.M., & McCarthy, J.F. (1998). Using reverse osmosis to obtain organic matter from surface and groundwater. *Water Research, 29*, 1471-1477.

Tenney, F.G., & Waksman, S.A. (1929). Composition of natural organic materials and their decomposition in soil: IV. The nature and rapidity of decomposition of the various organic complexes of different plant materials, under aerobic conditions *Soil Science, 28*, 55-84.

ter Braack, C.J.F, & Smilauer, P. (2012). *Canoco Reference Manual and User's Guide: Softward for Ordination (version 5.0)* Ithaca, NY, USA: Microcomputer Power.

Terajima, T., & Moriizumi, M. (2013). Temporal and spatial changes in dissolved organic carbon concentration and fluorescence intensity of fulvic acid like materials in mountainous headwaters catchments. *Journal of Hydrology, 479*, 1-12.

Thacker, SA, Tipping, E, Baker, A, & Gondar, D. (2005). Development and application of functional assays for freshwater dissolved organic matter. *Water research, 39*(18), 4559-4573.

Thomas, J.D. (1997). The role of dissolved organic matter, particularly free amino acids and humic substances, in freshwater ecosystems *Freshwater Biology 38*, 1-36.

Thrailkill, J, Byrd, PE, Sullivan, SB, Spangler, LE, & Taylor, CJ. (1983). Studies in Dye-Tracing Techniques and Karst Hydrogeology. *Available from the National Technical Information Service, Springfield VA 22161 as PB 83-235312, Research Report*(140).

Thurman, E.M. (1985). *Organic Geochemistry of Natural Waters* Dordrecht: Martinus Nijhoff/Dr. W. Junk Publishers.

Thurman, E.M., & Malcolm, R.L. (1981). Preparative isolation of aquatic humic substances. *Environmental Science & Technology, 15*(4), 463-466.

Tinti, A., Tugnoli, V., Bonora, S., & Francioso, O. (2015). Recent applications of vibrational mid-infrared (IR) spectroscopy for studying soil components: a review. *Journal of Central European Agriculture, 16*(1), 1-22.

Town, R.M., & Powell, H.K.J. (1993). Limitations of XAD resins for isolation of the non-colloidal humic fraction in soil extracts and aquatic samples. *Analytica chimica acta, 271*(2), 195-202.

Traina, S.J., Novak, J., & Smeck, N.E. (1990). An ultraviolet absorbance method of estimating the percent aromatic carbon content of humic acids. *Journal of Environmental Quality, 19*, 151-153.

Tranvik, L..J., Downing, J.A., Cotner, J.B., Loiselle, S.A., Striegl, R.G., Ballatore, T.J., . . . Weyhenmeyer, G.A. . (2009). Lakes and reservoirs as regulators of carbon cycling and climate. *Limnology and Oceanography, 54*(6), 2298-2314.

Tranvik, L.J., & von Wachenfeldt, E. (2010). Interactions of dissolved organic matter and humic substances. In G. E. Likens (Ed.), *Biogeochemistry of Inland Waters: A Derivative of Enclycopedia of Inland Waters* (pp. 464-470). San Diego, CA: Elsevier.

Tremblay, J-E., Belanger, S., Barber, D.G., Asplin, M., Martin, J., Darnis, G., . . . Gosselin, M. (2011). Climate forcing multiplies biological productivity in the coastal Arctic Ocean *Geophysical Research Letters, 38*, 1-5.

Tunlid, A., & White, D.C. (1990). Use of lipid biomarkers in environmental samples *Analytical Microbiology Methods* (pp. 259-274): Springer.

Tuschall, JR, Miles, CJ, & Brezonik, PL. (1985). Efficiency of isolating humus from natural waters using DEAE cellulose. *Organic Geochemistry, 8*(1), 137-139.

Valett, A.M., & Sheibley, R.W. (Eds.). (2009). *Ground Water and Surface Water Interaction*. San Diego: Elsevier.

Van Beynen, P.E., Ford, D.C., & Schwartz, H. (2000). Seasonal variability in organic substances in surface and cave waters at Marengo Cave, Indiana *Hydrological Processes, 14*, 1177-1197.

Van der Leeden, F., Troise, F., & Todd, D. . (1990). *The Water Encyclopedia*. Chelsea, MI: Lewis Publishers.

Vannote, R.L., Minshall, G.W., Cummins, K.W., Sedell, J.R., & Cushing, C.E. (1980). Journal of Fishery and Aquatic Sciences. *37, 130-137*.

Vestal, J.R., & White, D.C. (1989). Lipid analysis in microbial ecology: Quantitative approaches to the study of microbial communities. *BioScience, 39*(8), 535-541.

Vinson, D.S., Block, S.E., Crossey, L.J., & Dahm, C.N. (2007). Biogeochemistry at the zone of intermittent saturation: Field-based study of the shallow alluvial aquifer, Rio Grande, New Mexico. *Geosphere, 3*(5), 366-380.

Volk, C.J., Volk, C.B., & Kaplan, L.A. (1997). Chemical composition of biodegradable dissolved organic matter in streamwater *Limnology and Oceanography, 42*(1), 39-44.

Volkman, J.K. (2006). Lipid markers for marine organic matter *Handbook of Environmental Chemistry Part II* (Vol. N, pp. 27-70). Berlin: Springer-Verlag.

Von Lutzow, M., & Kogel-Knabner, I. (2009). Temperature sensitivity of soil organic matter decomposition - what do we know? . *Biology and Fertility of Soils, 46*, 1-15.

Wallenstein, M.D., & Hall, E.K. (2012). A trait-based framework for predicting when and where microbial adaptation to climate change will affect ecosystem functioning. *Biogeochemistry, 109*(1-3), 35-47.

Wehrli, B. (2013). Conduits of the carbon cycle. *Nature, 503*(21), 346-347.

Weishaar, J.L., Aiken, G.R., Bergamaschi, B.A., Fram, M.S., Fujii, R., & Mopper, K. . (2003). Evaluation of specific ultraviolet absorbance as an indicator of the chemical composition and reactivity of dissolved organic carbon. *Environmental Science & Technology 37*, 4702-4708.

Wershaw, R.L. (2004). Evaluation of Conceptual Models of Natural Organic Matter (Humus) from a Consideration of the Chemical and Biochemical Processes of Humification *Scientific Investigations Report 2004-5121*. Reston, VA: U.S. Geological Survey.

Wetzel, R.G. (1992). Gradient-dominated ecosystems: Sources and regulatory functions of dissolved organic matter in freshwater ecosystems. *Hydrobiologia, 229*, 181-198.

White, D.C. (1995). Chemical ecology: possible linkage between macro- and microbial ecology. *OIKOS, 74*, 177-184.

White, D.C., Bobbie, R.J., Morrison, R.J., Oosterhof, D.K., Taylor, C.W., & Meeter, D.A. (1977). Determination of microbial activity of estuarine detritus by relative rates of lipid biosythesis *Limnology and Oceanography, 22*, 1089-1099.

White, D.C., Davis, W.M., Nickols, J.S., King, J.D., & Bobbie, R.J. (1979). Determination of the sedimentary microbial biomass by extractable liquid phosphate *Oecologia, 40*, 51-62.

White, D.C., Flemming, C.A., Leung, K.T., & MacNaughton, S.F. (1998). In situ microbial ecology for quantitative appraisal, monitoring, and risk assessment of pollution remediation in soils, the subsurface, the rhizospere, and in biofilms *Journal of Microbial Methods, 32*, 93-105.

White, DC, & Ringelberg, D. (1998). Signature Lipid Biomarker Analysis. In R. Burlage, R. Atlas, D. Stahl, G. Geesey & G. Saylor (Eds.), *Techniques in Microbial Ecology* (pp. 255-272). New York: Oxford University Press.

Wilson, H.F., Saiers, J.E., Raymond, P.A., & Sobczak, W.V. (2013). Hydrologic drivers and seasonality of dissolved organic carbon concentation, nitrogen content, bioavailability, and export in a forested New England stream *Ecosystems, 16*, 604-616.

Wilson, Jr., J.F., Cobb, E.D., & Kilpatrick, F.A. (1986). *Fluorometric Procedures for Dye Tracing, Revised*. (TW3-A12). Washington, D.C.: US Government Printiing Office.

Wolkersdorfer, Christian, & LeBlanc, Jenna. (2012). Regulations, legislation, and guidelines for artificial surface water and groundwater tracer tests in Canada. *Water Quality Research Journal of Canada, 47*(1), 42-55.

Worthington, SRH, & Ford, DC. (2009). Self-organized permeability in carbonate aquifers. *Groundwater, 47*(3), 326-336.

Worthington, SRH, & Smart, C C. (2003). Empirical determination of tracer mass for sink to spring tests in karst. *GEOTECHNICAL SPECIAL PUBLICATION*, 287-298.

Worthington, Stephen RH. (2009). Diagnostic hydrogeologic characteristics of a karst aquifer (Kentucky, USA). *Hydrogeology Journal, 17*(7), 1665-1678.

Yamashita, Y., Fichot, C. G., Shen, Y., Jaffé, R., & Benner, R. (2015). Linkages among fluorescent dissolved organic matter, dissolved amino acids and lignin-derived phenols in a river-influenced ocean margin. *Frontiers in Marine Science, 2*, 92.

Zelles, L. (1997). Phospholipid fatty acid profiles in selected members of soil microbial communities. *Chemosphere, 35*(1), 275-294.

Zhang, Y-M., & Rock, C.O. (2008). Membrane lipid homeostasis in bacteria. *Nature Reviews Microbiology, 6*(3), 222-233.

Zhu, Z. (Ed.), Bergamaschi, B.A., Bernknopf, R., Clow, D., Dye, D, Faulkner, S., . . . Wein, A. (2010). *A method for assessing carbon stocks, carbon sequestion, and greenhouse-gas fluxes in ecosystems of the United States under present conditions and future scenarios*

## Appendix

Table A.1 Master Sample Analysis Table

| Carter Cave State Park | | | | | Sample Master List | | | | | | |
|---|---|---|---|---|---|---|---|---|---|---|---|
| | | | | | | CH 3 | | | CH 4 | | CH 5 |
| | ID | Type | Sample Date | Site | Physico | Corg | TN | Ions | DEAE | FTIR | PLFA |
| | 12D001 | water-filtered | 13-Dec-12 | LR | | X | | X | X | X | |
| | | water-unfiltered | | | X | X | | | | | |
| | | filter extracts | | | | | | | | | X |
| | | sediment extract | | | | | | | | | X |
| Winter | 12D002 | water-filtered | 13-Dec-12 | FF | | X | | X | X | X | |
| High | | water-unfiltered | | | X | X | | | | | |
| Flow | | Filters | | | | | | | | | X |
| | | Sediments | | | | | | | | | X |
| | 13F001 | water-filtered | 8-Feb-13 | LR | | X | | X | X | X | |
| | | water-unfiltered | | | X | X | | | | | |
| | | filter extracts | | | | | | | | | |
| Winter | | sediment extracts | | | | | | | | X | |
| High | 13F003 | water-filtered | 8-Feb-13 | FF | | X | | X | X | X | |
| Flow | | water-unfiltered | | | X | X | | | | | |
| | | filter extracts | | | | | | | | | X |
| | | sediment extracts | | | | | | | | X | X |
| | 13Ju001 | water-filtered | 2-Jun-13 | LR | | X | | X | X | X | |
| | | water-unfiltered | | | X | X | | | | | |
| Summer | | filter extracts | | | | | | | | | X |
| Low | | sediment extracts | | | | | | | | X | X |
| Flow | 13Ju003 | water-filtered | 2-Jun-13 | FF | | X | | X | X | X | |
| | | water-unfiltered | | | X | X | | | | | |

Table A.1.Cont.

| Carter Cave State Park | | | | | Sample Master List | | | | | | |
|---|---|---|---|---|---|---|---|---|---|---|---|
| | | | | | | CH 3 | | | CH 4 | | CH 5 |
| | ID | Type | Sample Date | Site | Physico | Corg | TN | Ions | DEAE | FTIR | PLFA |
| | | filter extracts | | | | | | | | | X |
| | | sediment extracts | | | | | | | | X | X |
| | 13Sp3.5 | water-filtered | 14-Sep-13 | LR | | X | | X | X | X | |
| | | water-unfiltered | | | X | X | | | | | |
| | | filter extracts | | | | | | | | | X |
| Summer | | sediment extracts | | | | | | | | X | X |
| Low | 13Sp2.5 | water-filtered | 14-Sep-13 | FF | | X | | X | X | X | |
| Flow | | water-unfiltered | | | X | X | | | | | |
| | | filter extracts | | | | | | | | | X |
| | | sediment extracts | | | | | | | | X | X |
| | 14Ja001 | water-filtered | 25-Jan-14 | LR | | X | | X | X | X | |
| | | water-unfiltered | | | X | X | | | | | |
| | | filter extracts | | | | | | | | | X |
| Winter | | sediment extracts | | | | | | | | | X |
| High | 14Ja002 | water-filtered | 25-Jan-14 | FF | | X | | X | X | X | |
| Flow | | water-unfiltered | | | X | X | | | | | |
| | | filter extracts | | | | | | | | | X |
| | | sediment extracts | | | | | | | | | X |
| | 14Mr001 | water-filtered | 15-Mar-14 | LR | | X | | | X | X | |
| | | water-unfiltered | | | X | X | | | | | |
| | | filter extracts | | | | | | | | | X |
| Winter | | Sediment ext. | | | | | | | | X | X |

Table A.1 Cont.

| Carter Cave State Park | | | | | Sample Master List | | | | | | |
|---|---|---|---|---|---|---|---|---|---|---|---|
| | | | | | | CH 3 | | | CH 4 | | CH 5 |
| | ID | Type | Sample Date | Site | Physico | Corg | TN | Ions | DEAE | FTIR | PLFA |
| High | 14Mr002 | water-filtered | 15-Mar-14 | FF | | X | | | X | X | |
| Flow | | water-unfiltered | | | X | X | | | | | |
| | | filter extracts | | | | | | | | | X |
| | | sediment ext. | | | | | | | | X | X |
| | 14Ju001 | water-filtered | 19-Jun-14 | LR | | X | | | X | X | |
| | | water-unfiltered | | | X | X | | | | | |
| | | filter extracts | | | | | | | | | X |
| Summer | | sediment extracts | | | | | | | | X | X |
| Low | 14Ju004 | water-filtered | 19-Jun-14 | FF | | X | | | X | X | |
| Flow | | water-unfiltered | | | X | X | | | | | |
| | | filter extracts | | | | | | | | | X |
| | | sediment extracts | | | | | | | | X | X |

## Vita

Teresa L. (Terri) Brown grew up in southwest Virginia and graduated from James Madison University with a B.S. in Geology in 1983. Her undergraduate research focused on the analysis of manganese-iron oxide coatings on stream sediments as an exploration tool for polymetallic sulfide mineral deposits. She worked as a hydrogeologist for more than 20 years before beginning graduate studies at the Department of Earth and Planetary Sciences (EPS) at the University of Tennessee, where she completed her Master of Science (M.S.) in Geology in 2009. Her M.S. research, which was partially funded by the Tennessee Department of Environment and Conservation, examined the characteristics of natural fluorophores in public groundwater supply sources in East Tennessee in relation to surface-water influence. Terri began her Ph.D. studies at Louisiana State University in 2010, and transferred back to UT in 2011 with her advisor, Dr. Annette Engel.